Role of Chronophin for glioma cell migration and invasion

Die Rolle von Chronophin für die Migration und Invasion von Gliomzellen

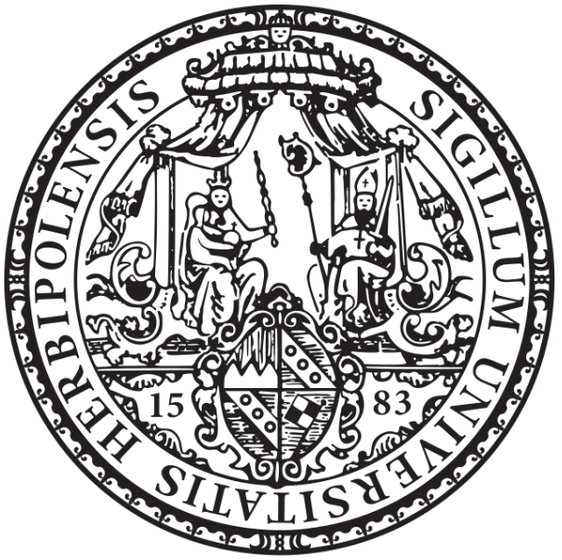

Doctoral thesis for a doctoral degree

at the Graduate School of Life Sciences,

Julius-Maximilians-Universität Würzburg,

Section Biomedicine

submitted by

Markus Schulze

from

Aschaffenburg

Würzburg, 2014

Submitted on: ……..……..

Office stamp

Members of the *Promotionskomitee*:

Chairperson:	**Prof. Dr. Jörg Schultz**
Primary Supervisor:	**Prof. Dr. Antje Gohla**
Supervisor (Second):	**Prof. Dr. Martin Eilers**
Supervisor (Third):	**Prof. Dr. Anna-Leena Sirén**

Date of Public Defence: ……

Date of Receipt of Certificates:……

Table of Contents

Figure Index

Abbreviations

´	minute(s)
´´	second(s)
2D	two dimensional
3D	three dimensional
A	ampere
ABC	avidin biotin complex
ADF	actin depolymerizing factor
ADP	adenosine diphosphate
APS	ammonium persulfate
Arp	actin related protein
ATP	adenosine triphosphate
AveExpr	average expression
bp	base pairs
BSA	bovine serum albumin
$CaCl_2$	calcium chloride
CD	cluster of differentiation
CDC	cell division cycle
CDKN2A	cyclin-dependent kinase inhibitor 2A
CDKN2B	cyclin-dependent kinase inhibitor 2B
cDMEM	complete Dulbecco's modified Eagle's medium
cDNA	complementary DNA
CEBPß	CCAAT/enhancer binding protein, beta
CFL1	cofilin-1
CFL2	cofilin-2
CHI3L1	chitinase 3-like 1
CIN	chronophin
CIP	calf intestinal phosphatase
CMV	cytomegalovirus
c-myc	v-myc avian myelocytomatosis viral oncogene homolog
CNS	central nervous system
CO_2	carbon dioxide
Ctl	control
CXCR	chemokine (C-X-C motif) receptor
d	diameter
D (amino acid)	aspartate
D (parameter)	distance from origin
DAB	3,3'-diaminobenzidine
DAPI	4',6-diamidino-2-phenylindole
DAVID	**D**atabase for **A**nnotation, **V**isualization and **I**ntegrated **D**iscovery
df	degree of freedom
DIC	differential interference contrast

DMEM	Dulbecco’s modified Eagle's medium
DMSO	dimethyl sulfoxide
DNA	deoxyribonucleic acid
dNTPs	deoxyribonucleotide triphosphate
E. Coli	Escherichia coli
ECM	extracellular matrix
EDIL3	EGF-like repeats and discoidin I-like domains 3
EDTA	ethylenediaminetetraacetic acid
EGF	epidermal growth factor
EGFR	epidermal growth factor receptor
EGFRvIII	epidermal growth factor receptor variant III
EGTA	ethylene glycol tetraacetic acid
ELISA	enzyme-linked immunosorbent assay
EthBr	ethidium bromide
FACS	fluorescence-activated cell sorting
F-actin	filamentous actin
FCS	fetal calf serum
FMI	forward migration index
x g	acceleration due to gravity (9.81 m/s^2)
G418	geneticin
GABA	gamma-aminobutyric acid
G-actin	globular actin
GABRA1	gamma-aminobutyric acid A receptor, alpha 1
GAPDH	glyceraldehyde 3-phosphate dehydrogenase
GBM	Glioblastoma multiforme
GEO	gene expression omnibus
GFAP	glial fibrillary acidic protein
GFP	green fluorescent protein
GO	gene ontology
GTPase	guanosine triphosphate hydrolase
h	hour(s)
H3F3A	H3 histone, family 3A
hCIN	human chronophin
HCl	hydrochloric acid
HEPES	4-(2-hydroxyethyl)-1-piperazineethanesulfonic acid
HIF1a	hypoxia inducible factor 1, alpha subunit
HRP	horseradish peroxidase
ICC	immunocytochemistry
IDH	isocitrate dehydrogenase
IHC	immunohistochemistry
IPA	ingenuity pathway analysis

KCl	potassium chloride
kDa	kilo Dalton
KH_2PO_4	potassium dihydrogen phosphate
LatA	latrunculin A
LB	Luria-Bertani
LIMK	LIM (Lin-11/Isl-1/Mec-3)-domain-containing protein kinase
logFC	logarithmic fold change
LPA	oleoyl-L-α-lysophosphatidic acid
MAX	MYC associated factor X
$MgCl_2$	magnesium chloride
MGMT	O-6-methylguanine-DNA methyltransferase
MgSo4	magnesium sulfate
MMP	matrix metalloproteinase
$MnCl_2$	manganese (II) chloride
mRNA	messenger RNA
MRT	magnetic resonance tomography
MXD	MAX dimerization protein
MXI1	MAX interactor 1, dimerization protein
Na_2HPO_4	di-sodium hydrogen phosphate
NaCl	sodium chloride
NaN_3	sodium azide
NaOH	sodium hydroxide
NEFL	neurofilament, light polypeptide
NF	neurofibromatosis
NGS	normal goat serum
NKX-2	NK2 homeobox
NMA	normal mouse astrocytes
NOD	non-obese diabetic
NP-40	nonylphenolethoxylate
O/N	over night
OLIG2	oligodendrocyte lineage transcription factor 2
P (amino acid)	proline
p53	tumor protein p53
PAGE	polyacrylamide gel electrophoresis
PAK	p21 protein (Cdc42/Rac)-activated kinase 1
PAR-2	protease activated receptor 2
PBS	phosphate buffered saline
P-cofilin	phosphorylated coflin
PCR	polymerase chain reaction
PDGFBB	platelet-derived growth factor beta polypeptide

.

PDGFRA	platelet-derived growth factor receptor, alpha polypeptide
PDXP	pyridoxal (pyridoxine, vitamin B6) phosphatase
PFA	paraformaldehyde
PI3K	phosphatidylinositol-4,5-bisphosphate 3-kinase
PIP2	phosphatidylinositol 4,5-bisphosphate
PIPES	piperazine-N,N'-bis(2-ethanesulfonic acid)
PMSF	phenylmethanesulfonyl fluoride
PTEN	phosphatase and tensin homolog
Rac	ras-related C3 botulinum toxin substrate
Ras	rat sarcoma viral oncogene homolog
Rembrandt	**RE**pository of **M**olecular **BRA**in **N**eoplasia **D**a**T**a
RhoA	ras homolog family member A
RISC	RNA induced silencing complex
RNA	ribonucleic acid
RNAi	RNA interference
ROCK	Rho-associated, coiled-coil containing protein kinase
RT	room temperature
RTEL1	regulator of telomere elongation helicase 1
RTK	receptor tyrosine kinase
SCID	severe combined immunodeficiency
SDS	sodium dodecyl sulfate
sec	seconds
shRNA	short hairpin RNA
siRNA	short interfering RNA
SLC12A5	solute carrier family 12 (potassium/chloride transporter), member 5
SNP	single nucleotide polymorphism
SOC	super optimal broth with catabolite repression
SP	specificity protein
SRE	serum response element
SRF	serum response factor
SSH (gene symbol)	slingshot protein phosphatase
SSH	suppression subtractive hybridization
STAT	signal transducer and activator of transcription
SYT1	synaptotagmin
T_A	annealing temperature
TAE	Tris-acetate-EDTA
TBS	Tris buffered saline
TCGA	The Cancer Genome Atlas
TEMED	tetramethylethylenediamine
TESK	testis-specific kinase
THBS1	thrombospondin 1
TM	trademark
Triton X-100	t-octylphenoxypolyethoxyethanol

Tween 20	polyoxyethylene (20) sorbitan monolaurate
TRE	tandem response element
uPA	plasminogen activator, urokinase
uPAR	plasminogen activator, urokinase receptor
v	volume
V	volt
V (amino acid)	valine
VEGFA	vascular endothelial growth factor A
WASP	Wiskott–Aldrich syndrome protein
w	weight
w/o	without
WHO	World Health Organization
WT	wild type

1. Introduction

1.1 The origins of gliomas

Gliomas are primary tumors of the central nervous system (CNS), which are derived from neural stem cells and/or more differentiated glial progenitor cells (see Fig. 1).

Different glioma entities are recognized in the CNS, according to their histological and biochemical similarity to the different possible cell types of origin. Gliomas are therefore subdivided in oligodendrogliomas, astrocytomas and ependymomas [2,3]. The most common form, the glioblastoma multiforme (GBM), belongs to the astrocytic tumors. Studies examining genetic mouse models of gliomas in p53 and NF1 deficient mice have collected evidence that gliomas arise from stem cells in the subventricular zone [4].

However, it has been shown recently that virally mediated tumor suppressor knockdown is able to induce gliomas from differentiated neuronal and glial cells [5].

Gliomas are classified into four different grades, according to the World Health Organization (WHO). Grade I comprises the most benign tumors, and grade IV the most malignant entities. The most common type of gliomas, the glioblastoma multiforme (GBM), belongs to the grade IV tumors and comprises more than 50 % of the gliomas in adulthood [6].

Due to the diffuse infiltration of the healthy brain parenchyma by the tumor cells and the tendency of the low grade lesions to progress to more malignant entities, already grade II tumors have a dismal prognosis [7]. The GBM is subdivided into primary and secondary GBMs. Secondary GBMs arise from lower grade gliomas, whereas primary GBMs arise *de novo*. These tumor types, although not distinguishable by histology, are characterized by different alterations on the molecular level, e.g. mutations of the isocitrate dehydrogenase genes, IDH1 and 2, which are nearly exclusively found in secondary GBMs. Except for ionizing radiation, no environmental risk factors for glioma development are known [8].

A genetic predisposition for glioma is present in individuals affected by the Li-Fraumeni syndrome, where the tumor suppressor protein p53 is frequently mutated, in patients suffering from neurofibromatosis, where NF1 or 2 are affected, and other rare genetic syndromes [8]. Besides these severe genetic syndromes, single nucleotide polymorphisms (SNPs) in the cyclin-dependent kinase inhibitor 2B (CDKN2B) and regulator of telomere elongation helicase 1 (RTEL1) genes have been linked to glioma susceptibility [9], as well as different SNPs in DNA repair genes [10].

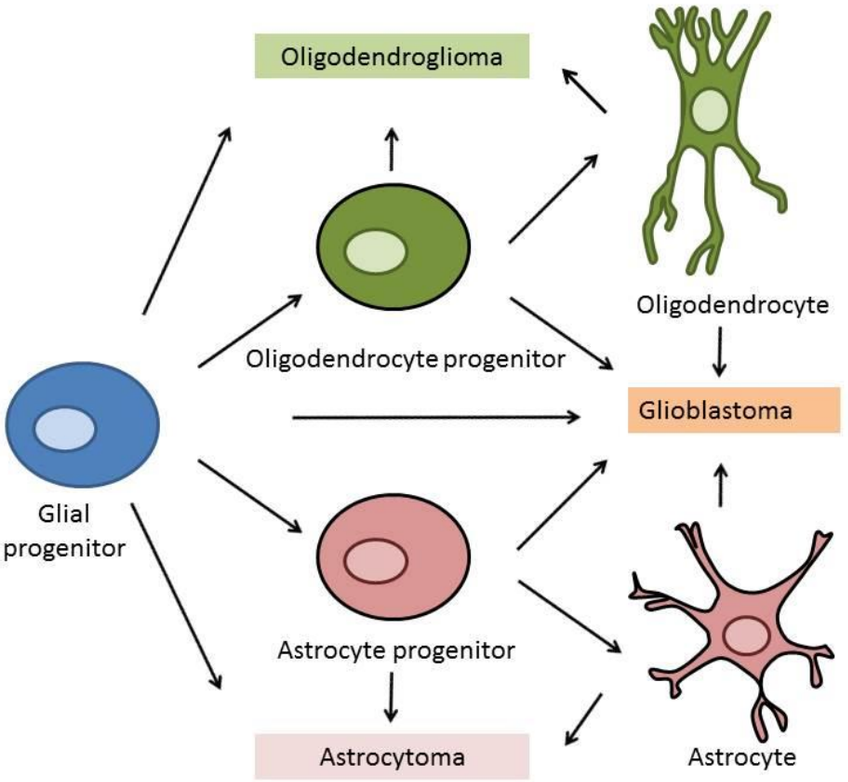

Figure 1: Cells of origin of different subtypes of gliomas.
Glial progenitors, astrocyte progenitors and differentiated glial cells can serve as cells of origin in the development of glioblastomas. Astrocytomas are thought to be derived from glial progenitors, astrocyte progenitors and/or mature astrocytes, modified after [4].

1.2 Diagnosis and therapeutic options

Most patients suffering from gliomas present themselves in the clinic with symptoms caused by elevated intracranial pressure. The pressure is increased by the tumor mass and by the edema accompanying it. Symptoms include seizures, headache and psychopathological symptoms [11]. Diagnosis of the tumor itself is performed with magnetic resonance tomography (MRT). The grading of the lesion is based on histological analysis. GBMs are characterized by a striking heterogeneity of the tissue. Necrotic areas, proliferating endothelial cells and pseudopalisading cells are typical features of a GBM (see Fig. 2) [6]. Other grading criteria include nuclear pleomorphisms, enhanced cellularity and mitotic activity [2]. Depending on the tumor localization, therapy includes, if possible, surgical

resection, chemotherapy with temozolomide and radiotherapy. If resection is impossible, the tissue is at least biopsied, to enable a grading of the tumor. Due to the massive infiltration of healthy brain parenchyma complete resection is impossible [12]. Unfortunately, gliomas are quite resistant to radiotherapy and treatment with the alkylating agent temozolomide. Resistance against temozolomide is conferred by the O-6-methylguanine-DNA methyltransferase (MGMT) that repairs O^6-methylguanine DNA-adducts.

Therefore, the methylation status of the MGMT promoter is nowadays analyzed very often, as methylation of the promoter is a prognostic factor as well as predictive for a patient's benefit from chemotherapy. However, other events, such as defects in DNA mismatch repair, contribute to temozolomide resistance, too [13].

Finally, increased intracranial pressure and invasion of vital brain regions lead to death. Besides temozolomide, many other drugs are currently under investigation in clinical trials. In addition, approaches consisting of immunotherapy and viral therapy are in development [14,15]. Identified tumor drivers, like the receptor tyrosine kinase (RTK) epidermal growth factor receptor (EGFR), are used for targeted therapies, e.g. the EGFR inhibitor Erlotinib. GBMs acquire resistance towards Erlotinib fast, the reason being among others parallel activation of different RTKs [16]. Anti-angiogenic therapy with bevacizumab, a monoclonal antibody targeting VEGF, has a significant impact on progression free survival [17]. However, there is evidence for increased invasion of glioma cells into the brain parenchyma after inhibition of the VEGF pathway [18]. Therefore, anti-angiogenic therapy combined with anti-invasive therapy would be a promising therapeutical approach, as it has been shown that inhibition of SRC family kinases with dasatinib blocks the increased invasion after bevacizumab application in an orthotopic xenograft mouse model [19].

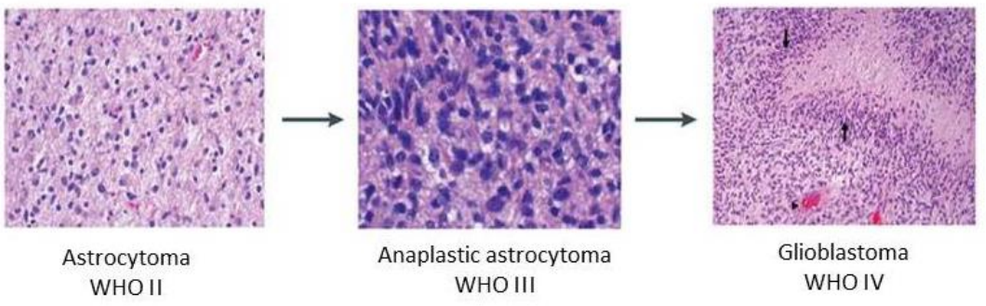

Figure 2: Hematoxylin and eosin staining of glioma sections.
Different grades of tumor lesions including a low grade astrocytoma, an anaplastic astrocytoma and a glioblastoma. The glioblastoma shows typical pseudopalisading cells (arrows) [7].

Moreover, anti-invasive therapy with imaprimine blue combined with doxorubicin chemotherapy has shown very promising effects on overall survival in a mouse model of glioma [20].

However, despite of aggressive therapy, GBMs have a dismal prognosis and a median survival time of about one year after diagnosis [8].

1.3 Molecular alterations in GBM

In the last decades, numerous expression and sequencing studies were performed, to establish a genome wide overview of aberrant expression patterns, mutations and gene copy number alterations in gliomas. The Cancer Genome Project (TCGA) has analyzed copy number alterations and mRNA expression patterns and in addition sequencing of the protein encoding genes of 22 GBM genomes was performed [21,22]. These studies have contributed significantly to our understanding of glioma initiation, progression and classification [23].

Frequently altered pathways include the p53, retinoblastoma and the RTK/Ras/PI3K signaling pathways [21]. GBMs can be classified into different, molecularly distinct, categories that are defined by the underlying genetic lesions. Classical categorization only distinguished primary and secondary GBMs, which cannot be separated based on histology. However, p53 mutations occur more frequently, and IDH mutations nearly exclusively, in secondary GBMs. Secondary GBMs are much less frequent than primary GBMs, and affect mostly younger patients.

Molecular analysis of primary and secondary GBMs revealed that there are three to four main categories of GBMs, the proneural, classical, mesenchymal and neural subtype [24]. As the neural subtype is less well defined than the other subtypes, it is not further discussed here. The **classical subtype** is characterized by epidermal growth factor receptor (EGFR) amplification, EGFR mutation or expression of a tumor specific EGFR variant, the EGFRvIII. EGFRvIII contains an in-frame deletion that comprises the ligand binding domain. The EGFRvIII is a constitutively active receptor variant [25], and EGFR and EGFRvIII cooperate to drive cell transformation and tumor progression [26]. This subtype normally does not contain p53 mutations. The retinoblastoma pathway is nearly exclusively disrupted by cyclin-

dependent kinase inhibitor 2A (CDKN2A) deletion in this subtype, and astrocytic markers are expressed [27].

The **proneural subtype**, which comprises most secondary GBMs, is characterized by p53 and IDH mutations, and tumors of this subtype frequently contain PDGFRA amplifications. Oligodendrocyte markers such as platelet-derived growth factor receptor, alpha polypeptide (PDGFRA), NK2 homeobox (NKX-2) and oligodendrocyte lineage transcription factor 2 (OLIG-2) are strongly expressed in this subtype [27]. In addition, further subtypes in the proneural subgroup have been identified that are characterized by H3F3A mutations, which are restricted to younger patients [28]. Moreover, a subgroup exists that shows global hypermethylation [29]. A trend towards overall prolonged survival is present in the proneural subtype, however, the more favourable prognosis in restricted to the tumors showing global hypermethylation [30].

Furthermore, the **mesenchymal subtype**, which contains NF1 deletions and mutations, and that shows expression of mesenchymal markers Met and CHI3L1, exists [27]. It has been shown that CEBPß and STAT3 activity are crucial for the establishment of the mesenchymal subtype [31].

The three mentioned subtypes, classical, proneural and mesenchymal have been identified (albeit named differently) by several groups and different approaches, including proteomic and mRNA expression analysis [24,27,32,33].

RTKs, like epidermal growth factor receptor (EGFR) and platelet-derived growth factor receptor A (PDGFRA), which are frequently overexpressed or mutated in GBMs, are not only drivers for glioma initiation, but also important signaling inputs for migration and invasion [34]. Stimulation of RTKs leads to signaling events that finally converge on reorganization of the tubulin and actin cytoskeleton.

1.4 The actin cytoskeleton in cell migration and invasion

The eukaryotic cytoskeleton consists of tubulin, actin and intermediary filaments.

These different structural components of the cell provide mechanical stability and enable cell locomotion [35]. Actin as well as tubulin are important for cell migration and are regulated in a coordinated fashion. Since this work focuses on the process of actin reorganization, only the actin cytoskeleton and the proteins involved in its reorganization are discussed in the following section. Actin is present in the cell in an equilibrium between G- and F-actin, and actin filaments can nucleate spontaneously, provided the G-actin concentration is sufficiently high. F-actin is a double helical, intrinsically polar filament. The more dynamic filament end, where actin subunits are rapidly added or removed, depending on the concentration of G-actin available for polymerization, is called barbed end. The less dynamic end of the actin filament is referred to as the pointed end. At the barbed end, actin is normally present in the ATP-bound state, whereas it is ADP-bound at the pointed end. Inside cells, actin is bound by variety of actin binding proteins [35].

The isolated proteins that are necessary for assembly of actin filaments and for the propulsion of beads in an *in vitro* motility assay are called minimal reconstituted motility machinery. It consists of actin, cofilin, capping protein, Wiskott-Aldrich syndrome-like (N-WASP), the Arp 2/3 complex and profilin [35]. N-WASP is an Arp 2/3 activator, whereas Arp 2/3 itself initiates branching from already existing filaments.

Cofilin´s most important cell biological functions are actin filament severing and enhancement of depolymerization at the pointed end [35,36].

The family of mammalian cofilin proteins consists of actin depolymerizing factor/ destrin (ADF), cofilin-2 (CFL2) and cofilin-1 (CFL1). These genes differ in tissue expression and function. CFL1 is ubiquitously expressed, whereas CFL2 is primarily found in muscle and ADF in epithelia [37]. The CFL1 gene is referred to as cofilin in the following sections.

Actin is part of a number of diverse cellular structures, and in cells at least 15 actin based structures are recognized [38].

Especially important for migration and invasion are lamellipodia, the lamellum, invadopodia, blebs and the different forms of stress fibers that are involved in the formation of these structures [1,39]. Stress fibers are subdivided into distinct entities, depending on type and localization (see Fig. 3). There are ventral stress fibers, dorsal stress fibers and transverse

arcs. Stress fibers are induced e.g. after RhoA stimulation, and exist *in vivo* in highly motile cells like myofibroblasts, or where cells are exposed to mechanical stress [1].

The lamellipodium is located at the leading edge, where a meshwork of growing actin filaments pushes the membrane forward [40].

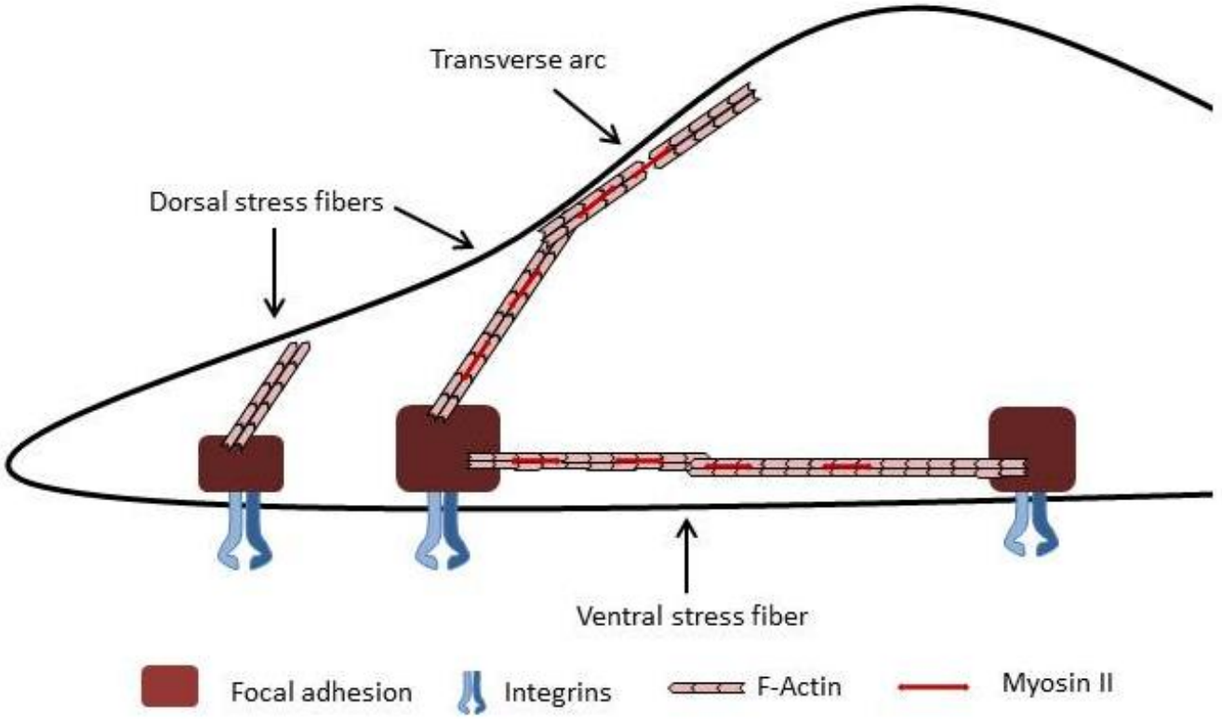

Figure 3: Stress fiber structures in eukaryotic cells.
Shown are dorsal and ventral stress fibers that are connected to the extracellular matrix *via* focal adhesions and integrins. Also shown is a transverse arc, modified after [1].

1.5 Signaling towards cofilin

The signaling towards cofilin is initiated at the plasma membrane by RTKs, G-protein coupled receptors or integrins.

Via PI3-Kinase and small GTPases of the Rho-family the signal is propagated, and finally cofilin phosphorylation is performed by LIMKs or TESKs. The F-actin binding of cofilin is regulated by phosphorylation of a single serine residue, serine 3 [41]. The phosphorylation on serine 3 abrogates the binding of cofilin to F-actin. Due to their sequence similarity and

conservation of the serine residue, it is at least possible that LIMKs, TESKs and the cofilin phosphatases regulate the phosphorylation of all three cofilin proteins. Phosphoregulation of cofilin-1 plays an important role in a variety of physiological and pathological situations [41], but also for the other two family members phosphorylation is an important regulatory mechanism. A critical role for phosphoregulation of cofilin-2 has been shown in the differentiation of smooth muscle cells [42] and ROCK dependent phosphoregulation of ADF has been shown to be implicated in the amoeboid type of migration of cancer cells [43].

LIMK1 and LIMK2 themselves are activated by kinases of the PAK or ROCK-family by phosphorylation on threonine residues 508 or 505, respectively (see Fig. 4) [44,45]. In contrast to the alterations and role of RTKs and PI3K in cell migration and invasion, which are well characterized, much less is known about their effector proteins Rho/ROCK and Rac/PAK in glioma. However, these are crucial for signal transmission and reorganization of the actin cytoskeleton [46].

The cellular role of the LIMK mediated phosphorylation of cofilin is explained by the **L**ocal **E**xcitation **G**lobal **I**nhibition (LEGI) model. This model postulates that cofilin is only activated focally where actin remodeling is taking place, and inhibited by phosphorylation on serine 3 in the rest of the cell [47]. LIMK mediated cofilin phosphorylation abolishes its severing activity. On the other hand, phosphorylation of cofilin also leads to cofilin recycling, and might play an important role in maintaining a very high local concentration of active cofilin in structures important for invasion, e.g. invadopodia [41]. In the process of cofilin recycling phosphorylation of actin bound cofilin leads to the dissociation of actin and cofilin. The phosphoralyted cofilin can then be reactivated by dephosphorylation by cofilin phosphatases, e.g. SSHs and CIN.

Previous work in our laboratory has revealed that LIMKs are highly upregulated in astrocytic tumors on protein level, whereas the cofilin phosphatase CIN is downregulated on protein level [48]. Importantly, ROCK has already been shown to contribute to tumor formation in the skin [49] and the importance of LIMKs for cancer cell invasion has been shown in a variety of experimental model systems [50-52].

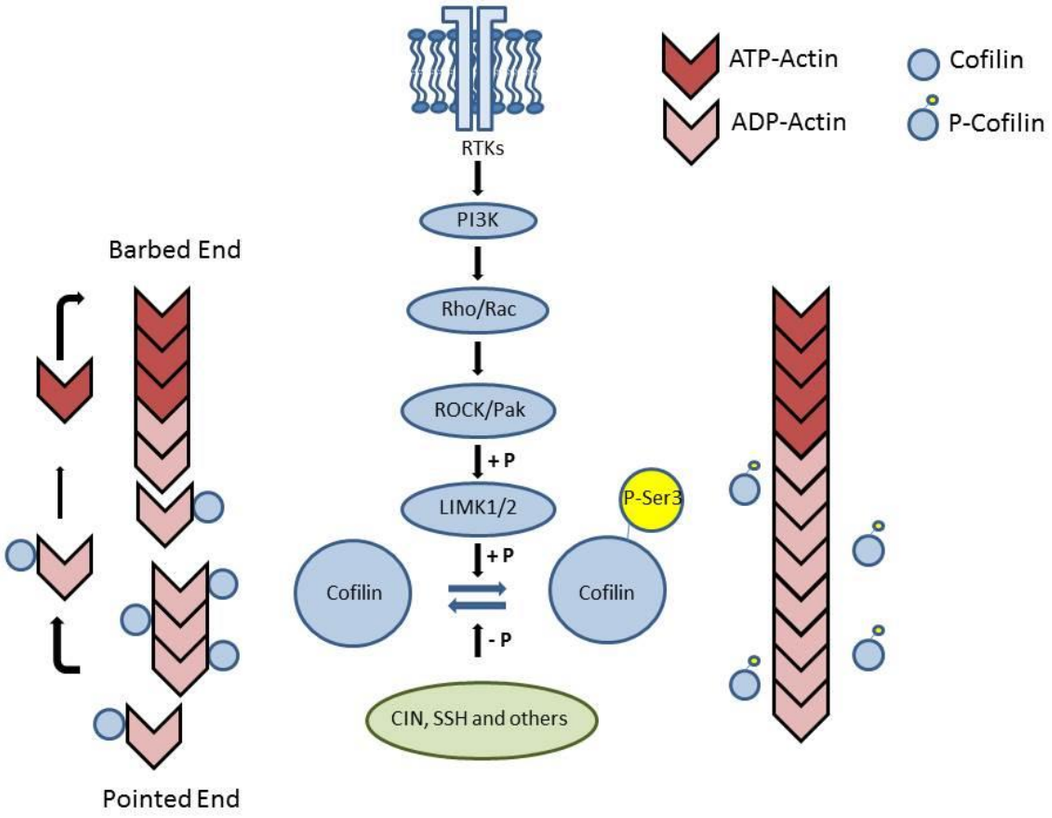

Figure 4: The regulatory pathway of cofilin phosphorylation.
Actin turnover is initiated by receptor tyrosine kinase signaling. Subsequently, PI3K and the small GTPases Rho/Rac are activated. These in turn activate ROCK and Pak proteins, respectively, which in turn phosphorylate the LIMKs. The LIMKs phosphorylate cofilin on serine 3, and abolish its actin binding. CIN, SSH1-3 and other phosphatases can dephosphorylate cofilin, modified after [41,53].

The role of CIN and LIMKs has until now not been examined in glioma. This is however important, due to the fact that ROCK proteins have a variety of substrates besides LIMKs [54], and the ROCK inhibitor induced phenotypes do not need to be necessarily induced by a change in cofilin phosphorylation. In this study, cell migration and invasion are examined after deregulation of CIN. CIN, a cofilin phosphatase, is strongly downregulated in glioma specimens. Therefore, the pathophysiological changes in the phosphoregulation of cofilin are mimicked more closely here than by overexpression of a constitutively active mutant of cofilin, which has been performed by others.

Besides phosphorylation, cellular cofilin activity is furthermore controlled by PIP2-binding and intracellular pH [55]. In metastatic breast cancer cells, PIP2 hydrolysis is especially important for the initial cofilin activation during chemotaxis at the leading edge [56]. PH

dependent cofilin regulation has been shown to influence invadopodium turnover [57]. Invadopodia are invasive, matrix resolving, F-actin rich structures specifically induced by cancer cells [58].

1.6 Cofilin in cell migration and invasion

Cofilin activity is needed for invasion and metastasis, which was shown in a study on metastatic mammary carcinoma cells [46]. In these cells, cofilin activation is coupled to cell polarization and stimulus induced induction of lamellipodia [59]. Mechanistically, cofilin creates barbed ends together with the Arp 2/3 complex at the leading edge of these cells, driving cell locomotion [47]. However, the significance and importance of barbed end initiation by cofilin in cells is discussed controversially [35,60], and there are also studies pointing out the importance of cofilin in cellular actin recycling and regulation of the G-actin level [61].

Cofilin overexpression could be a mechanism that leads to an increase in cofilin activity and drives cancer invasion. There are some reports on cofilin protein overexpression in cancer [62-64]. However, none of the studies cited above [62-64] has examined the cofilin regulatory pathways. It is therefore unclear if cofilin activity is indeed higher in the examined cancers and if one of the other above mentioned regulatory mechanisms is deregulated as well. Whereas at least some cofilin activity is crucial for invasion in mammary carcinoma cells [46], the studies examining LIMKs have found that an increase in cofilin phosphorylation, and therefore global inactivation, is accompanied by enhanced invasion [52].

There are also conceptual controversies if enhanced or diminished cofilin phosphorylation drives invasion. On the one hand, an increase in actin dynamics through an increase in active cofilin could speed up actin remodeling, and therefore enhance invasion [46]. On the other hand, inactivation of cofilin might lead to an increased build up of cellular force [65].

In glioma, only few studies have been conducted that address the question if higher or lower cofilin activity drives invasion, again yielding controversial results. A recent report links ROCK1 expression and activity and glioma invasion [66]. The ROCK-inhibitors fasudil and

Y-27632 have been shown to induce apoptosis and to decrease invasiveness of glioma cells *in vitro*, and to enhance survival of mice in a glioma xenograft model *in vivo* [67]. Others have shown that treatment of glioma cells with Y-27632 increases invasion in an *in vitro* transwell setup [68] and that a knockdown of cofilin leads to a reduction of motility *in vitro*, whereas overexpression of a constitutively active cofilin mutant GFP chimera enhances cell migration *in vitro* and invasiveness *in vivo* [69].

These differences could be partly explained by the fact that cofilin has a concentration dependent influence on cell motility, with highest motility occurring at intermediate expression levels [70]. Given that the expression differences measured are well correlated with overall cofilin activity in the experimental system used in this study, an intermediate level of cofilin activity would be optimal for cell migration. Therefore, activating cofilin in an experimental system where cofilin activity is low as well as inactivating cofilin in a system where cofilin activity is already high could both lead to an increase in motility.

There is only one study available on the regulation of the cofilin pathway in gliomas, which has reported evidence for an upregulation of cofilin with increasing grade of malignancy [69].

1.7 Cellular functions of chronophin (CIN/PDXP)

Chronophin (CIN/PDXP) belongs to the haloacid dehalogenase superfamily (HAD) of phosphatases. The catalytic core consists of a modified Rossmann fold [71], and it contains the typical catalytic motif DxDx(V/ T), with the catalytic aspartate residue in position 25 in the human enzyme.

It has been identified initially as pyridoxal phosphate phosphatase, as a phosphatase for activated vitamin B6 [72,73]. After that, CIN was identified as cofilin specific phosphatase [74].

Moreover, CIN was found in a screen for phosphatases that regulate NCOA3. NCOA3 is an important factor for the regulation of the transcriptional response to estrogen in the cell. Alterations in estrogen signaling are well known to be involved in breast cancer. CIN

knockdown leads to an enhanced transcriptional response after estrogen stimulation, including an increase in c-myc expression [75].

On the cellular level, CIN depletion in HeLa cells leads to an increase in p-cofilin and an increase of F-actin, which is most prominent in mitotic cells [74]. Other studies emphasize the importance of CIN at the leading edge, where it is functioning downstream of PAR2 [76] and has an influence on the number of cofilin induced barbed ends in neutrophils [60].

CIN is highly expressed in the brain on mRNA level as well as on protein level [74]. Here, however, expression in nearly all examined regions is very strong [77].

In rat brains, astrocytes and neurons are positive for CIN, but in human samples the staining is predominantly found in astrocytes and microglia [78]. In clinical samples of human glioma specimens and normal brain tissue, a staining of astrocytes and neurons could be detected with an extensively characterized antibody (Sondergeld, unpublished). As mentioned above, there are reports on CIN function in both neuronal cells and astrocytes. CIN has been implicated in astroglial apoptosis [79], and acts as an HSP90 interacting ATP sensor in neuronal cells [80].

Interestingly, CIN maps to a genomic locus that is lost in more than 40 % of primary GBMs, on which the affected tumor suppressor is unknown [81]. tween

1.8 C-myc in glioma

The transcription factor c-myc plays a role in cell proliferation, induction of apoptosis and tumorigenesis. Due to the fact that many c-myc target genes are involved in biosynthetic processes, an important and cell type independent function of c-myc is biomass accumulation [82].

On a mechanistic level, c-myc can act as a general transcriptional amplifier of already transcriptionally active genes in lymphocytes and embryonic stem cells [83,84]. However, c-myc mediated gene repression, e.g. for CDKN2B, is also important [85] and studies on c-myc promoter binding and transcriptional regulation have found a significant role for c-myc in gene repression in cancer cells [86]. The coactivator max is an obligate partner for c-myc, with which it forms a heterodimer. This heterodimer can bind canonical E-Boxes, which have the consensus-sequence CANNTG [87]. A heterodimer consisting of the constitutively expressed proteins max and MNT is thought to establish a basal transcriptional activity at

the promoters that are also recognized by the myc/max and MXD/max heterodimers (see Fig. 5). The MXD proteins can also form heterodimers with max and can replace c-myc, and are therefore considered as negative regulators of myc/max dependent transcription.

Max and the myc-family members c-myc, N-myc and L-myc are expressed in glioma, and expression correlates with malignancy grade [88]. Furthermore, a high percentage of glioma overexpresses at least one myc protein [89].

C-myc is essential for tumor propagating cell renewal in a genetic mouse glioma model [90], and can transform differentiated astrocytes [91]. Especially interesting is that MXI1, a MXD family member, has been described as tumor suppressor in glioma cells [92]. The MXI1 gene maps to a genomic locus that is lost in ~65 % of GBMs [3]. In addition, there is crosstalk between RhoA signaling and myc dependent transcription. Increasing c-myc expression reduces the RhoA induced actin structures in NIH3T3 fibroblasts [93]. There is also a link between myc expression and LIMK1 activity. On a mechanistic level, increased cofilin phosphorylation after LIMK1 overexpression leads to a decrease in STAT3- tyrosine phosphorylation and c-myc repression [94].

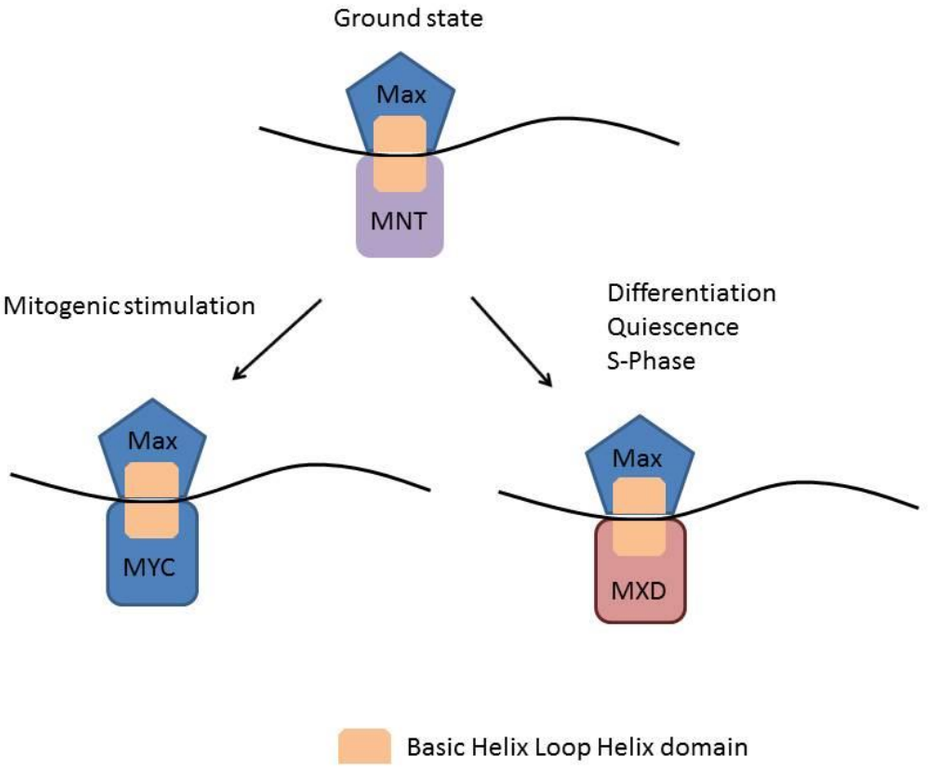

Figure 5: Transcriptional regulation of c-myc by MXD proteins.
MXD proteins like MXI1 are thought to be negative regulators of c-myc induced transcription by competing with c-myc for the obligate cofactor max, modified after [87].

2. Aims of the study:

Cofilin is a crucial regulator of actin cytoskeletal dynamics and upregulation of the kinases controlling cofilin phosphorylation has been linked to increased invasiveness in breast and prostate cancer.

Proteins controlling the phosphorylation of cofilin are deregulated in human astrocytic tumors. Whereas the LIMK2 that phosphorylates cofilin, is strongly upregulated, the cofilin phosphatase chronophin is downregulated.

In this work, we focused on the consequences of loss of chronophin expression in glioma cells, due to the fact that its role for cell migration and glioma progression has not been examined so far.

The aim of the study was therefore

-to characterize the motile behavior of glioma cells after chronophin deregulation in 2D migration assays

-to determine the changes in invasive behavior after chronophin deregulation in transwell invasion assays

-to analyze the effects of manipulating cofilin phosphorylation levels in invasion and migration assays with cofilin-phoshorylation mutants and/or ROCK-inhibitors

-to perform orthotopic implantation experiments to model cell growth and invasion *in vivo*

-to analyze the transcriptome of glioma cells after chronophin depletion in high throughput transcriptomic assays

Therefore, this study should contribute substantially to the understanding of chronophin´s role in glioma pathogenesis and to the understanding of the regulation of cofilin phosphorylation in gliomas. Further, the kinases upstream of cofilin might emerge as promising therapeutic targets for anti-invasive therapy in gliomas.

3. Materials

3.1 List of manufacturers and distributors

Number	Company
1	5 Prime GmbH, Gaithersburgh, MD, USA
2	Abcam, Cambridge, UK
3	Adolf Kuehne AG, Schindellegi, Switzerland
4	Agilent, Böblingen, Germany
5	Alpha Innotech, Santa Clara, CA, USA
6	American Type Culture Collection ATCC, Manassas, VA, USA
7	Applichem, Darmstadt, Germany
8	B. Braun, Melsungen, Germany
9	Chemicon, Temecula, CA, USA
10	BD Becton Dickinson GmbH, Heidelberg, Germany
11	BDK Luft- und Reinraumtechnik GmbH, Sonnenbühl, Germany
12	Beckman Coulter, Krefeld, Germany
13	Biochrom AG, Berlin, Germany
14	Biometra, Goettingen, Germany
15	Bio-Rad, Munich, Germany
16	Braun, Tuttlingen, Germany
17	Calbiochem, Darmstadt, Germany
18	Cell Signalling Technologies, Danvers, CO, USA
19	Clontech, Palo Alto, CA, USA
20	Cytoskeleton Inc., Denver, CO, USA
21	Dharmacon RNAi Technologies, Schwerte, Germany
22	Eppendorf, Hamburg, Germany
23	Fermenta, St. Leon-Roth, Germany
24	Fresenius Kabi Deutschland GmbH, Bad Homburg, Germany
25	Fujifilm, Tokyo, Japan
26	GE Healthcare, Munich, Germany
27	Greiner bio-one, Frickenhausen, Germany
28	Hartenstein, Würzburg, Germany
29	Heraeus, Hanau, Germany
30	Hettich, Tuttlingen, Germany
31	Ibidi, Martinsried, Germany
32	Idea Scientific, Minneapolis, MN, USA
33	Invitrogen, Karlsruhe, Germany
34	Leibniz institute DSMZ, German Collection of microorganisms and cell cultures
35	Leica microsystems, Wetzlar, Germany
36	Lonza, Cologne, Germany
37	Merck, Darmstadt, Germany
38	Millipore, Billerica, MA, USA
39	MWG Biotech, Ebersberg, Germany
40	Nalgene, Rochester, NY, USA
41	NEB, New England, USA

Number	Company
42	Nikon, Tokyo, Japan
43	Openbiosystems, Huntsville, AL, USA
44	PAN Biotech GmbH, Aidenbach, Germany
45	peqlab, Erlangen, Germany
46	Perkin Elmer, Waltham, MA, USA
47	Prior Scientific GmbH, Jena, Germany
48	Promega, Heidelberg, Germany
49	Qiagen, Hilden, Germany
50	R and D, Minneapolis, MN, USA
51	Roth, Karlsruhe, Germany
52	Sarstedt, Nuembrecht, Germany
53	Seton Scientific, Petaluma, CA, USA
54	Sigma Aldrich, Munich, Germany
55	Southern-Biotech, Birmingham, AL, USA
56	Starlab GmbH, Hamburg, Germany
57	Thermo-Fisher Scientific - Germany GmbH, Schwerte, Germany
58	Tocris Bioscience, Wiesbaden-Nordenstadt, Germany
59	Vector, Burlingame, CA, USA
60	Wako Chemicals GmbH, Neuss, Germany
61	DAKO, Hamburg, Germany
62	Okolab, Ottaviano, NA, Italy
63	Leitz, Grand Rapids, MI , USA

3.2 Chemicals

Chemical	Manufacturer
4-(2-hydroxyethyl)-1-piperazineethanesulfonic acid (HEPES)	7
4',6-diamidino-2-phenylindole (DAPI)	54
Acetic acid	36
Acrylamide 30 % / Bisacrylamide 0.8 %	51
Adenosine triphosphate (ATP)	54
Agarose	51
Ammonium persulfate (APS)	36
Ampicillin sodium salt	51
Aprotinin	54
Aqua ad injectibila	24
Bovine serum albumin fraction V	7
Bromophenol blue	54
Calcium chloride ($CaCl_{2)}$	7
Carbenicillin	54
Deoxyribonucleotide triphosphate (dNTP)	41
Di-sodium hydrogen phosphate dihydrate ($Na_2HPO_{4)}$	7
Ethanol 100 %	51
Ethanol 70 %	54
Ethanol Rotipuran p.a.	51
Ethidium bromide	54
Ethylenediaminetetraacetic acid (EDTA)	54
Ethylene glycol tetraacetic acid (EGTA)	54
Fluorescence mounting medium	55
Glucose	7
Glycerol anhydrous	7
Glycin	51
Hexadimethrine bromide	54
Hydrochloric acid	54
Hydrogen peroxide	51
Igepal	54
Isopropanol	54
Kanamycin sulfate	51
LB agar	7
LB medium	51
Leupeptin	54
Magnesium chloride ($MgCl_2$)	7
Manganese (II) chloride ($MnCl_2$)	7
Methanol	54
Mayer´s hemalaun	51
Sodium pyrophosphate	7

Chemical	Manufacturer
Sodium hydroxide (NaOH)	7
Nonfat dry milk powder	7
Nonylphenol ethoxylates (NP-40)	54
Normal goat serum	44
Orange G	51
Paraformaldehyde (PFA)	51
Peptone	7
Phenylmethanesulfonylfluoride (PMSF)	54
Phosphatase inhibitor cocktail 1	54
Phosphatase inhibitor cocktail 3	54
PhosTag	60
Piperazine-N,N'-bis(2-ethanesulfonic acid) (PIPES)	7
Potassium acetate	7
Potassium chloride (KCl)	36
Potassium dihydrogen phosphate (KH_2PO_4)	36
RNAse free water	51
RNAse A	54
RNAse-exitus plus™	28
Roti-Histol	7
siRNA resuspension buffer	21
Sodium azide (NaN_3)	36
Sodium chloride (NaCl)	51
Sodium dodecyl sulfate (SDS)	51
ß-Glycerophosphate	36
ß-Mercaptoethanol	54
SYBR Green	36
Tetramethylethylenediamine (TEMED)	51
Tris base	51
Tris-HCl	7
Triton X-100	36
Tween 20	54
Urea	7
Yeast extract	7

3.3 Primers

Custom Primers	39

3.4 DNA and Protein ladders

100 bp DNA Ladder Plus	41
1 kb DNA Ladder	41
Precision Plus Protein™ Standards Dual Color	15

3.5 Plasmids

pCDNA3	33
peGFPN1	19
pIRESNeo2	19
hCIN//pCMVSport6	43
hCFL1//pCMVSport6	43
SHC 002	54
TCN0000050046	54

3.6 Immunocytochemistry reagents

Chronophin antibody, rabbit, monoclonal	18
Alexa Fluor 546 Phalloidin	33
Alexa Flour 488 conjugated goat anti-rabbit, highly cross absorbed	33
Vinculin antibody, mouse, monoclonal	54

3.7 Immunohistochemistry reagents

Biotynilated goat anti-rabbit HRP conjugate	59
ABC complex	59
DAB substrate	59
Cytochrom C-Oxidase IV antibody, rabbit, monoclonal	18
Tissue-Tek® O.C.T. compound	28
Mounting medium	57

3.8 Antibodies for immunoblotting

Target	Manufacturer	Dilution	Source
GAPDH	18	1:1000	rabbit, monoclonal, clone 14C10
ß-Actin	38	1:10000	mouse, monoclonal, clone MAB1501
α-Tubulin	54	1:10000	mouse, monoclonal, clone DM1A
Chronophin	18	1:1000	rabbit, monoclonal, clone C85E3
Rac 1/2/3	18	1:1000	rabbit, polyclonal, clone
RhoA	18	1:1000	rabbit, monoclonal, clone 67B9
P-Ser3-Cofilin	18	1:1000	rabbit, monoclonal, clone 77G2
Cofilin-1	18	1:1000	rabbit, polyclonal
MMP9	8	1:1000	rabbit, polyclonal
MMP14	2	1:1000	rabbit, polyclonal
MMP2	8	1:1000	mouse, monoclonal, clone VB3
uPA	54	1:1000	mouse, monoclonal, clone 3B8
uPAR	50	1:500	mouse, monoclonal, clone 62022
GFP	33	1:1000	rabbit, polyclonal
c-myc	18	1:1000	rabbit, monoclonal
secondary anti-rabbit HRP conjugated	57	1:10000	goat, polyclonal
secondary anti-mouse HRP conjugated	57	1:10000	goat, polyclonal

3.9 Bacterial strains and cell lines

DBTRG-05-MG	34
U87	6
GBM6840	Dr. S.S. Tony To, Departement of Health Technology and Informatics, The Hong Kong Polytechnic University, Hongkong, China
E. Coli DH5α	33

3.10 Tissue culture reagents

Dulbecco´s phosphate buffered saline	44
Dulbecco´s modified Eagle´s medium w/o phenolred 4.5 g/l glucose	44
Dulbecco´s modified Eagle´s medium 4.5 g/l glucose	44
HAM´s F10 4.5 g/l glucose	44
Fetal calf serum	13
L-glutamine	44
Penicillin / streptomycin	44
Geneticindisulfate (G418)	51
Lipofectamine 2000	33
Opti-MEM	33
Puromycin	17
Trypsin / EDTA	44
Dimethyl sulfoxide	7
Latrunculin A	54
Oleoyl-L-α-lysophosphatidic acid sodium salt (LPA)	54
Bradykinin	54
Epidermal growth factor, human (EGF)	54
Platelet-derived growth factor BB, human (PDGFBB)	54
Y-27632	54
Fasudil	58
Fibronectin, human	17
Collagen I, rat tail	54
Collagen IV, human	54
Vitronectin, human	54
Poly-L-lysine	54
Soybean trypsin inhibitor	54

3.11 Tissue culture materials

Bovine serum albumin	7
Calcein AM	33
Cell culture flasks 75 cm^2	57
Cellulose acetate filter 0.45 µm FiltropurS 0.45	52
Cryo 1°C freezing container	40
Falcon tube 15 ml	10
Falcon tube 50 ml	10
Hoechst 33342	33
Kryo vials	40
Matrigel coated 24-well plate inserts, pore size 8 µm	10
Plastic pipettes 5 ml, 10 ml, 25 ml, 50 ml	27
Polystyrene round-bottom tube 5 ml	10
Sterile filter 0.2 µm FiltropurS 0.2	52
Surgical disposable scalpel	8
Tissue culture dishes Ø 15, 30 and 100 mm	57
White 96-well plate with lid	46

3.12 Other materials

Cell scraper	28
Cotton swabs	28
Cover slips	51
Glass slides	28
Glass slides superfrost	28
Hard Shell® 384-well PCR plates	15
Hematocytometer	28
Hydrophobic barrier pen	61
Hybond C nitrocellulose membrane	26
Omnifix®-F syringes and needles	8
Open top tubes thickwall polyallomer	53
PCR Sealers™ Microseal® ´B´ film	15
PCR tubes, 0.2 ml	28
Pipette tips 10, 200 and 1000 µl	22
Reaction tubes 0.5, 1.5 and 2.0 ml	22
Reaction tubes 1.5 ml, Biopur®	22
Whatman paper	28

3.13 Enzymes and reaction buffers

DNA-Polymerases	
Dream Taq DNA polymerase	23
Hot Taq DNA polymerase	1
Platinum Pfx polymerase	33
10 x Hot Taq buffer	1
10 x Dream Taq buffer	23
10 x Pfx buffer	33
$MgSO_4$	33
Restriction Enzymes	
BamHI	41
EcoRI	41
XhoI	41
EcoRV	41
NotI	41
StuI	41
DPNI	41
Ligases	
T4 DNA Ligase	41

3.14 Kits

Cignal Finder™10-Pathway Reporter Array Cancer	49
Cignal™ Reporter Assay c-myc	49
Cignal™ Reporter Assay SRE	49
Dual-Glo® Luciferase Assay System	48
G-LISA Rac1,2,3 Activation Assay Biochem Kit (colorimetric format)	20
G-LISA RhoA Activation Assay Biochem Kit (colorimetric format)	20
pGEM®-T Easy Vector System	48
Plasmid plus Midi Kit	49
QIAquick Gel Extraction Kit	49
RevertAid™ H Minus First Strand cDNA Synthesis Kit	23
SuperSignal® West Pico Chemiluminescent Substrate	49
SV Total RNA Isolation System	48

3.15 Solutions and buffers

3.15.1 Bacterial culture

SOC medium

In dH_2O

Peptone		20.0 g
Yeast extract		5.0 g
NaCl		0.5 g
KCl	(0.25 M)	10.0 ml
$MgCl_2$	(2 M)	5.0 ml
Glucose	(1 M)	20.0 ml

Adjust pH = 7.0, add dH_2O to 1 L, autoclave

LB medium

In dH_2O

25 g LB medium powder per 1 L dH_2O, autoclave

LB agar

In dH_2O

40 g LB agar powder per 1 L dH_2O, autoclave

Kanamycin stock solution

50 mg/ml in dH_2O

Ampicillin stock solution

50 mg/ml in dH_2O

Carbenicillin stock solution

50 mg/ml in 50 % ethanol

3.15.2 Mini-Plasmid preparation

S1-solution

in dH_2O	
EDTA (pH = 8.0)	10 mM
RNAse A	100 µg/ml
Tris-HCl (pH = 8.0)	50 mM

S2-solution

in dH_2O	
NaOH	200 mM
SDS	1 % (w/v)

S3-solution (pH = 5.2)

in dH_2O	
Potassium acetate	3 M
Acetic acid	pH adjustment

3.15.3 SDS-PAGE

10 x Running buffer SDS gels

in dH_2O	
Tris base	150 mM
Glycine	2 M
SDS	1 % (w/v)

4 x Stacking gel buffer

in dH_2O	
Tris base	0.5 M
Adjust pH = 6.8	
SDS	0.4 % (w/v)

4 x Running gel buffer

in dH_2O	
Tris base	1.5 M
Adjust pH = 8.8	
SDS	0.4 % (w/v)

4 x Laemmli buffer (lysis buffer)

Bromophenol blue	2.0 mg
ß-Mercaptoethanol	1.6 ml
SDS	3.2 g
Glycerol	16.0 ml
Tris-HCl pH 6.8	20.0 ml

Phostag lysis buffer

Aprotinin	5.0 µg/ml
Glycerol	10.0 % (v/v)
Igepal	1.0 % (v/v)
Leupeptin	1.0 µg/ml
Sodium pyrophosphate	1.5 mM
Phosphatase inhibitor cocktail 1	1:1000
Phosphatase inhibitor cocktail 3	1:1000
PMSF	1.0 mM
ß-Glycerophosphate	1.0 mM
Tris-HCl (pH = 8.0)	20.0 mM

Phostag solution D

in dH_2O containing 3 % methanol (v/v)	
Phostag	5 mM

Phostag solution E

in dH_2O	
$MnCl_2$	10 mM

3.15.4 Immunoblotting

Blotto buffer

In dH_2O	
Nonfat dry milk	5.0 % (w/v)
Tris-HCl, pH=8.0	50.0 mM
NaCl	80.0 mM
$CaCl_2$	2.0 mM
NP-40	0.2 % (v/v)

Antibody dilution buffer

In dH_2O	
BSA	1.0 % (w/v)
HEPES	10.0 mM
NaCl	0.5 M
NaN_3	0.02 % (w/v)
Tween 20	0.2 % (v/v)

Towbin buffer

In dH_2O	
Tris base	3.0 g
Glycine	14.4 g
dH_2O	800 ml
Methanol	200 ml

Anode 1 buffer, for low molecular weight proteins

In dH_2O	
Tris base	0.3 M
Methanol	40.0 % (v/v)

Anode 2 buffer, for low molecular weight proteins

In dH_2O

Tris base	25.0 mM
Methanol	40.0 % (v/v)

Cathode buffer, for low molecular weight proteins

In dH_2O

Tris base	25.0 mM
Glycine	40.0 mM
Methanol	10.0 % (v/v)

Anode 1 buffer, for high molecular weight proteins

In dH_2O

Tris base	0.3 M
Methanol	20.0 % (v/v)

Anode 2 buffer, for high molecular weight proteins

In dH_2O

Tris base	25.0 mM
Methanol	20.0 % (v/v)

Cathode buffer, for high molecular weight proteins

In dH_2O

Tris base	25 mM
Glycine	40 mM
Methanol	10 % (v/v)
SDS	0.005 % (w/v)

3.15.5 Immunocytochemistry and immunohistochemistry

1 x PBS

In dH_2O

KCl	0.2 g
KH_2PO_4	0.2 g
Na_2HPO_4	1.15 g
NaCl	8.0 g

Adjust pH = 7.4, add dH_2O to 1 L.

10 x TBS

In dH_2O

Tris-HCl	24.0 g
Tris base	5.6 g
NaCl	88.0 g

Adjust pH to 7.6, add dH_2O to 1 L.

Paraformaldehyde for ICC

In 1 x PBS

Paraformaldehyde	4 % (w/v)

Adjust pH to 7.2

ICC blocking buffer

In 1 x PBS

Normal goat serum	10.0 % (v/v)
Saponin	0.3 % (w/v)

ICC antibody dilution buffer

In 1 x PBS

Normal goat serum	1.0 % (v/v)
Saponin	0.3 % (w/v)

IHC blocking buffer

In 1 x PBS

Normal goat serum	10.0 % (v/v)
Triton X-100	0.3 % (v/v)

IHC antibody dilution buffer

In 1 x PBS

Normal goat serum	1.0 % (v/v)
Triton X-100	0.3 % (v/v)

3.15.6 Agarose gel electrophoresis

10 x TAE-buffer

In dH_2O

Tris base	242.0 g
Acetic acid	57.1 ml
EDTA 0.5 M, pH=8.0	100.0 ml

Adjust volume to 5L

5 x Orange G loading dye

In dH_2O

EDTA	10 µM
Glycerol	65 % (v/v)
Orange G	0.2 % (w/v)
Tris base	50 µM

3.15.7 Actin spin down assay

Spin down buffer 1

PIPES, pH=6.9	50.0 mM
NaCl	50.0 mM
EGTA	5.0 mM
Glycerol	5.0 %
$MgCl_2$	5.0 mM
Igepal	0.1% (v/v)
Triton X-100	0.1% (v/v)
Tween 20	0.1% (v/v)
ß-Mercaptoethanol	0.1% (v/v)

Spin down buffer 2

In spin down buffer 1

ATP	1 mM
Aprotinin	5 µg/ml
Leupeptin	1 µg/ml
PMSF	1 mM

3.15.8 Cell culture

Puromycin

10 mg/ml in cell culture grade dH_2O

Hexadimethrine bromide

8 mg/ml in cell culture grade dH_2O

Complete medium GBM6840

In DMEM 4.5 g/l glucose

Fetal calf serum	10 % (v/v)
L-glutamine	2 mM
Penicillin	100 U/ml
Streptomycin	100 µg/ml
(Puromycin	1.0 µg/ml, for transduced cells only)

Complete medium U87

In DMEM 4.5 g/l glucose

Fetal calf serum	10 % (v/v)
L-glutamine	2 mM
Penicillin	100 U/ml
Streptomycin	100 µg/ml

Complete medium DBTRG-05-MG

In HAM´s F10 4.5 g/l glucose

Fetal calf serum	10 % (v/v)
L-glutamine	2 mM
Penicillin	100 U/ml
Streptomycin	100 µg/ml
(Puromycin	0.5 µg/ml, for transduced cells only)

Starving medium:

Medium w/o FCS

Starving medium + BSA

Medium w/o FCS + 0.1 % BSA (w/v)

Freezing medium

In complete medium

FCS	20 % (v/v)
DMSO	10 % (v/v)

3.16 List of devices used

Device		Application
Leica SP5 microscope	35	Confocal microscopy
Leica DM 4000 B	35	Microscopy for histology
NikonT_i eclipse	42	Epifluorescence microscopy/live imaging
Prior Stage Pro Scan	47	Epifluorescence microscopy/live imaging
FACS Calibur™	9	Flow cytometry
Envision 2104 multilabel reader	46	Fluorescence/luminescence measurements
BDK S-1200	11	S1 cell culture
BDK SK-1500	11	S2 cell culture
LAS-1000	25	Western blot
Fluor Chem Q imaging system	4	Western blot, DNA gel visualization
Incubator BD6220	57	Cell culture
BD6220	29	Bacterial culture
Shaker ISF-1-V	3	Bacterial culture
C1000™ thermal cycler	15	Polymerase chain reaction
CFX384™ real time system	15	Real-time PCR
Trans Blot® semi-dry transfer cell	15	Semi-dry western blot
GENIE® blotter	32	Wet-tank blotting
DNA gel electrophoresis system	15	DNA gel electrophoresis
Lumen 200 Pro	47	Epifluorescence microscopy/live imaging
Mini-Protean SDS gel electrophoresis	15	SDS gel electrophoresis
NanoDrop 2000c spectrophotometer	45	RNA and DNA measurement
Hera Cell 240	29	S2 incubator
Centrifuge 5702 R	22	S2 centrifuge
TFX-35 M	14	Cloning
Hettich Universal 16 R	30	DNA preparation
Hettich Universal 16 R	30	S1 cell culture
Cryostat CM 3050S	35	Cryo sections
Ultracentrifuge Optima™ TLX	12	Spin down assay
Cell culture microscope	63	Cell counting
Temperature and CO_2 controlled humidified microscope stage	62	Live cell imaging

4. Experimental procedures

4.1 RNA specific methods

4.1.1 Isolation of total RNA

Total RNA was isolated from GBM6840 cells with the SV Total RNA Isolation System Kit from (48). Isolation of total RNA is necessary for gene expression analysis of mRNAs by microarray and PCR based technologies. All steps were performed with special RNAse free materials and all pipettes and equipment were cleaned with 70 % ethanol and RNAse-Exitus plus before performing the experiment.

Cells were grown in Ø 10 cm cell culture dishes, and 600,000 cells were seeded per dish 48 h before harvest in complete DMEM. Then, the supernatant was aspirated and cells were washed with ice cold PBS. The cells were lysed immediately in 175 µl prechilled RNA-lysis buffer on ice, and collected with a cell scraper. Then, the lysate was passed three times through a 20 gauge and three times through a 25 gauge needle with a syringe to shear genomic DNA, and the lysate was then transferred in a 1.5 ml tube. Then, 350 µl RNA dilution buffer were added and the solution was mixed by inverting the tube three times. The solution was heated at 70 °C for 3´ to denature RNA secondary structures. Afterwards, the solution was centrifuged at 18,000 x *g* for 10´ and the supernatant was transferred into a fresh 1.5 ml tube. 200 µl 95 % ethanol were added and the solution was mixed by pipetting. Then the solution was pipetted into the spin basket assembly provided in the kit, and centrifuged for 1´ at 18,000 x *g* to bind the RNA to the column. The column was washed with 600 µl RNA wash buffer, and centrifuged for 1´ at 18,000 x *g*. Then, the DNAse-mix was added that digests the genomic DNA in the sample.

The following DNase-mix was prepared per column:

Yellow core buffer:	40.0 µl
$MnCl_2$ 0.09 M	5.0 µl
DNase I	5.0 µl
	50.0 µl

The 50.0 µl DNAse-mix were applied to the column, and incubated for 15´ at RT.
Then, 200 µl DNAse stop solution were added, and the columns were centrifuged for 1´ at 18,000 x *g*. After that, the column was washed as before with 600 µl and 250 µl RNA wash buffer again. Then, the RNA was eluted from the column with 100 µl RNAse free water and the liquid was collected by centrifugation for 1´ at 18,000 x *g*. The RNA was immediately frozen in liquid nitrogen, and stored at -80°C.

4.1.2 Labeling and microarray

Total RNA was measured with an Experion Bio-analyzer system to assure quality of the RNA, hybridization to Agilent microarrays was performed by Dr. Michael Krause (Institut für Molekularbiologie und Tumorforschung, Marburg) and analysis of the raw data was performed by Lukas Rycak at the Microarray Core facility at the University of Marburg.
The platform used was a Human GE 4 x 44k Microarray Kit (Agilent G4845A), labeling and hybridization were performed with the Quick-Amp Labeling Kit (2 color) (Agilent 5190-0444) The microarray scanner and software used were the Agilent Microarray Scanner G2505C and Feature Extraction v10.5.1.1 (4).

4.1.3 cDNA synthesis

cDNA synthesis is needed for converting the RNA template as generated in 4.1.1 into a DNA template suitable for PCR applications. All steps were performed with special RNAse free materials and all pipettes and equipment were cleaned with 70 % ethanol and RNAse-Exitus plus before performing the experiment.

The cDNA synthesis was performed with the RevertAid H Minus First Strand cDNA Synthesis Kit from (23).

From each RNA sample

500 ng Total-RNA	x µl
Random hexamer primer	1.0 µl
dH_2O, RNAse free	add 11.0 µl
Total volume	11.0 µl

were gently mixed and centrifuged briefly. Then, the samples were incubated at 65° C for 5´ to denature RNA secondary structures and then the tubes were chilled on ice.

For every sample

5 x Reaction buffer	4.0 µl
RiboBlock RNAse inhibitor (20U/µl)	1.0 µl
10 mM dNTPs	2.0 µl
Reverse Transcriptase	2.0 µl
Total volume	20.0 µl

were added, gently mixed and centrifuged briefly.

The samples were then incubated for 5´ at RT and incubated for 1 h at 42°C to synthesize the cDNA. Afterwards, the samples were incubated at 70°C for 5´ to stop the reaction and subsequently the cDNA was stored at -20°C.

4.2 DNA specific methods

4.2.1 Transformation of competent *E. coli*

Chemically competent *E. coli* DH5α were thawn for 10´ on ice, and then the DNA to be transformed, 500 ng plasmid DNA or 8.0 µl from a ligation reaction, was added to 200 µl bacteria solution. The cells were incubated with the DNA for 45´ on ice, and then a heat shock was performed for 45´´ at 42°C in a water bath. Then, the bacteria were again incubated for 5´ on ice, and afterwards 600 µl RT SOC medium were added. The cells were allowed to grow for 1.5 h at 700 rpm and 37°C, to allow for the expression of the plasmid encoded resistance gene. Then, the bacteria were collected by centrifugation for 5´ at 1,844 x *g*. The supernatant was discarded, the pellet was resuspended in the back flow of medium left, and plated on LB agar plates containing the selection antibiotics kanamycin or ampicillin.

4.2.2 Gateway cloning

First, a PCR product was generated as described in 4.2.3 in a total volume of 150 µl PCR reaction. It was purified as described in 4.2.5. Then, A-overhangs were added to the blunt end PCR product by a standard Taq-polymerase. Per PCR-product

Purified PCR product	44.0 µl
Taq	0.5 µl
10 x Taq- buffer	5.0 µl
10 mM dNTPs	0.5 µl
Total volume	50.0 µl

were mixed in a PCR tube, and incubated for 20´ at 72°C in a thermocycler. Then, the PCR-product was run on a 1 % agarose gel, excised from it and purified with the QIAquick gel extraction kit as described in 4.2.5. Afterwards, the ligation reaction was performed at 4°C O/N.

Per reaction

T4 DNA Ligase	1.0 µl
2 x Rapid ligation buffer	5.0 µl
PCR product	3.0 µl
pGEMT Easy vector	1.0 µl
Total volume	10.0 µl

were mixed in a 0.5 ml reaction tube. The ligated DNA was transformed as described in 4.2.1.

4.2.3 Cloning-PCR

Amplification of specific DNA sequences by polymerase chain reaction is needed for cloning reactions. To ensure the sequence integrity of the amplified fragments, a proof reading DNA polymerase, Platinum Pfx, from (33) was used for this application. Primers used and annealing temperatures (T_A) are listed in table 1.

Per reaction

10 x Pfx buffer	2.5 µl
Pfx-polymerase	0.5 µl
$MgSO_4$	0.5 µl
dNTPs	0.5 µl
Enhancer	2.5 µl
Primer mix (10 µM each)	2.5 µl
Template	1.0 µl (25 ng Plasmid DNA)
dH_2O	add 25.0 µl
Total volume	25.0 µl

were mixed.

Table 1: Primers used for cloning PCR reactions.

Target	Forward	Cutting site	T_A	Elongation time
hCFL1	ATATACTCGAGGCCACCATGGCCTCCGGTGTGGCTGTCT	XhoI	56°C	2´
hCFL1	Reverse	BamHI		
	ATATAGGATCCCCTCCCAAAGGCTTGCCCTCCAGGGAG			

The reactions were cycled in a thermocycler under the following conditions:

Denaturation	95°C	5´	
Denaturation	95°C	1´	35 x
Annealing	T_A	1´	
Elongation	68°C	x	
Final	68°C	10´	
Hold	12°C		

4.2.4 Preparation of agarose gels for DNA electrophoresis

1 % w/v agarose was mixed with 150 ml 1 x TAE buffer, and heated until boiling in a microwave. Then, the solution was cooked three times for 10´´, and subsequently cooled down to 60°C. Then, the solution was poured into a gel casting frame.

4.2.5 Purification of DNA from agarose gels and PCR reactions

PCR products or digested DNA fragments were generated as described in 4.2.3 or 4.2.6 and the DNA was extracted from agarose gels with the QIAquick Gel extraction Kit. The DNA was mixed with Orange G loading dye and run on 1 % agarose gels at constant voltage (85 V) for 50´. Then, the gels were stained in ethidium bromide and the bands at the expected length

were cut out. Then, the gel slices were weighed, and three volumes of buffer QG were added. The gel slice was dissolved for 10´ at 50°C and mixed vigorously several times during the incubation time. For PCR products that were purified without separation on a gel, five volumes of buffer QG were added to the PCR reaction directly.

Then, one volume of isopropanol was added to the solution. Afterwards, the solution was applied to a spin column that was provided in the kit, and centrifuged at 14,000 x *g* for 1´. The column was washed with 750 µl buffer PE, and the flow through was discarded. Then, the column was dried by centrifugation at 14,000 x *g* for 1´. Afterwards, the DNA was eluted with 50 µl dH_2O.

4.2.6 Restriction digestion and cloning

hCIN//pCMVSport6 and pCDNA3 were digested with EcoRI and XhoI.

For this reaction

Plasmid DNA	4.0 µl = 4.0 µg
BSA 100 x	0.5 µl
EcoRI-buffer	5.0 µl
dH_2O	38.5 µl
EcoRI	1.0 µl
XhoI	1.0 µl
Total volume	50.0 µl

were mixed and the reaction mixtures were incubated 4 h at 37°C.

hCIN//pCMVSport6 and pIRESNeo2 were digested with EcoRV and NotI.

For this reaction

Plasmid DNA	4.0 µl = 4.0 µg
BSA 100 x	0.5 µl
Buffer 3	5.0 µl
dH_2O	38.5 µl
EcoRV	1.0 µl
NotI	1.0 µl
Total volume	50.0 µl

were mixed and the reactions were incubated 4 h at 37°C.

hCFL1//pGEMTeasy and pEGFP-N1 were digested with BamHI and XhoI.

For this reaction

pEGFP-N1/CFL1//pGEMTeasy	6.0 µg (= 6.0 µl/10 µl)
BamHI	1.0 µl
XhoI	1.0 µl
Buffer 3	5.0 µl
dH_2O	37.0 / 33.0 µl
Total volume	50.0 µl

were mixed and the reactions were incubated 4 h at 37°C.

4.2.7 Ligation

For each ligation reaction

Ligation buffer	2.0 µl
Insert DNA	5.0 µl
Plasmid DNA	1.0 µl
T4 DNA Ligase	1.0 µl
dH_2O	11.0 µl
Total volume	20.0 µl

were mixed and incubated in a thermocycler for 48 h at 16°C. Afterwards, the DNA was transformed as described in 4.2.1.

4.2.8 Preparation of agar plates

Autoclaved LB agar was heated until cooking in a microwave and subsequently cooled down to 50°C. Then, ampicillin or kanamycin stock solution was diluted 1:1000 in the agar solution and the agar containing antibiotics was poured into petri dishes.

4.2.9 Plasmid isolation from *E. coli*, Mini-Prep format

The Mini-Prep is suitable for isolation of DNA for cloning and sequencing applications. A single colony of *E. Coli* DH5α was grown in 5 ml LB-medium O/N at 37°C and 180 rpm. Then, 2 ml of the solution were centrifuged for 5´ at 1,844 x *g*. The supernatant was discarded, and the pellet was resuspended in 300 µl prechilled buffer S1. Then, 300 µl buffer S2 were added, the solution was mixed by inverting eight times, and the bacteria were lysed for 5´ at RT. Then, 300 µl S3 were added, the solution was mixed by inverting eight times, and incubated for 30´ on ice. Afterwards, the solution was centrifuged for 10´ at 18,407 x *g*, and the pellet was discarded. DNA was precipitated from the supernatant with 700 µl

isopropanol, and was collected by centrifugation for 20´ at 18,407 x *g* and 4°C. The pellet was washed in 500 µl 70 % ethanol, centrifuged for 10´ at 18,407 x *g* and dissolved in 50 µl dH_2O.

4.2.10 Plasmid isolation from *E. coli*, Midi-prep format

The DNA Midi-prep is used for generation of large amounts of plasmid DNA suitable for cell culture applications. It was performed with the Plasmid Plus Midi Kit from (49). *E. coli* DH5α transformed as described in 4.2.1 were grown in 50 ml LB medium O/N at 37°C at 180 rpm. Then, the cells were collected by centrifugation for 15´ at 4°C and 2,325 x *g*. Afterwards, the supernatant was discarded and the pellet resuspended in 4 ml buffer P1. Then 4 ml buffer P2 were added, and the solution was incubated at RT for 5´. Then, 4 ml buffer P3 were added, and the solution was incubated on ice for 15´. The solution was centrifuged again for 30´ at 4°C and 2,325 x *g* and the pellet was discarded. The supernatant was recentrifuged for 15´ at 4°C and 2,325 x *g*. Then, a QIAGEN Tip 100 was equilibrated with 5 ml buffer QBT. The supernatant was applied to the column, and the column was allowed to empty by gravity flow. Afterwards, the column was washed three times with 10 ml buffer QC. The DNA was eluted with 5 ml buffer QF, and precipitated with 3.5 ml isopropanol. The DNA was collected by centrifugation at 2,325 x *g* for 30´ and 4°C. Then, the pellet was washed in 70 % ethanol and dried. Finally, the DNA was dissolved in 100 µl cell culture grade dH_2O and the concentration was determined with the NanoDrop 2000c spectrophotometer.

4.2.11 Site directed mutagenesis

To study the impact of amino acid exchanges mimicking a non-phosphorylatable cofilin (S3A), a phosphorylated cofilin (S3E), or for creation of a chronophin construct lacking the shRNA target site (named hereafter ΔshRNA), the sequences of the plasmids that were cloned as described in 4.2.6 and 4.2.7 had to be mutated. The approach used was PCR based, and the mutations to be inserted were included in the synthesized primer pairs that were used for a PCR with the non-mutated construct as a template.

The PCR-setup was as described in 4.2.3, the primers used are given in table 2. For hCIN, two overlapping PCR products had to be generated, which are named hCINΔshRNA left and hCINΔshRNA right hereafter.

Table 2: Primers used for mutagenesis PCRs.

Construct	**Primer**	**Sequence**
CFL1-S3A	forward primer	GCCACCATGGCCGCCGGTGTGGCTG
CFL1-S3E	forward primer	GAGGCCACCATGGCCGAGGGTGTGGCTGTCTCT
hCINΔshRNA left	forward primer	AGCTCGGATCGATATCGTCGA
hCINΔshRNA right	forward primer	GCCCCTACATGTTTGAATGTATCACGGAGAACTTCAGC
CFL1-S3A	reverse primer	CGGTGGTACCGGCGGCCACACCGAC
CFL1-S3E	reverse primer	CTCCGGTGGTACCGGCTCCCACACCGACAGAGA
hCINΔshRNA left	reverse primer	GCTGAAGTTCTCCGTGATACATTCAAACATGTAGGGGC
hCINΔshRNA right	reverse primer	AATCCATAGGGGACCAGCTT

4.2.11.1 Mutagenesis of hCIN//pIRESNeo2 to hCINΔshRNA//pIRESNeo2

For hCIN, a mutagenesis and cloning protocol was performed with the primer pairs given in table 2. The PCR reactions were mixed according to the protocol in 4.2.3.

First, two PCR-products were created, that contained 3 silent mutations in the shRNA target site and a sequence overlap. Counted from the translational start site, in position 657 a cytosine was exchanged to thymine, in position 660 a guanine was exchanged to adenine and in position 663 a cytosine was exchanged to thymine (see Fig. 6).

```
Mutated Sequence  GCCCCTACATGTTTGAATGTATCACGGAGAACTTCAGC
                  |||||||||||||  ||  ||  ||||||||||||||||||
PDXP human 644    GCCCCTACATGTTCGAGTGCATCACGGAGAACTTCAGC    681
```

Figure 6: Alignment of human CIN and the mutated primer sequence.

The hCINΔshRNA left product was 760 bp, and the hCINΔshRNA right product was 476 bp long. Then a fill up PCR was performed with the overlapping fragments, to create one insert of 1220 bp suitable for cloning into the hCIN//pIRESNeo2 construct. In the fill up PCR, both products were combined to create a single long product. Then, purification, digestion and ligation of the product were performed as described in 4.2.5, 4.2.6 and 4.2.7, respectively. The restriction sites used were EcoRV and StuI.

Cycling conditions hCINΔshRNA left PCR product:

Denaturation	95°C	5´	
Denaturation	95°C	1´	35 x
Annealing	57°C	1´	
Elongation	68°C	2´30´´	
Final	68°C	7´	
Hold	12°C		

Cycling conditions hCINΔshRNA right PCR product:

Denaturation	95°C	5´	
Denaturation	95°C	1´	35 x
Annealing	57°C	30´´	
Elongation	68°C	1´	
Final	68°C	7´	
Hold	12°C		

Cycling conditions fill up PCR:

Denaturation	95°C	5´	
Denaturation	95°C	1´	12 x
Elongation	68°C	2´30´´	
Final	68°C	10´	
Hold	12°C		

4.2.11.2 CFL1-S3A-GFP and CFL1-S3E-GFP

For the CFL1-S3A and CFL1-S3E mutants, a standard PCR reaction of the CFL1//pEGFP-N1 construct was performed.

Per reaction

10 x Pfx buffer	5.0 µl
Pfx-polymerase	1.0 µl
$MgSO_4$	1.0 µl
dNTPs	1.0 µl
Enhancer	5.0 µl
Primer mix (10 µM each)	1.25 µl
Template	1.0 µl (25 ng – 500 ng plasmid DNA)
dH_2O	add 50.0 µl
Total volume	50.0 µl

were mixed and the reactions were cycled in a C1000 thermal cycler under the following conditions:

Denaturation	95°C	5´	
Denaturation	95°C	1´	18 x
Annealing	55°C	1´	
Elongation	68°C	10´	
Final	68°C	7´	
Hold	12°C		

Afterwards, 1 µl DPNI was added to digest methylated parental plasmids, and the reaction was incubated for 3 h at 37°C. Then, another 0.5 µl DPNI were added, and the reaction was again incubated for 2 h at 37°C. Then, the DNA was transformed as described in 4.2.1.

4.2.12 Semiquantitative PCR

The semiquantitative PCR is used to measure relative transcript abundances in different biological samples. 1:5 diluted cDNA as prepared in 4.1.3 was used as a template for this reaction. Annealing temperatures (T_A) and primer sequences for all templates are shown in table 3. For target amplification, the DreamTaq DNA-polymerase from (23) was used.

Table 3: Primer sequences and conditions for semiquantitative PCR.

Target	Forward Primer	Reverse Primer	Length in bp	T_A	Cycles
GAPDH	CCCTTCATTGACCTCAACTA	CCAAAGTTGTCATGGATGAC	401	57.0	25
CIN	TGCAACCCCCTCCCAGCAGT	TCCACTCGGGCTCCAGGACG	397	59.0	28
CFL1	ATGCCCTCTATGATGCAACC	GCTTGATCCCTGTCAGCTTC	152	54.3	25
CFL2	TGGTTATATGCCTCCCTTGC	GCCTCACAGAACTGCAATCA	177	54.3	25
ADF	CGTAAATGCTCCACACCAGA	AGCATTCCCACAAAATGCTT	164	54.3	25
MMP2	CACTTTCCTGGGCAACAAAT	CTGAGCGATGCCATCAAATA	382	58.0	30
MMP9	CACTGTCCACCCCTCAGAGC	GCCACTTGTCGGCGATAAGG	263	58.0	33
MMP14	CATTGGAGGAGACACCCACT	GGTGTCAAAGTTCCCGTCAC	352	58.0	32
uPAR	CATGCAGTGTAAGACCAACGGGGA	AATAGGTGACAGCCCGGCCAGAGT	254	58.5	33
uPA	TGAGGTGGAAAACCTCATCC	GCAGCACACAGCATTTTGGTG	321	58.5	30
CathepsinB	AGAATGGCACACCCTACTGG	AACCACAGGCTGGGATGTAG	333	59.0	30
c-myc	CCTACCCTCTCAACGACAGC	CTCTGACCTTTTGCCAGGAG	228	59.0	30
c-JUN	CCCCAAGATCCTGAAACAGA	CCGTTGCTGGACTGGATTAT	168	54.3	25
STAT3	CAGTCAGTGACCAGGCAGAA	GCTGCAACTCCTCCAGTTTC	289	54.3	25
p53	GTGGAAGGAAATTTGCGTGT	AGCTGTTCCGTCCCAGTAGA	220	52.3	25
SP1	CTTCTTACCCCAGCCTACCC	AGGCTCAGCCATAGGGAAAT	279	54.3	25

For each PCR reaction per cDNA sample:

10 x buffer	2.5 µl
cDNA	1.0 µl
DreamTaq	0.3 µl
dNTPs 10mM	0.5 µl
dH_2O	18.2 µl
Total volume	22.5 µl

were mixed and 2.5 µl primer mix (10 µM each) was added.

Then the PCR reactions were cycled in a C1000 thermal cycler.

95°C	5´	
95°C	30´´	x X cycles, T_A and the number of cycles are given in table 3
T_A	30´´	
72°C	1´	
72°C	10´	

After cycling, the reactions were mixed with Orange G loading dye and separated on a 1 or 3 % TAE-agarose gel depending on the size of the PCR product. The agarose gel was stained for 15´ in dH_2O containing 0.5 µg/ml ethidium bromide, 5´ destained in dH_2O and then a picture was taken. Then, the band intensities were measured with ImageJ ver. 1.45i and normalized to the GAPDH level.

4.2.13 Real-time quantitative PCR

Real-time quantitative PCR is performed to accurately measure the relative amount of template in a PCR reaction. The primers used are given in table 4. The measurement of double stranded DNA was performed with a CFX384 real-time system that monitors the increase in fluorescence of the dsDNA binding dye SYBR Green.

Table 4: Primers used for real-time PCR.

Target	Forward Primer	Reverse Primer
MXI1	ATGGAGCGGGTGAAGATG	ATGAAGAGGCGTAGCCATGT
VEGFA	GGATTTTGGAAACCAGCAGA	GTCACTCACTTTGCCCCTGT
THBS1	TGCTATCACAACGGAGTTCAGT	GCAGGACACCTTTTTGCAGATG
CIN	CTGGAGACCGACATCCTCTTT	TTCTAGGCGGGAGACTCCTG
GAPDH	CATGAGAAGTATGACAACAGCCT	AGTCCTTCCACGATACCAAAGT
EDIL3	TCGAAGACATTGCACTTTGC	GTCCATGTTGAGCGTTCTGA

The following reagents were mixed in Hard Shell 384-well PCR plates:

cDNA	2.0 µl
10 x HotTaq buffer	1.25 µl
10 x SYBR Green	0.25 µl
dH_2O	7.775 µl
dNTPs (10 mM)	0.25 µl
HotTaq	0.075 µl
Total volume	12.1 µl

Afterwards, 0.4 µl primer mix were added per well (10 µM each).

Cycling conditions in the CFX-Cycler:

94°C 2´

94°C 20´´
56°C 20´´ } 40 x
65°C 40´´

65°C 1´

+ melt curve

The cycler determines the threshold cycle C_T for every sample. Afterwards, the relative expression in the different goups compared to the Ctl shRNA cells was calculated by the $2^{-\Delta\Delta CT}$ method [95]. To calculate the ΔC_T, the C_T of the housekeeping gene, GAPDH, is substracted from the C_T of the target gene, e.g. CIN for every sample. Then, from this ΔC_T value the ΔC_T value of the means of the control group are substracted, yielding the $\Delta\Delta C_T$ [95].

4.3 Protein biochemistry

4.3.1 SDS-PAGE

SDS-Polyacrylamide gel electrophoresis is used for separation of proteins by their molecular mass. All protein lysates were prepared in 1 x Laemmli-buffer and run on 12 % SDS-gels. The gel casting was performed with equipment from the Mini-Protean SDS gel system. First, the short plates and spacer plates (1 mm gel thickness) were assembled with the casting frame on the casting stand. Then, for the separating gel the following reagents were mixed for two gels:

H_2O	3.5 ml
Acrylamide 30 % / Bisacrylamide 0.8 %	4.0 ml
4 x Tris-HCl/SDS pH = 8.8	2.5 ml

Then, 75 µl 10 % APS and 7.5 µl TEMED were added, and the gels were covered with isopropanol. After polymerization of the separating gel was completed, the isopropanol was discarded and the gels were covered with a stacking gel. For the stacking gel, the following reagents were mixed for two gels:

H_2O	2.48 ml
Acrylamide 30 % / Bisacrylamide 0.8 %	0.52 ml
4 x Tris-HCl/SDS pH = 6.8	1.0 ml

20 µl 10 % APS and 5 µl TEMED were added to induce polymerization.
The electrophoresis equipment used was a Mini-Protean SDS gel electrophoresis system.
Electrophoresis was performed at a constant voltage for 30´ at 80 V (stacking gel) and for 1 h 20´ at 120 V (separating gel).
Then the protein was transferred on nitrocellulose using a semi-dry blotting device as described in 4.3.2.

4.3.2 Semi-dry western blotting

Western blotting describes the transfer of protein from a SDS gel to a membrane suitable for immunoblotting.

For proteins of up to 40 kDa molecular weight, the low molecular weight buffers were used, for proteins > 40 kDa, high molecular weight buffers were used.

The gel was washed in cathode buffer for 10´, and the blotting sandwich was assembled as shown in figure 7. Two whatman papers were equilibrated in anode buffer 1. Another was incubated in anode buffer 2 and three in cathode buffer. Transfer was performed at 70 mA for 30´ for low molecular weight proteins, and for 1 h for high molecular weight proteins.

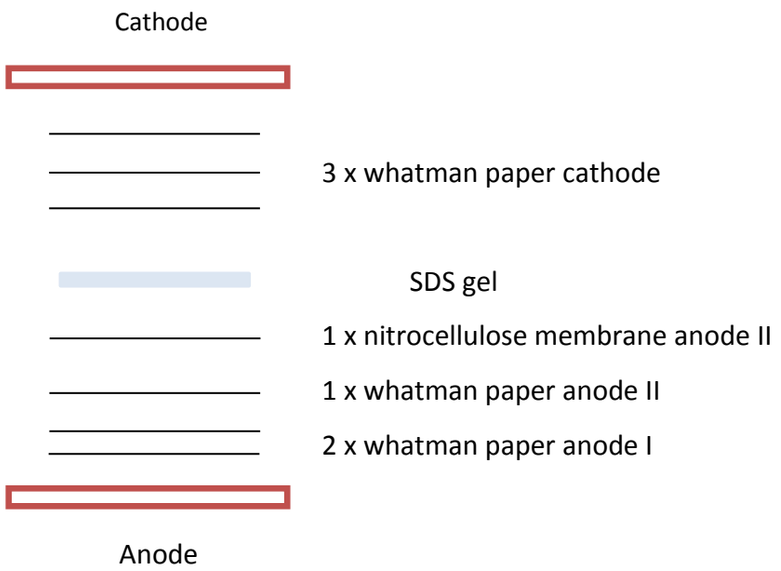

Figure 7: Sandwich for semi-dry western blotting.

4.3.3 Phostag SDS-PAGE

The analysis of phosphocofilin was performed with standard SDS-PAGE gels containing 1 µM Phostag, which allows for separation of phosphorylated and unphosphorylated proteins [96]. The gel was washed in 10 mM EDTA in Towbin buffer after electrophoresis and washed three times for 5´ in Towbin blotting buffer afterwards. For two separating gels,

H_2O	3.5 ml
Acrylamide 30 % / Bisacrylamide 0.8 %	4.0 ml
Phostag solution D	50.0 µl
Phostag solution E	50.0 µl
4 x Tris-HCl/SDS pH = 8.8	2.5 ml

were mixed. Then, 75 µl 10 % APS and 7.5 µl TEMED were added to start polymerization of the acrylamide, and the gels were covered with isopropanol. After polymerization of the separating gel was completed, the isopropanol was discarded and the gels were covered with a stacking gel. For the stacking gel the following reagents were mixed for two gels:

H_2O	2.48 ml
Acrylamide 30 % / Bisacrylamide 0.8 %	0.52 ml
4 x Tris-HCl/SDS pH = 6.8	1.0 ml

20 µl 10 % APS and 5 µl TEMED were added to induce polymerization of the acrylamide. Electrophoresis was performed at a constant current for 70´ at 30 mA.
Then, the proteins were transferred on a nitrocellulose membrane using a wet-tank transfer as described in 4.3.4.

4.3.4 Wet-tank transfer

The Phostag gels were blotted on a nitrocellulose membrane in a wet-tank blotting device, the GENIE blotter. The whatman paper and the nitrocellulose membrane were equilibrated in Towbin buffer prior to assembly of the blotting sandwich. The sandwich was assembled as

shown in figure 8. The protein was transferred on a nitrocellulose membrane at constant voltage of 12 V for 1 h.

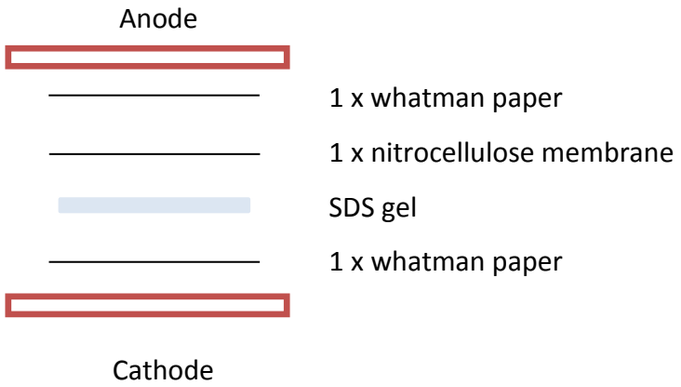

Figure 8: Sandwich for wet-tank protein transfer.

4.3.5 Detection of proteins after western blotting

The membranes were blocked in blotto buffer for 30´. Then, the membranes were rinsed in dH_2O, and incubated in primary antibody diluted in antibody diluent O/N. All antibodies used and dilutions are given in 3.8 in material and methods. The next day, the membranes were rinsed three times in dH_2O and incubated with secondary antibody diluted 1:10,000 in blotto buffer. After 1.5 h incubation at RT, the membranes were rinsed three times in dH_2O and incubated with picoluminescence substrate for exactly 2´. Then, the luminescence signal was recorded in a LAS1000 or Fluor Chem Q Imaging system. Band intensities were quantified with ImageJ ver. 1.45i or AlphaView ver. 2.0.1.1 and normalized to the respective GAPDH, ß-actin or α-tubulin level. The cofilin antibody used recognizes cofilin-1 but crossreacts with cofilin-2. The ratio of p-cofilin/total cofilin was calculated by $\% P - Cofilin = \frac{P-Cofilin}{(P-Cofilin+Cofilin)}$.

4.4 Cell culture techniques

4.4.1 Cell lines and cell culture

Eukaryotic cells were cultured with sterile equipment and all working steps were performed under a BDK-S 1200 laminar flow hood. The cell lines HEK293T, GBM6840 and U87 were cultured in complete DMEM medium and DBTRG-05-MG cells were cultured in complete HAM´s F10. Origin and marker positivity are important characteristics for the cell lines used and can be important for their reactivity to stimuli and their behavior in cell culture experiments. DBTRG-05-MG are glioma cells, established from a secondary GBM that occurred in a 59 year old female individual and stain for Vimentin but not GFAP [97]. GBM6840 cells were established from a GBM from a 17 year old female individual, and are strongly positive for both Vimentin and GFAP [98]. U87 are established from a grade IV astrocytoma that occurred in a 44 year old male individual [99].

Both media, HAM´s F10 and DMEM, were supplemented with L-glutamine, 100 u/ml penicillin and 100 µg/ml streptomycin. The cells were incubated in a humidified incubator at 37°C and 7 % CO_2. Cells were checked on a regular basis for mycoplasma, and contaminated cultures were discarded immediately. Cells were cultured to 80 – 90 % confluency, and then splitted 1:10 (GBM6840, HEK293T) or 1:4 (DBTRG-05-MG and U87). For this purpose, the medium was aspirated from the adherent cells. Then, the cells were washed with 5 ml of sterile DPBS. After that, 3 ml trypsin/EDTA were added to the culture dish, and then a volume was aspirated leaving the cells covered with trypsin/EDTA. The cells were allowed to detach for 3´ at 37 °C, and were subsequently resuspended in 10 ml complete medium. For a 1:10 dilution, 1 ml cell suspension was plated onto a new cell culture dish. The total volume in the 75 cm^2 cell culture flasks or Ø 10 cm cell culture dishes was 12.5 ml.

Cultures of primary mouse astrocytes were kindly provided by Alexandra Bohl (Institut für Pharmakologie, Universität Würzburg).

4.4.2 Freezing cells

For long term storage, cells need to be cryoconserved. For that purpose, cells grown to 80 % confluency on 75 cm^2 cell culture flasks or Ø 10 cm cell culture dishes were harvested by trypsinization as described in 4.4.1. Then, the cells were resuspended in 5 ml complete medium and collected by centrifugation for 5´ at 99 x *g*. The cell pellet was resuspended in freezing medium and immediately transferred into a cryo vial and put on ice. Then, the vials were transferred in a cryo box, and stored at -80°C O/N. On the next day, the vials were transferred into liquid nitrogen.

4.4.3 Thawing cells

For rethawing, the cells were first thawn in a waterbath at 37°C, until only a small ice crystal was left in the cryo vial. Then, the content of the cryo vial was mixed with 5 ml prewarmed complete medium in a 15 ml falcon tube, and then the cells were collected by centrifugation for 5´ at 99 x *g*. The cell pellet was resuspended in 3 ml complete medium, and then the cells were plated on 75 cm^2 cell culture flasks or Ø 10 cm cell culture dishes in a total volume of 12.5 ml medium.

4.4.4 RNA interference (RNAi)

RNA interference can be used to downregulate gene expression by targeting specific mRNAs. It is a conserved mechanism in eukaryotes for gene-silencing and anti-viral defense. Double stranded RNA molecules, siRNAs or miRNAs, mediate in general a silencing mechanism for homologous sequences [100]. However, the mechanisms can be diverse and silencing can be performed by mRNA degradation, translational silencing, and other mechanisms [101]. The most relevant mechanism by which the transfected RNAs in the experiments target mRNAs is the cleavage dependent mechanism.

Here, after entry into the cells, an RNA induced silencing complex (RISC) is formed, processed, and mRNAs complementary to the guide strand are degraded [101], as shown in figure 9.

For silencing mRNAs in cell culture, double stranded small interfering RNAs are transfected into cells, or short hairpin RNA encoding plasmids are stably transduced into target cells [100]. The sequences used for hCIN or the respective control sequences are given in table 5.

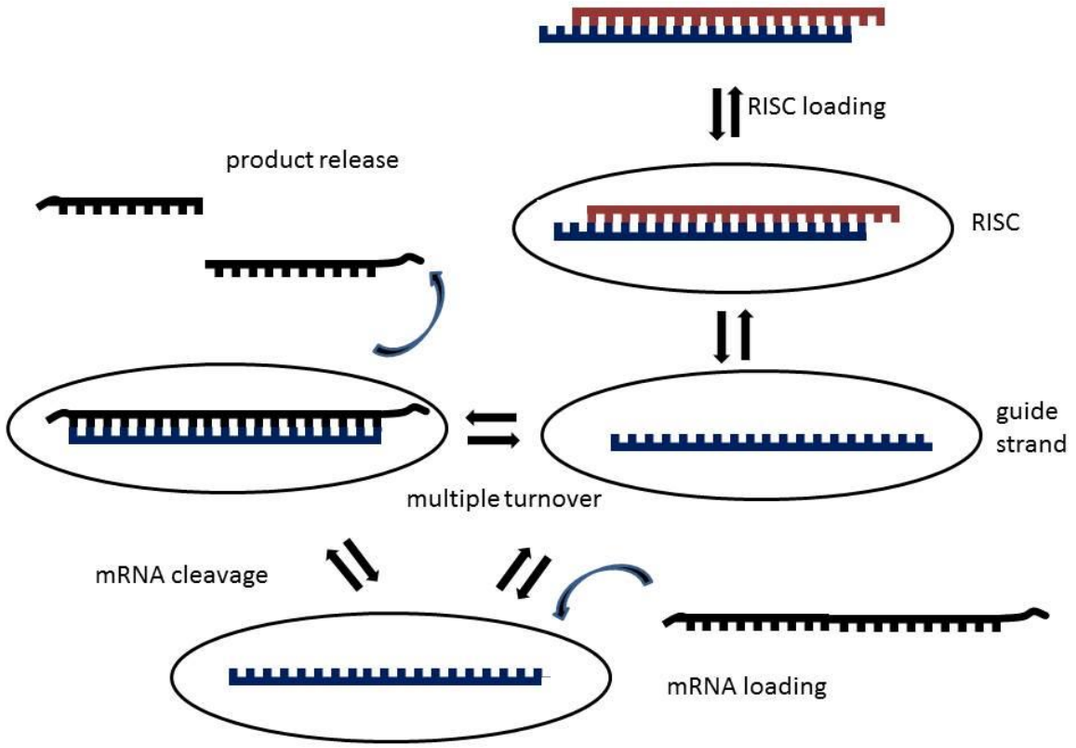

Figure 9: Mechanism of RNAi induced gene silencing.
The guide strand (blue) is loaded onto the RISC whereas the passenger strand (red) is degraded. A mRNA molecule (black) that is complementary to the guide strand is degraded. Modified after [100].

4.4.5 Transfection

Transfection is used for transfer of DNA or RNA into eukaryotic cells. The transfection reagent used was Lipofectamine 2000. Ø 6 cm plates with adherent cells were washed with 1 ml prewarmed Opti-MEM, and 3 ml Opti-MEM were added to the plate. For a Ø 6 cm dish, 250 µl Opti-MEM were mixed with the indicated RNA or DNA concentration and in parallel, 250 µl Opti-MEM were mixed with 3 µl Lipofectamine 2000, and incubated for 5´ at RT in polystyrene tubes.

Then, the solutions were mixed and incubated for another 20´ at RT to allow transfection complex formation. Afterwards, the solution was added to the cell culture plates in a dropwise fashion. The cells were incubated in the Opti-MEM medium containing transfection complexes for 4 h, and then the medium was exchanged to complete medium.

The expression plasmid for human c-myc was kindly provided by the group of Prof. Dr. Martin Eilers (Lehrstuhl für Biochemie und Molekularbiologie, Biozentrum Universität Würzburg).

4.4.6 Establishment of virally transduced cell lines

Cells can be genetically modified at high efficiency with virally mediated DNA transfer. First, the DNA that is supposed to be transferred into the target cells needs to be packaged into viral particles. All steps were performed under aseptic conditions in a S2 cell culture laboratory.

HEK293T cells were transfected at 70 % confluency as described in 4.4.5 to produce lentiviral particles carrying vectors with a non targeting control shRNA and a chronophin targeting shRNA. These plasmids SHC002 and TCN0000050046 were purchased from (54), and the target sequences are shown in table 5.

The plasmids for the packaging, pVSVG, pMDL, pAdvantage and pRSV were kindly provided by Dr. Stefan Kissler (Rudolf Virchow Center for experimental Biomedicine, Würzburg).
Per plate, 30 µl Lipofectamine 2000 and

pVSVG	2.0 µg
pMDL	1.5 µg
pAdvantage	2.0 µg
pRSV	1.5 µg
shRNA coding plasmid	5.0 µg

were used. Supernatants were collected three and four days after transfection, sterile filtered with 0.45 µm filters and viral particles were collected by ultracentrifugation. After collection of the particles, they were stored at -80°C. DBTRG-05-MG cells were infected at 70 % confluency and afterwards the infected clones were selected with 0.5 µg/ml puromycin.

Table 5: siRNA and shRNA sequences.

Target	Type	Sense	Antisense
hCIN	siRNA	UCGAGUGCAUCACGGAGAAUU	UUCUCCGUGAUGCACUCGAUU

Target	Type	Sequence 5´-3´
none (control)	shRNA	CCGGCAACAAGATGAAGAGCACCAACTCGAGTTGGTGCTCTTCATCTTGTTGTTTTT
hCIN	shRNA	CCGGCCTACATGTTCGAGTGCATCACTCGAGTGATGCACTCGAACATGTAGGTTTTTG

4.4.7 Establishment of stably transfected cell lines

For the establishment of stably transfected cell lines, cells were transfected as described in 4.4.5 with 1.0 µg pIRESNeo2 or pEGFP-N1 vector. After 24 h, the medium was exchanged, and 400 µg/ml G418 were added to the complete culture medium. The cells were cultured for another two weeks until G418 resistant clones had been selected.

4.4.8 Preparation of paraformaldehyde

First, the PFA was weighed in. Here, the amount needed to get 4 % (w/v) of the final volume of PFA solution to be prepared was used. Then, dH_2O equal to 2/3 of the total volume of PFA solution to be prepared was heated to 60°C.
The PFA was added to the water under the fume hood, and then 2N NaOH was added until the solution became clear. Afterwards, 3 x PBS equal to 1/3 of the total volume of PFA solution to be prepared was added and the pH was adjusted to 7.2 with HCl.

4.4.9 Plate coating

The plates to be coated were first washed with sterile dH_2O, and then coated for 1.5 h at 37°C, 7 % CO_2 with 10 µg/ml collagen I in 0.05 M HCl, 10 µg/ml collagen IV in 0.05 M HCl, 100 µg/ml poly-L-lysine in PBS, 0.5 µg/ml vitronectin in dH_2O or 10 µg/ml fibronectin in PBS.
Afterwards, the plates were washed with sterile dH_2O, and the water was removed by flicking. Then, the plates were blocked with 0.5 % BSA in DMEM for 30´ at 37°C and 7 % CO_2. Afterwards, the plates were washed with sterile dH_2O and dried O/N.

4.4.10 Immunocytochemistry and phalloidin staining

Cells were seeded at a density of 9,300 cells/cm^2 on collagen IV coated coverslips. Growth was allowed O/N and afterwards cells were starved for 4 h in starving medium. For the inhibitor treatment, cells were incubated with 10 µM Y-27632 or 0.1 % (v/v) DMSO as control for 2 h. Cells were immediately fixed in 4 % PFA at RT for 15´. Cells were washed with PBS, and permeabilized and blocked with ICC blocking buffer. Afterwards, cells were washed in PBS + 0.3 % saponin and stained in ICC antibody dilution buffer O/N at 4°C with vinculin primary antibody. On the next day, the slides were washed three times in PBS + 0.3 % saponin and incubated with Alexa Fluor 488 anti-rabbit IgG or anti-mouse IgG (diluted 1:200 in antibody dilution buffer) and Alexa Fluor 546 phalloidin (diluted 1:50 in antibody dilution buffer) for 2 h at RT. The slides were washed again three times in PBS + 0.3 %

saponin. Then, the slides were counterstained with DAPI, at a concentration of 1 µg/ml for 10´. Afterwards, the coverslips were washed twice in PBS, mounted in fluorescence mounting medium and the cells were visualized with confocal microscopy using a Leica SP5. At least 30 sections in the z-axis of slice thickness 0.695 µm were imaged, and from the acquired stacks maximum projections of these z-stacks were calculated with the Leica Application Suite Advanced Fluorescence Software for three independent experiments.

4.4.11 Immunocytochemistry CIN staining

Cells were seeded at a density of 9,300 cells/cm^2 on glass coverslips. Growth was allowed for 48 h. Then the cells were fixed in 4 % PFA at RT for 15´. Cells were washed with PBS, and permeabilized and blocked with ICC blocking buffer. Afterwards, cells were washed in PBS + 0.3 % Saponin and stained in antibody dilution buffer O/N at 4°C with α-CIN antibody diluted 1:50. On the next day, the coverslips were washed in PBS + 0.3 % saponin and incubated with Alexa Fluor 488 anti-rabbit IgG (diluted 1:200) and Alexa Fluor 546 phalloidin (diluted 1:50) for 2 h at RT. The coverslips were washed again three times in PBS + 0.3 % saponin. Then, the coverslips were counterstained with DAPI, at a concentration of 1 µg/ml for 10´. Afterwards, the coverslips were washed twice in PBS, mounted in fluorescence mounting medium and the cells were visualized with confocal microscopy using a Leica SP5.

4.4.12 Immunocytochemistry and F-actin staining of stimulated cells

Cells were seeded at a density of 9,300 cells/cm^2 on glass coverslips. Growth was allowed for 24 h and afterwards the cells were starved O/N in DMEM w/o FCS. The cells were stimulated with LPA at a concentration of 1 µM, 50 ng/ml PDGFBB, 100 ng/ml EGF or 1 µM Bradykinin diluted in starving medium or pure starving medium (unstimulated) for 10´.
Afterwards, the cells were immediately fixed in 4 % PFA at RT for 15´. The coverslips were washed with PBS, and permeabilized and blocked with ICC blocking buffer. Afterwards the coverslips were washed in PBS + 0.3 % saponin and incubated with Alexa Fluor 546

phalloidin diluted 1:50 in ICC antibody dilution buffer for 2 h at RT. Then, the coverslips were counterstained with DAPI, at a concentration of 1 µg/ml for 10´. Afterwards, the coverslips were washed twice in PBS, mounted in fluorescence mounting medium and the cells were visualized with confocal microscopy using a Leica SP5. At least 30 sections in the z-axis of slice thickness 0.695 µm were imaged, and from the acquired stacks maximum projections of these z-stacks were calculated with the Leica Application Suite Advanced Fluorescence Software for three independent experiments.

4.4.13 Actin spin down assay

Cells were seeded at a density of ~20,000 cells/cm^2, growth was allowed for 24 h and the cells were then starved O/N in starving medium. Afterwards, lysis was performed in 500 µl 37°C prewarmed spin down buffer 2. All other equipment and the centrifuge were prewarmed to 37°C before the experiment, too.

The lysates were homogenized by aspirating them five times through a syringe with a 30 gauge needle and were then incubated at 37°C for 10´.

Afterwards, the F-actin and G-actin containing fractions were separated by ultracentrifugation. 350 µl lysate were centrifuged in an Optima TLX ultracentrifuge at 100,000 x *g* at 37°C. The supernatant containing G-actin was collected immediately after centrifugation, and the pellet containing F-actin was resuspended in 350 µl 8 M urea. The actin in the pellet was depolymerized by incubation for 1 h on ice.

Afterwards, the fractions were mixed with Laemmli-buffer, and processed for standard SDS-PAGE. F/G-actin levels were estimated *via* western blot. The ß-Actin antibody was used for detection of actin in the fractions.

4.4.14 Chemotaxis-assay on collagen IV

For chemotaxis-assays, GBM6840 control shRNA and CIN shRNA cells were seeded at a concentration of 3 x 10^6 cells/ml on collagen IV coated µ-slide chemotaxis chambers in a total volume of 7 µl per chemotaxis chamber. Cells were allowed to adhere O/N, and starved in medium w/o FCS for 6 h on the next day. Then, 8 µl DMEM containing 100 ng/ml EGF or 10 % FCS were added on one reservoir side. Build up of the chemoattractant gradient was allowed for 2 h, and afterwards a time lapse DIC movie was recorded in a humidified, temperature and CO_2 controlled microscope stage incubator. A picture per position was recorded every 20´ for 24 h. At least 30 cells per condition were tracked and analyzed.
The forward migration index for each cell was then calculated by dividing the displacement on the chemoattractant gradient axis through the accumulated distance of each cell.

4.4.15 2D-Migration 8-well setup

For the assays with the ROCK-inhibitors, CFL1-S3A mutant and U87 cells, 8-well µ-slides were coated with 10 µg/ml collagen IV as described in 4.4.17.

GBM6840 and U87 cells were seeded at a density of 6,000 cells/cm^2 in starving medium with BSA and allowed to adhere for 6 h. Afterwards, cells were preincubated with 10 µM fasudil, 10 µM Y27632, or 0.2 % DMSO as a control for 30´. All inhibitors used were dissolved in sterile DMSO, stored at -20°C and thawed maximally three times. The GFP expressing cells used here had been sorted for GFP-expression by C. Linden (Institut für Virologie und Immunbiologie, Würzburg) as described in 4.5.2.

DIC-movies were recorded for 12 h in a humidified, temperature and CO_2 controlled microscope stage incubator. At least 50 cells per condition were tracked and analyzed with ImageProPlus, ver. 7.0. Two parameters were calculated from the measurements, the accumulated distance as well as the distance from origin for each object/tracked cell. The accumulated distance is the sum of the travelled distances (d_1, d_2,…d_i) between the timepoints t_0 and the last timepoint t_i and is thus expressed as $\sum di$. The distance from origin

(D) is measured by the software as the distance between the starting point of an object at t_0 and its position at the last timepoint t_i (see Fig. 10).

The directionality of each object is then calculated by $Directionality = \frac{D}{accumulated\ distance}$

.

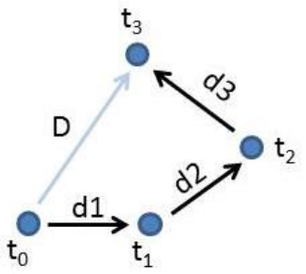

Figure 10: Parameters used for the calculation of accumulated distance and distance from origin.
The travelled distances between the timepoints t_0 and the last timepoint t_3 are denoted as d_1, d_2 and d_3. The distance from origin (D) is the distance between the position of the object at first and the last time point timepoint.

4.4.16 Transwell assay

Cells were grown to 90 % confluency, trypsinized, resuspended in complete medium and counted in a hematocytometer. Afterwards, the cells were centrifuged and resuspended in starving medium and resuspended to a density of 5.0 x 10^4 cells/ml. 2.5 x 10^4 cells from the lines GBM6840, U87 or DBTRG-05-MG were seeded per upper compartment of a growth factor reduced matrigel-coated transwell chamber with 8 µm pore size in a 24-well plate format. The effective growth area of the transwell membrane used was 0.3 cm^2. EGF at a concentration of 100 ng/ml was added to the lower compartment of the chamber to stimulate the migration of the glioma cells. Cells were allowed to migrate for 24 h, and afterwards non-invading cells were removed with a cotton swab from the upper side of the insert, and the cells on the lower side of the membrane were fixed with methanol. Afterwards, cells were stained with 1 µg/ml DAPI in PBS for 10´, washed twice in PBS, the membranes were cut out from the culture inserts and transferred on microscopy glass slides. After cutting out the membrane, a circle of d = ~ 3,400 µm was left from it. Therefore, the area of the membrane was ~ 9.08 mm^2, and the area on which counting was performed was

~ 3.45 mm^2, or ~ 38 % of the total membrane area. Fluorescent micrographs were taken with a 4 x objective on an inverted microscope in the DAPI channel, one micrograph was taken per membrane and analyzed afterwards. Automated object counting of the nuclei on the membrane was performed with ImageProPlus, ver. 7.0.

4.4.17 Proliferation assay

For the analysis of cell proliferation, 1,000 (U87 and GBM6840) or 2,000 (DBTRG-05-MG) cells were seeded per well on 96-well plates, and a separate well was prepared for every time point. 6 h after seeding, the medium was exchanged. Then, every 24 h for five days, one well from each condition was stained with 1 µM Hoechst 33342 for 1 h at 37°C and 7 % CO_2. Then, one picture was taken from the center of the well on each day for each condition with a 10 x objective on a NikonT_i eclipse microscope equipped with a DAPI filter, and automated image analysis was performed with ImageProPlus 7.0 to automatically count the number of nuclei per well.

4.4.18 Cytokinesis assay

Cells were seeded at a density of 5,000 cells/cm^2 on 8-well Ibitreat slides. They were incubated at 37°C, 7 % CO_2 in an humidified incubator for 16 h, afterwards media were exchanged to the respective starving medium and the cells were allowed to recover for 6 h. As the cells in the transwell assay as described in 4.4.16 were also seeded in starving medium, this was done to make the condition between the two assays comparable. Afterwards, DIC movies were taken on a NikonT_i eclipse microscope, and the number of completed mitoses was determined. Only mitoses were counted, which started and whose cytokinesis was completed within the observation period, and at least 100 cells were followed over the time course.

4.4.19 Cell roundness and cell area scoring

Cells were seeded at a density of 9,300 cells/cm^2 on collagen IV coated coverslips. Growth was allowed O/N and afterwards cells were starved for 4 h in starving medium. Cells were fixed in 4 % PFA at RT for 15´. Then cells were stained with Alexa Fluor 546 phalloidin diluted 1:50 in PBS supplemented with 0.3 % saponin and 0.1 % BSA. Fluorescent micrographs were taken employing a 20 x objective on a NikonT_i eclipse microscope and automatically analyzed with ImageProPlus 7.0. At least 100 cells were scored for each condition. The perimeter is calculated as the chain code length of the outline. The area is determined by counting the number of pixels within the object including the outline. The roundness R is then calculated by $R = \frac{perimeter^2}{4 \times \pi \times area}$.

4.4.20 Adhesion Assay

The plates for the adhesion assay were coated on the day before the assay as described in 4.4.9. Tissue culture treated, 96-well plates with clear bottom and black walls were used. 400,000 cells were seeded 48 h prior to the assay on a Ø 10 cm dish in complete medium. The cells were starved in starving medium with 0.1 % BSA. Then, the cells were labeled with 1 µg/ml calcein AM in starving medium w/o phenol red for 15´ at 37°C and 7 % CO_2. Afterwards, the cells were trypsinized, and the trypsin reaction was stopped in 5 ml starving medium w/o phenol red supplemented with 0.1 % BSA and 0.5 mg/ml soybean trypsin inhibitor. The cells were allowed to recover for 30´ at 37°C and 7 % CO_2. The cells were counted and the cell number was adjusted to 100 cells/µl. Then, the cell suspension was incubated on the different substrates for 10´, 20´ or 40´. After incubation, the plates were washed twice with PBS, and then 100 µl of lysis buffer containing 50 mM Tris and 1 % Triton X-100 were added and the plate was incubated at RT for 15´. Then, the fluorescence intensity in every well was measured with an Envision 2104 multilabel reader.

4.4.20 Cignal Cancer Panel, c-myc luciferase assays and SRE-luciferase assay

To analyze the effect of CIN deregulation on the activity of a variety of cancer relevant transcription factors, a luciferase based reporter assay was performed. In this assay, a tandem repeat transcriptional element (TRE) for a specific transcription factor is used that controls the expression of a firefly luciferase. As an internal control, a Renilla luciferase is cotransfected, which is expressed under the control of a constitutively active pCMV promoter (see Fig. 11). 5000 cells were seeded per well of white 96-well plate 48 h before the assay. Then, the cells were transfected with 50 ng reporter plasmid mix per well and 4 pmol siRNA /well or 10 ng hCIN//pCDNA3 and 0.2 µl Lipofectamine 2000. The cells were grown for 24 h in medium w/o phenol red supplemented with 0.5 % (Cignal Cancer Panel, SRE) or 5 % FCS (c-myc, SRE) after transfection. The volume of medium used was 75 µl/well. Afterwards, the luciferase activity was measured with the Dual Glo luciferase assay system. 75 µl Dual Glo Luciferase reagent were added, incubation was performed for exactly 15´ at RT, and the Firefly luminescence intensity was measured in an Envision 2104 multilabel reader. Afterwards, the Dual Glo Stop and Glo Reagent was added, incubation was performed for exactly 15´ at RT, and the Renilla luminescence intensity was measured in an Envision 2104 multilabel reader.

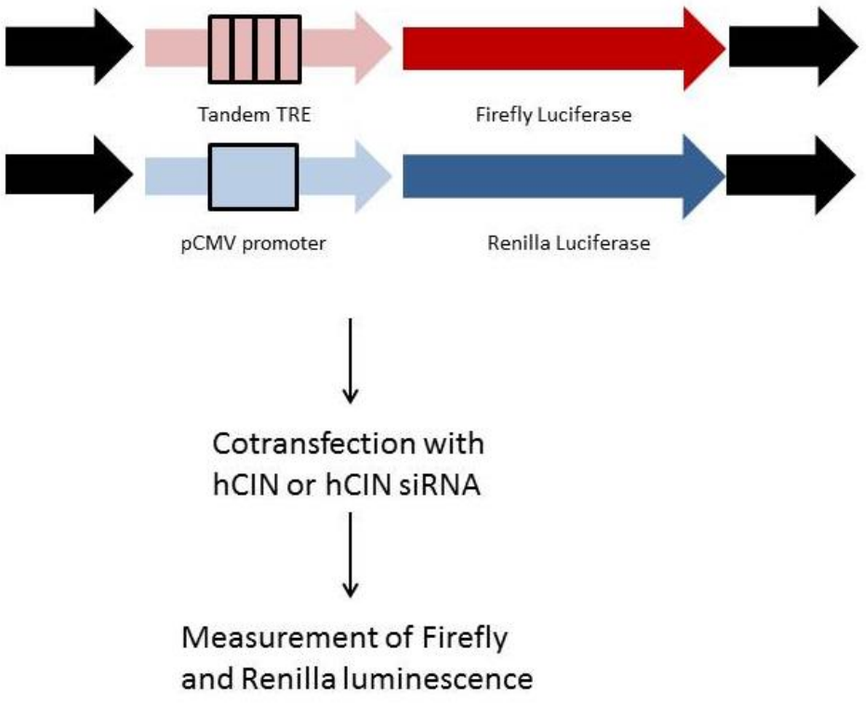

Figure 11: Principle of the luciferase based promoter activity assay.
A tandem repeat transcriptional element (TRE) for a specific transcription factor is transfected into cells that controls the expression of a firefly luciferase. As an internal control, a Renilla luciferase is cotransfected, which is expressed under the control of a constitutively active pCMV promoter. A hCIN encoding plasmid or a human CIN targeting siRNA was cotransfected. Afterwards, Firefly and Renilla luminiscence were measured. Modified after [102].

4.4.21 Small GTPase activity assays

The measurement of GTP-bound, active Rho- and Rac 1/2/3 was performed with commercially available ELISA based activity assays containing a RhoA-GTP or Rac 1/2/3-GTP binding 96-well plate. On these plates, a RhoA-GTP or Rac 1/2/3-GTP binding domain of a Rho effector is bound.

Cells were seeded at a density of ~20,000 cells/cm^2 and grown for 24 h. Afterwards the medium was exchanged to starving medium and the cells were starved O/N. Afterwards, cells were washed with ice-cold PBS, immediately lysed in lysis buffer, frozen in liquid nitrogen and stored at -80°C until measurement. Aliquots of the lysates were taken for western blot and RhoA and Rac 1/2/3 protein detection. The samples were incubated on a 96-well plate coated with a Rho-GTP or Rac 1/2/3-GTP binding protein of a Rho effector binding specifically RhoA or Rac 1/2/3. Afterwards, the plate was washed with washing buffer, incubated with primary antibody and secondary antibody, and a HRP-based colorimetric detection of the bound RhoA-GTP and Rac1/2/3-GTP, respectively, was performed.

The absorbance of each sample was measured in duplicate wells and measured in an Envision 2104 multilabel reader.

4.5 Flow cytometry based methods

4.5.1 F-actin FACS

Cells were seeded at a density of ~20,000 cells/cm^2 and starved O/N in starving medium containing 0.1 % BSA. Afterwards, the cells were trypsinized briefly for 90´´, resuspended in starving medium and immediately fixed in 2 % PFA for 15´ at RT (see Fig. 12). Afterwards, cells were permeabilized with 0.5 % saponin for 15´, washed twice with PBS + 0.5 % saponin and stained with Alexa Fluor 546 Phalloidin diluted 1:25 in PBS, supplemented with 0.1 % BSA and 0.5 % saponin, for 1 h at RT. Then cells were washed again three times in PBS containing 0.5 % saponin, and analyzed in a FACS Calibur flow cytometer.

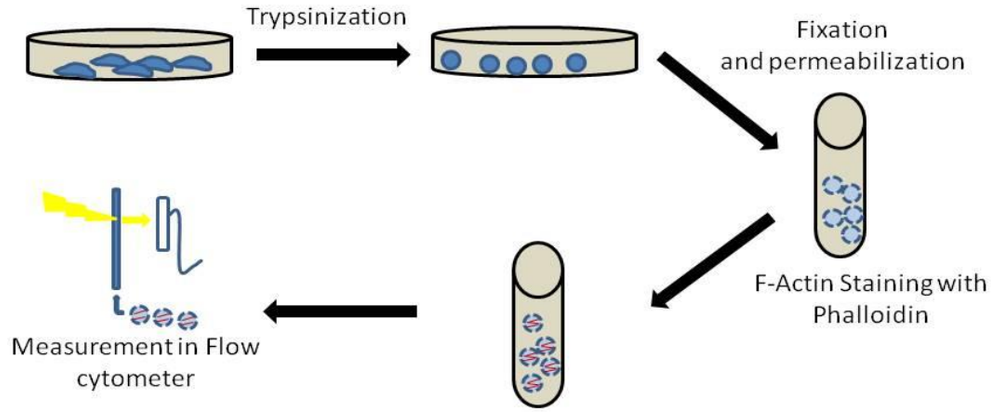

Figure 12: Principle of the FACS based measurement of total F-actin levels.
The cells were trypsinized, permeabilized and stained with Alexa Fluor 546 phalloidin. Afterwards, the cells were analyzed in a flow cytometer.

4.5.2 Cell sorting

Cells were sorted by Christian Linden (Institut für Virologie und Immunbiologie, Würzburg) in the Core Facility for Cell Sorting in Würzburg. The cells were sorted for GFP expression on a FACS Aria III Flow cytometer, and cells were gated as GFP$^+$ that were more than 1.3 x above the highest background fluorescence level measured in control cells.

4.5.3 GFP-expression analysis

The analysis of GFP expression was performed with a FACS Calibur flow cytometer. The cells were harvested by trypsinization, resuspended in complete medium and analyzed in the FL-1 channel.

4.6 *In vivo* assays

4.6.1 GFP-Luciferase transduction

For transduction of the FUGLW vector [103], lentiviral particles were created, and all steps were performed in a S2 laboratory under a laminar flow hood. The FUGLW vector encodes a luciferase-GFP fusion gene and was kindly provided by Dr. A. Beilhack (Medizinische Klinik und Poliklinik II, Universitätsklinikum Würzburg).
2.5 x 10^6 HEK293T cells were seeded 24 h prior to transfection in DMEM complete medium on a Ø 10 cm dish. Then 1 ml Opti-MEM plus 30 µl Lipofectamine 2000 (1) and 1ml Opti-MEM plus

pVSVG	5.0 µg
pPAX2	5.0 µg
pAdvantage	2.0 µg
FUGLW	5.0 µg

(2) were mixed and incubated for 5´ at RT. Then, solution (1) and (2) were mixed, and incubated for another 20´ at RT. Then, the transfection mix was applied drop by drop to the HEK293T-cells, and after 3 h the medium was exchanged to complete medium. After 72 h and 96 h, the virus containing supernatant was harvested from the cells, and cellular debris

was removed by centrifugation at 800 x *g* and 4°C. The supernatant was filtered with a 0.45 µm cellulose acetate filter. 60 % confluent GBM6840 cells were transduced in complete medium containing 8 µg/ml hexadimethrine bromide, and the cells were incubated for 24 h in the virus containing supernatant. The cell lines used for FUGLW transduction all originated from GBM6840 cells. These cells were first transduced with a control or CIN targeting shRNA [48], hereafter named Ctl shRNA and CIN shRNA. Then, the cells were transfected with the pIRESNeo2 empty vector or the hCINΔshRNA//pIRESNeo2 construct that was created as described in 4.2.11.1, and stably transfected cell lines were selected as described in 4.4.7 .

Finally, Ctl shRNA transduced pIRESNeo2 transfected, CIN shRNA transduced pIRESNeo2 transfected and CIN shRNA transduced hCINΔshRNA//pIRESNeo2 transfected cells were used for the FUGLW transduction. These cells are hereafter named control, CIN knockdown and rescue, respectively.

4.6.2 Clone picking

Clones were picked from GFP-Luciferase expressing cells, which were transduced as described in 4.6.1. The protocol used for single cell clone picking was based on the serial dilution of cells in a 96-well plate [104]. 200 µl of a cell suspension containing 5 x 10^4 cells/ml in complete DMEM were pipetted into the first well of a 96-well plate. Then, eight serial 1:2 dilutions were prepared from that well in complete DMEM in a total volume of 200 µl in the wells. Then, from each of these eight wells another twelve 1:2 dilutions were prepared, again in a final volume of 200 µl. 24 h later, it was checked in which wells single cells were present, and those clones were grown for three weeks at 37°C and 7 % CO_2 in a humidified incubator. Finally, GFP expression was examined as described in 4.5.3. Then, clones were selected that had a high GFP expression. These were then examined for their CIN expression. CIN knockdown clones were selected, in which the CIN protein levels were reduced to less than 20 % of the respective control cells. Rescue cells were selected, in which the CIN protein level was increased back to the level in control cells ± 20 %.

4.6.3 Orthotopic implantation

The control, CIN knockdown and rescue cell clones generated as described in 4.6.2 were injected into NOD-SCID mice by Prof. Dr. Anna Leena Sirén. NOD-(Non obese diabetic) SCID (severe combined immunodeficeny) mice are genetically engineered immunocompromised mice that lack natural killer cells and in which T- and B-cell development is blocked [105]. Immunocompromised mice are used to prevent rejection of the tumor xenograft by the immune system [106].

Injection was performed according to the following protocol.

Under aseptic conditions, mice were anesthetized by intraperitoneal injection of ketamine (0.1 mg/g) and xylazine (0.005 mg/g). After removal of the periosteum the cranium was accessible. A 10 µl Hamilton microsyringe equipped with a 33 gauge needle was centered above the Bregma, and placed 1.0 mm posterior and 2.0 mm lateral over the midline. Through a hole in the cranium, the needle was inserted 3.0 mm under the dura mater. Then, 10,000 cells in a total volume of 5 µl were injected into the brain. The needle was removed and the wound was closed with Etilon 3.0. 10 mice per group were injected. Due to the fact that some animals died during the experiment and others showed no luminescence signal in the cerebrum, three animals were lost per group. All mice were female and approximately 10 weeks old. The animals were controlled daily for weight loss and behavioral deficits.

4.6.4 *In vivo* luciferase imaging

The luciferase imaging was performed by Dr. Sabrina Kraus (Medizinische Klinik und Poliklinik II, Universitätsklinikum Würzburg) and Prof. Dr. Anna Leena Sirén (Neurochirurgische Klinik und Poliklinik, Universitätsklinikum Würzburg) according to the following protocol.

The animals were anesthetized with a mixture of ketamine (100 mg/kg) and xylazine (10 mg/kg) containing 150 mg/kg luciferin by intraperitoneal injection. After exactly 10´, the bioluminescence intensity of the whole animal was measured in a bioluminescence imager in dorsal position, and the images were analyzed with the Living image 4.0 Software. The first measurement was performed on day 1 after surgery for all mice, and repeated on day 3,

7, 11, 15 and 20 after surgery. The anesthetized animals were killed on day 20 directly after luminescence imaging by decapitation. Afterwards, the brain was removed from the skull, and an *ex vivo* imaging was performed in the bioluminescence imager. Then, the brains were conserved as described in 4.6.5.

4.6.5 Cryo sections

Cryo sections from the mice from the experiments described in 4.6.3 and 4.6.4 were prepared as follows. First, brains were removed from the mice and fixed in 4 % ice cold PFA for 24 h at 4°C. Then, the brains were transferred in 20 % sucrose in TBS. After incubation for 24 h at 4°C the brains were frozen slowly in liquid nitrogen. For this purpose, the brains were glued to a piece of aluminum foil with Tissue-tek and only the edge of the foil was submerged in the liquid nitrogen until the tissue was frozen. When the tissue was frozen, the whole brain was submerged in liquid nitrogen and then stored at -80°C.
For the preparation of the sections, the brains were glued to a stamp with Tissue-tek, and 18 µm thick coronal sections (containing both hemispheres) were prepared with a Cryostat CM 3050S. These were transferred on poly-L-lysine coated superfrost glass slides. The cerebral hemispheres were cut and preserved as completely as possible, and from the 21 brains at least 160 sections were cut per brain. The sections were stored at -80°C.

4.6.6 Immunohistochemistry

For Immunohistochemistry, frozen sections were prepared as described in 4.6.5. The slides were thawed for 20´ at RT prior to the staining procedure. The slides were rehydrated in 1 x TBS for 10´, and the brain sections on the slides were surrounded with a hydrophobic barrier pen. To quench endogenous peroxidase activity, the brain sections were incubated for 15´ at RT in 100 % methanol containing 3 % H_2O_2.Then, the slides were washed in 1 x TBS for 5´. The sections were blocked for 1 h in IHC blocking buffer. Then, the slides were incubated with primary antibody in IHC antibody dilution buffer O/N at 4°C. In order to specifically detect the implanted human glioblastoma cells, an antibody was used that only recognizes

the human Cytochrom C Oxidase IV, and not the murine antigen. This rabbit human Cytochrom C Oxidase IV antibody was diluted 1:1000, and every 20th section from every brain was stained and examined systematically for presence of tumor cells. To exclude staining artifacts the slides with control, knockdown and rescue cell injected brains were always stained in parallel and mixed. On the next day, the sections were washed three times in 1 x TBS + 0.3 % Triton X-100 for 5´. Then, a biotinylated goat anti-rabbit secondary antibody was applied to the sections in TBS + 1 % BSA for 1 h at RT. Afterwards, the slides were incubated with avidin coupled horse radish peroxidase (ABC complex) diluted in TBS for 30´ at RT. Then, the slides were washed three times in TBS. After that, the DAB staining was developed with DAB substrate for 10´ at RT, and the reaction was stopped by rinsing the slides in running tap water for 5´. The slides were counterstained in Mayer´s hemalaun for 2´, again rinsed in running tap water, and dehydrated in alcohol and Roti-Histol. The slides were mounted in mounting medium and covered with a coverslip.

4.7 *In silico* analyses

4.7.1 Rembrandt data mining

The Rembrandt database from the National Cancer Institute (http://rembrandt.nci.nih.gov) was accessed on the 23.8.2013 [107], and the expression ratios of the indicated probesets in the individual samples compared to the geometric mean of the non tumor samples were downloaded. The specific _at and a_at probesets were analyzed for the genes indicated, and the more unspecific x_at, _s_at probesets were excluded from the analysis. Then, the relative gene expression in GBM compared to the normal brain tissue was calculated. In total, 28 normal brain samples and 221 GBM samples were analyzed. All available GBM and normal brain samples available were analyzed, with the exception that re-resection GBM samples were excluded.

4.7.2 GEO-Analysis

The Gene Expression Omnibus (GEO) Database, http://www.ncbi.nlm.nih.gov/geo/, was accessed on 5.3.2012 and the MASS normalized raw data for the GEO Accession GSE 4290 [108] and the raw data for GSE12657 (unpublished) were downloaded. All further analysis steps were performed with R ver. 13.2.1. The data from GSE12657 were normalized with the RMA algorithm. Lists were generated containing the symbols for all significantly deregulated genes at an adjusted $p \leq 0.05$ and a logFC ≥ 0.5 in GEO Accession GSE 4290 and all significantly regulated genes ($p \leq 0.05$) from GSE12657 from the comparison pilocytic astrocytoma versus GBM. Then, the symbols from the lists were compared to the list of deregulated genes contained in table 8, and all genes regulated in the same direction were extracted.

4.7.3 DAVID-Analysis

The Database for Annotation, Visualization and Integrated Discovery (DAVID) [109,110], http://david.abcc.ncifcrf.gov/, was accessed on 9.10.2012. The transcripts from the list in table 8 were categorized according to the Gene Ontology (GO) database.

4.7.4 Ingenuity Pathway Analysis

The analysis of transcription factor networks was performed with Ingenuity Pathway analysis, Ingenuity®Systems, www.ingenuity.com.

This software determines potentially affected transcriptions factors from a gene list as shown in table 8. All identified transcription factors were exported that fulfilled the following criteria: The hit had to be significant with a p-value ≤ 0.05 and the number of regulated target molecules had to be at least 10 % of the molecules within the given data set. The cutoff of 10 % of the initial data set size was chosen due to the following reasons: IPA

identifies many significantly regulated transcription factors with only very few regulated molecules. Due to the few molecules found in the data set, these hits do not seem to be biologically meaningful. On the other hand, due to the different sizes of the data sets used in this analysis, it would have been hard to define an absolut number of regulated molecules. The IPA software also automatically generates graphical networks of the results, as shown in figure 34.

4.8 Data analysis

All graphs shown in this thesis were created with the commercially available GraphPad Prism ver. 5.0. All statistical analyses were carried out with R ver. 13.2.1, a software that is freely available at http://www.r-project.org/. Parameters given for the statistical analyses include the p-value, standard error of the mean and the degrees of freedom. The p-value is the measure for the probability that the measured result could have arisen by chance if the null hypothesis is true. The null hypothesis is always: The means are the same. The degrees of freedom is the sample size minus the number of parameters estimated from the data [111]. For all continuous variables normal distribution and normal distribution of the residuals were assumed and a t-test was performed for comparison of means. A result was regarded as statistically significant, when $p < 0.05$. For count data, like from the transwell experiments, normal distribution of the residuals cannot be assumed [111]. Therefore, a rank based test, the Kruskal-Wallis test was performed that does not assume normal distribution of the residuals [112].

5. Results

5.1 Cofilin and CIN expression in human glioma cells

We tested which of the three cofilin family members, cofilin-1 (CFL1), cofilin-2 (CFL2) and actin depolymerizing factor (ADF), are expressed in GBM6840 cells. Among these, CFL1 was the most abundant member in GBM6840 cells (assuming that the PCR reactions for these different gene products were equally efficient). CFL2 and ADF were also expressed, but at rather low levels (see Fig. 13 A and B). Furthermore, the CIN protein expression level of selected human glioma cell lines was checked, given previous findings from our group that most cell lines from rat and human gliomas do not express CIN [48]. After normalization to GAPDH protein levels, it became apparent that DBTRG and GBM6840 cells expressed CIN at a level comparable to normal mouse astrocytes and were therefore suitable for shRNA mediated knockdown experiments (see Fig. 13 C). Interestingely, both the CIN and the GAPDH bands appeared at a lower molecular weight in the mouse sample than in the human samples. The murine CIN protein is 292 amino acids long and indeed shorter than the human protein with 296 amino acids, which resulted in a different behavior in the SDS-PAGE run. For the GAPDH protein, the molecular mass for the longest isoform in the human is 36.1 kDa. The longest isoform in the mouse has a molecular mass of 38.7 kDa, the shorter isoform 35.8 kDa. If the mouse astrocytes expressed the shorter GAPDH isoform this might explain the lower apparent molecular weight of GAPDH in the murine samples.

The DBTRG-05-MG cells were newly transduced with a CIN targeting shRNA or a control shRNA, whereas GBM6840 cells were already available as transduced cell line previously generated in our laboratory [48]. U87 cells expressed only low levels of CIN, and were used for reexpression experiments with a full length hCIN.

To examine the subcellular localization of CIN, one of the CIN expressing cell lines, GBM6840, was immunostained for CIN and F-actin. CIN localized to the nucleus and the cytoplasm in GBM6840 (see Fig. 13 D). Immunostainings of GBM6840 cells were visualized by confocal microscopy, shown is a single optical slize of 0.7 µm thickness.

These experiments identified DBTRG-05-MG and GBM6840 cells as suitable cell lines for CIN knockdown experiments, and the cell line U87 as a good model for reexpression analyses.

Furthermore, as CFL1 was shown to be the most abundant ADF/cofilin family member in GBM6840, a rationale was created for the Phostag based analysis of the p-cofilin/total cofilin level with an antibody that recognizes CFL1 and CFL2, but not ADF.

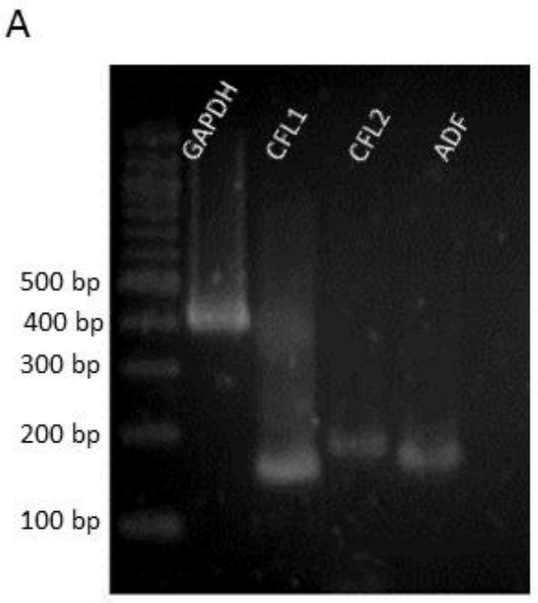

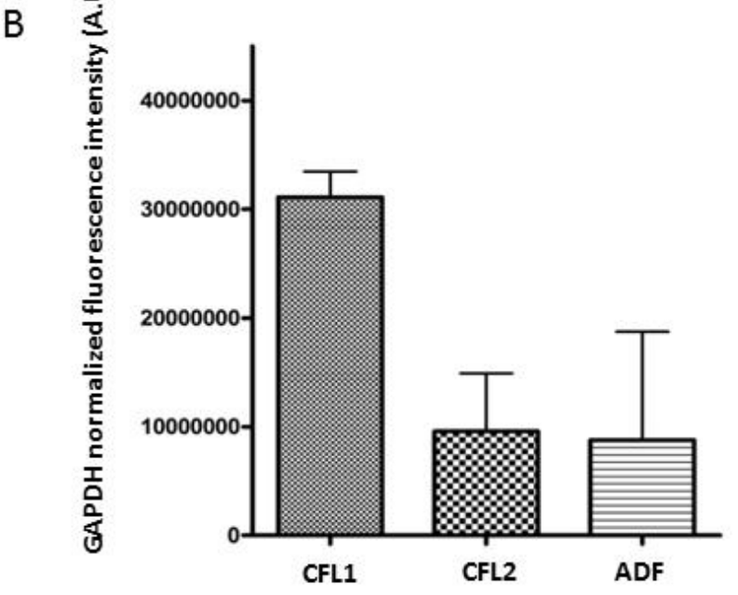

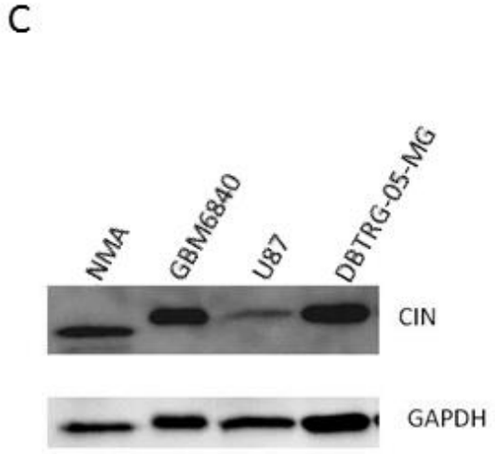

D

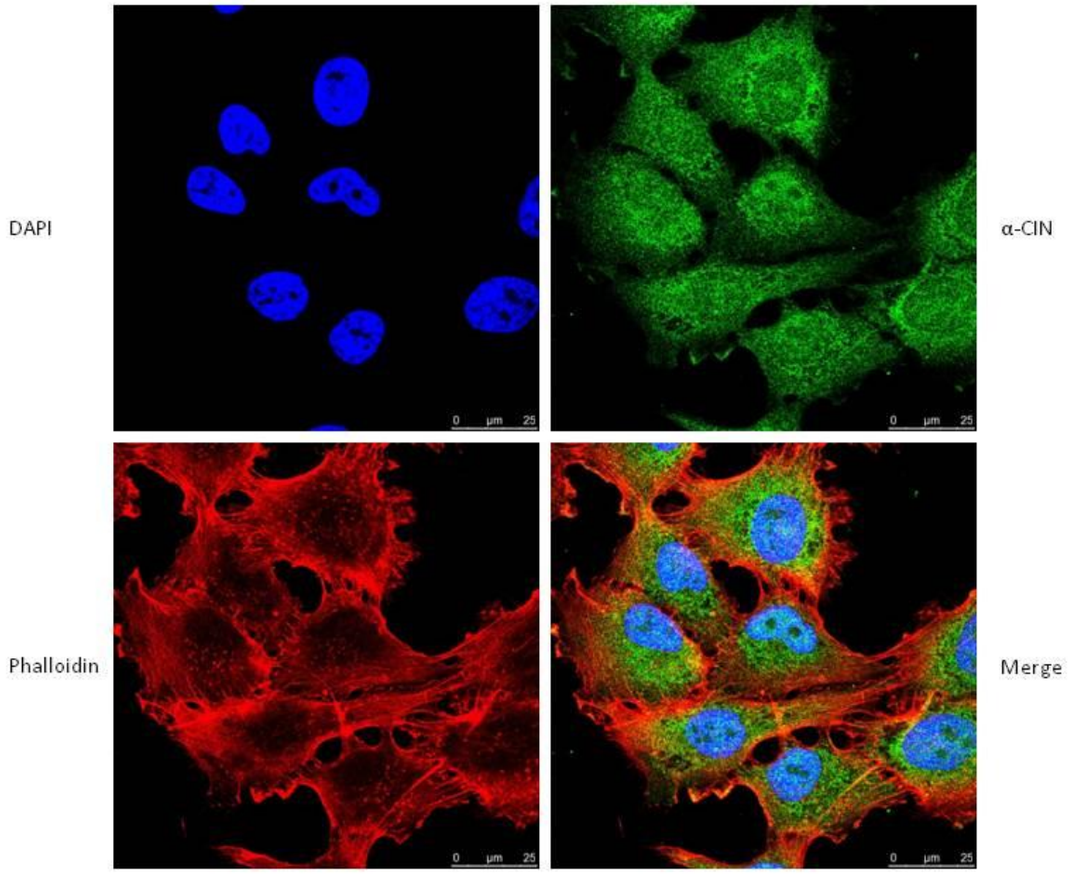

Figure 13: Cofilin and CIN expression in human glioma cells.
(A) Representative ethidium bromide stained agarose gel of a semiquantitative PCR showing PCR product abundance for the three cofilin/ADF family members in GBM6840. GAPDH was used as loading control.
(B) Quantification of n=3 experiments as shown in (A). Shown is the mean GAPDH normalized fluorescence intensity of cofilin/ADF-transcripts + SEM.
(C) Western blot with α-CIN antibody in normal mouse astrocytes (NMA), and the human glioma cell lines GBM6840, U87 and DBTRG-05-MG. GBM6840 and DBTRG-05MG cells expressed CIN at levels comparable to NMAs. U87 cells expressed only very low amounts of CIN. GAPDH was used as loading control.
(D) Immunocyctochemistry for CIN in GBM6840 cells. CIN localized to the nucleus and the cytoplasm. GBM6840 cells were stained for F-actin with Alexa Fluor 546 phalloidin, with α-CIN antibody and secondary Alexa Fluor 488 labeled anti-rabbit antibody and the nuclei were stained with DAPI. GBM6840 cells were visualized by confocal microscopy, shown is a single optical slize of 0.7 µm thickness.

5.2 Changes in cofilin phosphorylation after CIN deregulation

As CFL1 was the most abundant transcript in GBM6840, we focused on CFL1 in the assays in which cofilin protein phosphorylation was analyzed. The ratio of Ser3-phosphocofilin to total (phosphorylated and unphosphorylated) cofilin was analyzed by western blot detection of cofilin after Phostag SDS-PAGE.

The compound Phostag added to a SDS gel can lead to retardation of the phosphorylated protein as compared to non-phosphorylated protein [113,114]. For cofilin a pan-specific antibody is available that can detect both phosphorylated cofilin and the non-phosphorylated form.

This is especially interesting for cofilin proteins, as these proteins are regulated by phosphorylation on a single serine residue, serine 3 [41]. This modification regulates the actin binding of cofilin proteins, and is regulated, among other phosphatases, by CIN [74].

As controls, calf intestinal phosphatase (CIP) dephosphorylated lysates were loaded on the gels. After CIP treatment, the retarded phosphoprotein band was no longer present. Probing the membrane with a P-Ser3-cofilin specific antibody only yielded the retarded band in the non-dephosphorylated lysate, and no signal in the dephosphorylated lysate (see Fig. 14 A).

When the lysates from GBM6840 control and CIN shRNA cells were probed with the total cofilin antibody after Phostag SDS-PAGE, a substantial increase in the p-cofilin/total cofilin ratio in GBM6840 after CIN knockdown was detectable (see Fig. 14 D).

The p-cofilin/total cofilin ratio increased from 0.24 ± 0.04 in Ctl shRNA cells to 0.41 ± 0.03 in CIN shRNA cells, this difference was statistically significant (two-tailed t-test, $p=0.0155$, $df=6$, $n=4$). Whereas DMSO treatment did not change the p-cofilin content significantly (mean Ctl shRNA + DMSO= 0.23 ± 0.02, two-tailed t-test $p=0.8816$, $df=5$, $n=3$). To check if increased phosphorylation in CIN shRNA cells is dependent on ROCK activity, the cells were treated with the ROCK inhibitor Y-27632. At a concentration of 10 µM Y-27632, the p-cofilin content was reduced back to control levels. Therefore, CIN counteracts the ROCK and LIMK mediated cofilin phosphorylation, the regulatory pathway as shown in figure 4.

There was a significant difference in the p-cofilin/total cofilin ratio between Ctl shRNA and CIN shRNA cells after DMSO treatment (two-tailed t-test, p=0.0169, df=4, n=3), as well as between CIN shRNA cells treated with DMSO or Y-27632 (two-tailed t-test, p=0.0065, df=4).

The cell lines U87 and DBTRG-05-MG contained a higher p-cofilin/total cofilin ratio than GBM6840 cells. In these cell lines, only minor changes of about 5 % of the p-cofilin/total cofilin ratio after CIN deregulation could be detected (see Fig. 14 F).

Nonetheless, the difference was statistically significant in U87 cells (two-tailed t-test, p= 0.0132, n=3, df=4), where the p-cofilin/total cofilin ratio dropped from 0.85 ± 0.009 in cells stably transfected with pIRESNeo2 empty vector to 0.81 ± 0.003 in hCIN expressing cells.

In DBTRG-05-MG cells the p-cofilin/total cofilin ratio increased from 0.73 ± 0.04 in Ctl shRNA cells to 0.79 ± 0.02 in CIN shRNA cells. This difference was not statistically significant (two-tailed t-test, p=0.2497, n=3, df=4).

These experiments established the Phostag based separation of cofilin and p-cofilin as a valuable tool for the quantification of p-cofilin/total cofilin levels.

Furthermore, it was verified that the p-cofilin/total cofilin ratio increased after CIN knockdown and decreased after CIN expression, although it has to be mentioned that the phenotype was rather mild in U87 and DBTRG-05-MG cells.

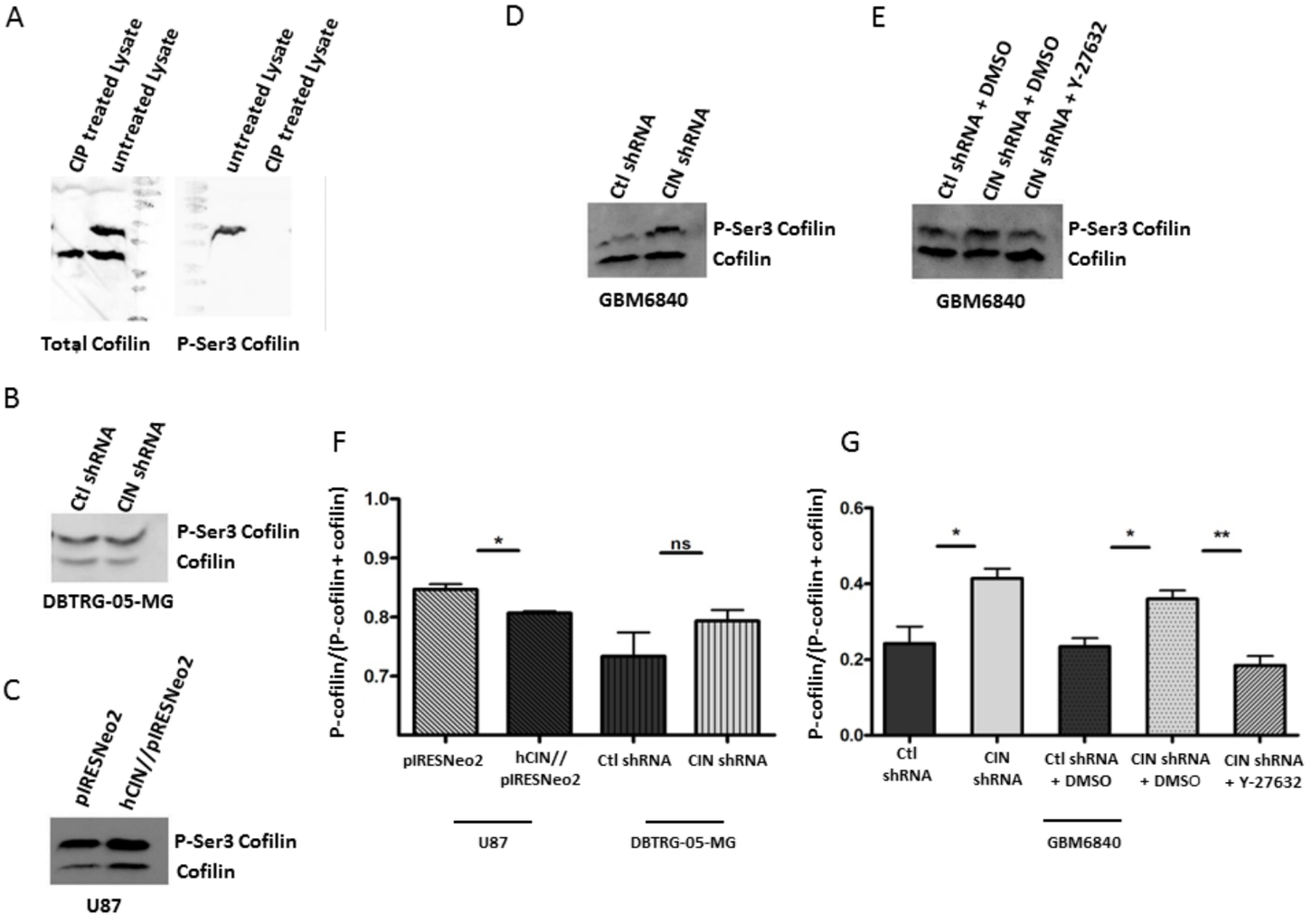

Figure 14: Analysis of cofilin phosphorylation in human glioma cells.
(A) Western blot with α-cofilin antibody after separation of p-cofilin and cofilin by Phostag SDS-PAGE. After Phostag SDS - PAGE and western blot there was a retarded band visible, that was well recognized by the P-Ser3 specific cofilin antibody. This band could be removed by treating the lysate with CIP.
(B) Representative western blot with α-cofilin antibody after Phostag SDS-PAGE in DBTRG-05-MG.
(C) Representative western blot with α-cofilin antibody after Phostag SDS-PAGE in U87.
(D) Representative western blot with α-cofilin antibody after Phostag SDS-PAGE in GBM6840.
(E) Representative western blot with α-cofilin antibody after Phostag SDS-PAGE in GBM6840 after treatment with 10 µM Y-27632 or DMSO (control).
(F) Quantification of n=3 independently harvested lysates as shown in (B) and (C). The p-cofilin/total cofilin ratio decreased after CIN expression in U87 cells, and increased after CIN knockdown in DBTRG-05-MG.
(G) Quantification of n=4 independently harvested lysates as shown in (D), and n=3 as shown in (E). The p-cofilin/total cofilin ratio increased after CIN knockdown. Whereas DMSO treatment had no effect on the p-cofilin/total cofilin ratio, Y-27632 treatment reduced it back to control levels in CIN shRNA cells.

5.3 Regulation of cofilin phosphorylation in human glioma cells

To test which upstream signaling events are able to increase p-cofilin levels as seen after CIN knockdown in glioma cells, substances were applied to GBM6840 cells which are supposed to activate Rac, CDC42 and RhoA respectively. The activation of the small GTPase Rac is well known to induce lamellipodia, CDC42 activation leads to induction of filopodia and RhoA activation induces stress fibers in other cell types [115]. For Rac, 50 ng/ml platelet-derived growth factor BB (PDGFBB) or 100 ng/ml epidermal growth factor (EGF) were used. RhoA activity was stimulated with 1 µM oleoyl-L-α-lysophosphatidic acid (LPA) and CDC42 with 1 µM bradykinin.

Stimulation with EGF and PDGFBB led to intense ruffling activity at the cell edge, indicative of increased Rac activity. After bradykinin stimulation, numerous filopodia were visible, which are well known to form in a CDC42 dependent manner. Finally, after incubation with LPA, an increase in actin stress fibers was observed. Stress fibers are known to form in a RhoA dependent fashion (see Fig. 16, n=3). In conclusion, after stimulation with these substances, the in the literature for fibroblasts reported actin phenotypes were observed in the glioma cells, too [116].

Interestingly, only LPA stimulation, and therefore RhoA activation, was accompanied by a substantial and significant (two-tailed t-test, $p=0.0251$, $df=2$, $n=2$, see Fig. 15 H and I) increase in p-cofilin levels.

To characterize the activity of signaling pathways regulating cofilin phosphorylation in glioma cells, RhoA and Rac 1/2/3 G-Lisa experiments were performed, to measure the levels of active RhoA and Rac 1/2/3. These proteins are, besides CDC42, important nodes in the signaling towards cofilin phosphorylation, and can activate kinases mediating cofilin phosphorylation [46].

Whereas there was no significant difference in Rac 1/2/3 activity (two-tailed t-test, $p=0.6321$, $n=3$ $df=4$, see Fig. 15 A), there was an increase in RhoA activity in CIN shRNA cells as compared to Ctl shRNA cells in GBM6840 (see Fig. 15 B).

Absorbance at 490 nm increased significantly (two-tailed t-test, $p=0.0197$, $n=4$, $df=6$) from 0.34 ± 0.03 in Ctl shRNA cells to 0.44 ± 0.02 in CIN shRNA cells.

Expression of RhoA and Rac 1/2/3 was not significantly different on protein level (RhoA, two-tailed t-test, p= 0.7907, df=6, n=4; Rac 1/2/3, two-tailed t-test, p= 0.5575, df=4; see Fig. 15 D, E, F).

After stable hCIN expression in U87, there was no change in RhoA activity (two-tailed t-test, p=0.9112, df=6, n=4, see Fig. 15 C). In pIRESNeo2 empty vector transfected cells absorbance values were 1.72 ± 0.12 and in hCIN expressing cells 1.71 ± 0.04. The CIN expression was controlled *via* routine western blotting (see Fig. 15 G).

These experiments suggested that Rac activities are not affected by CIN expression levels in glioma cells. In contrast, Rho activities were increased in GBM6840 after CIN knockdown. Moreover, RhoA activation *via* LPA stimulation, but not Rac or CDC42 activation, led to an increase in the p-cofilin/total cofilin ratio, emphasizing the importance of RhoA signaling for the regulation of the p-cofilin/total cofilin level in glioma cells.

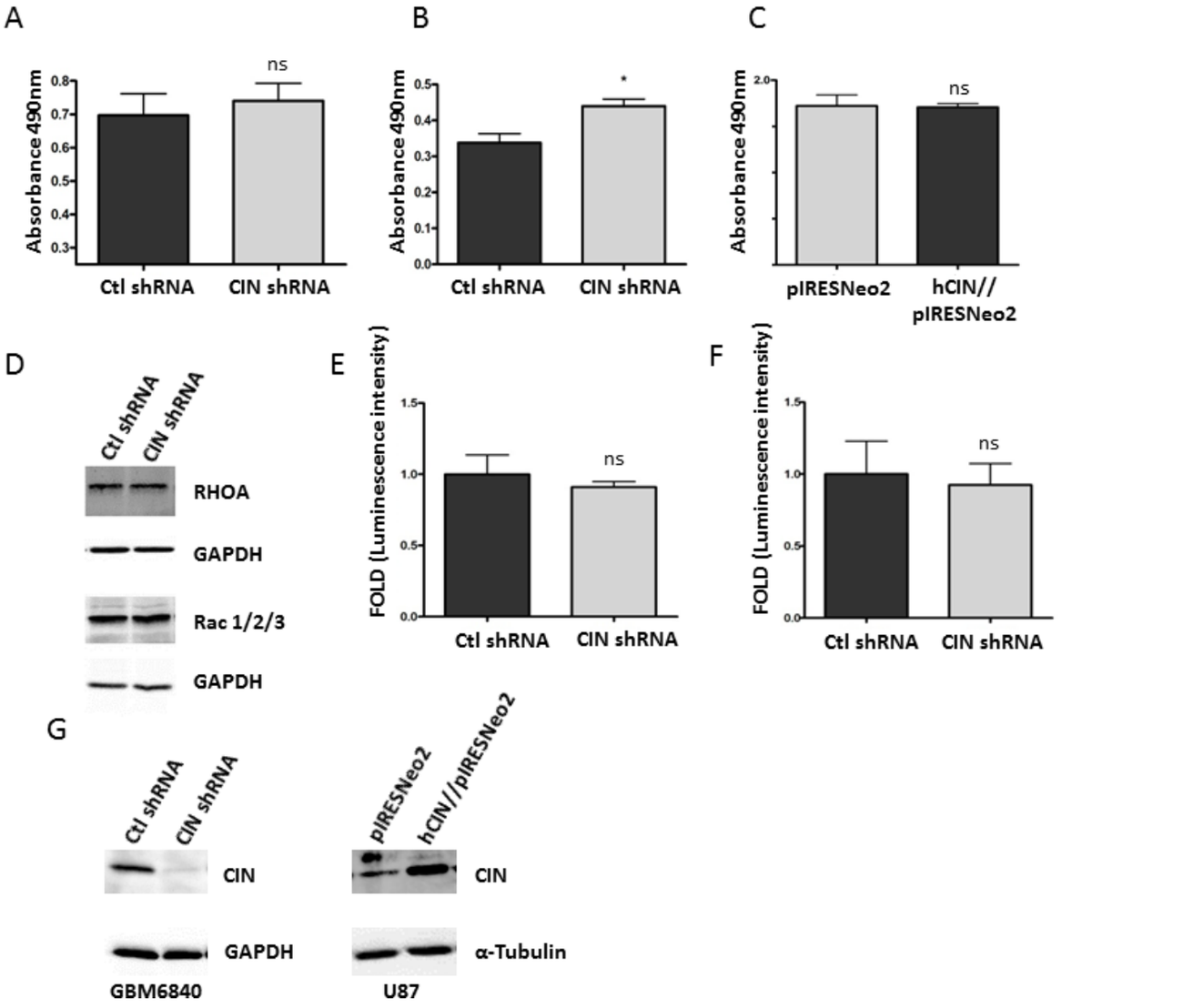
A
Absorbance 490nm
ns
Ctl shRNA
CIN shRNA
B
Absorbance 490nm
*
Ctl shRNA
CIN shRNA
C
Absorbance 490nm
ns
pIRESNeo2
hCIN// pIRESNeo2
D
Ctl shRNA
CIN shRNA
RHOA
GAPDH
Rac 1/2/3
GAPDH
E
FOLD (Luminescence intensity)
ns
Ctl shRNA
CIN shRNA
F
FOLD (Luminescence intensity)
ns
Ctl shRNA
CIN shRNA
G
Ctl shRNA
CIN shRNA
CIN
GAPDH
GBM6840
pIRESNeo2
hCIN//pIRESNeo2
CIN
α-Tubulin
U87

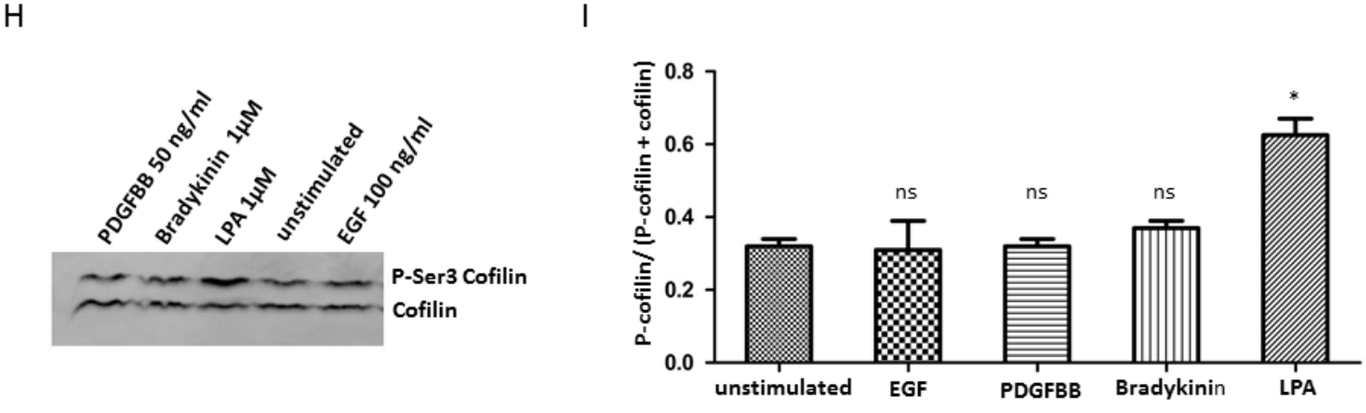
H
PDGFBB 50 ng/ml
Bradykinin 1μM
LPA 1μM
unstimulated
EGF 100 ng/ml
P-Ser3 Cofilin
Cofilin
I
P-cofilin/ (P-cofilin + cofilin)
ns
ns
ns
*
unstimulated
EGF
PDGFBB
Bradykinin
LPA

Figure 15: Regulation of cofilin phosphorylation in human glioma cells.
(A) Quantification of n=3 Rac 1/2/3 G-Lisa experiments in GBM6840. Shown are means + SEM.
(B) Quantification of n=4 RhoA G-Lisa experiments in GBM6840. Shown are means + SEM. There is a significant increase in RhoA activity in CIN shRNA cells.
(C) Quantification of n=3 RhoA G-Lisa experiments in U87. Shown are means + SEM.
(D) Representative western blot with α-RhoA and α-Rac 1/2/3 antibody in GBM6840. GAPDH was used as loading control.
(E) Quantification of n=4 as shown in (D) for RhoA, the intensities were normalized to the GAPDH level.
(F) Quantification of n=3 as shown in (D) for Rac 1/2/3, the intensities were normalized to the GAPDH level.
(G) Representative western blot with α-CIN antibody in GBM6840 and U87, GAPDH or α-Tubulin were used as loading control.
(H) Representative western blot with α-cofilin antibody after Phostag SDS-PAGE and differential stimulation of GBM6840 cells. Only LPA-treatment led to a substantial increase in p-cofilin levels, n=2.
(I) Quantification of n=2 as shown in (H).

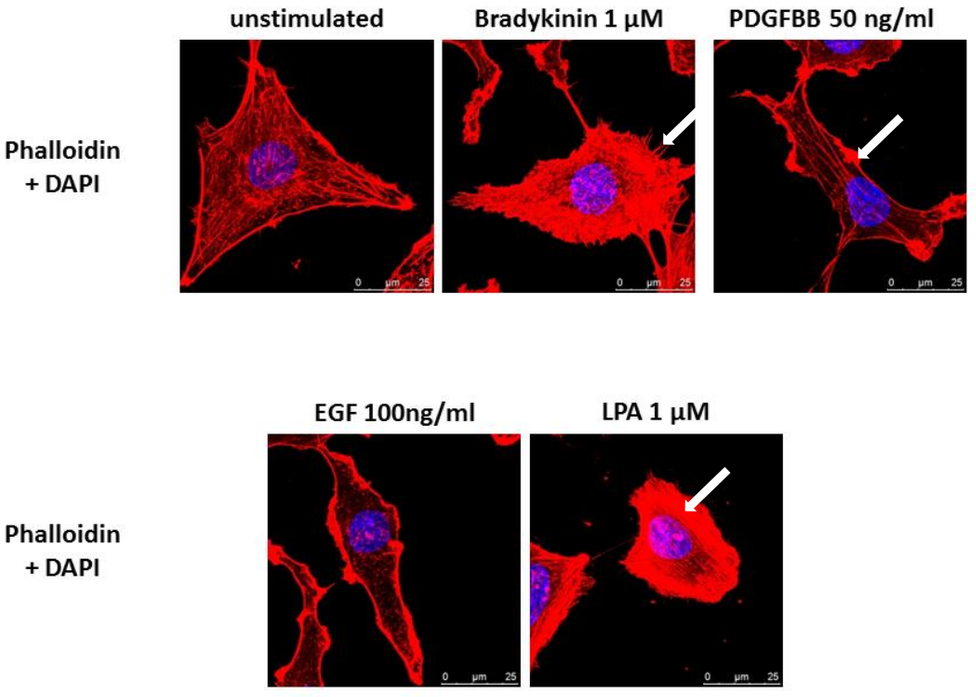

Figure 16: The actin cytoskeleton after stimulation of different small GTPases.
Shown are phalloidin stainings of the actin cytoskeleton in GBM6840.
As compared to control cells, EGF and PDGFBB stimulated cells showed an increase in ruffling activity (arrow). LPA stimulation led to the build up of extensive stress fiber networks (arrow). Bradykinin induced numerous filopodia (arrow). Cells were visualized by confocal microscopy, at least 30 slices were imaged and 3D reconstructions (maximum projection) were calculated from the DAPI and Alexa Fluor 546 phalloidin stainings with the Leica LAS AF software.

5.4 Quantification of F-actin levels *via* flow cytometry

Phosphorylation on serine-3 inhibits the F-actin binding of cofilin, and phosphorylation is therefore a very important mechanism for regulation of its activity [41]. Reduction of cofilin protein levels lead to an increase in total F-actin in carcinoma cells [117].

Levels of total F-actin in glioma cells were determined by flow cytometry. U87 and GBM6840 cells were trypsinized shortly, fixed and stained with fluorescently labeled phalloidin that specifically binds to F-actin.

This technique has been used in adherent cells previously [93]. To test if the measured signals in the trypsinized cells correlated with the F-actin content of the adherent glioma cells, different controls were performed to test if stimulus induced changes of the F-actin content in adherent cells can be measured in the flow cytometry based assay.

1 µM latrunculin A, 250 nM LPA or an equivalent volume of starving medium (unstimulated) were applied to the cells. Latrunculin A sequesters G-actin and inhibits F-actin assembly [118]. In contrast, LPA activates RhoA, and increases stress fiber bundling and the cellular F-actin content [119]. As expected, LPA led to an increase in fluorescence labeling, whereas latrunculin A treatment led to a nearly complete extinction of the signal (see Fig. 17 A and D).

In U87 cells, hCIN expression led to a significant reduction of the phalloidin staining, (two-tailed t-test, $p=0.0094$, $df=4$, $n=3$) from 124.0 ± 6.02 arbitrary units (A.U.) in U87 cells stably transfected with the pIRESNeo2 empty vector to 95.57 ± 0.70 A.U. in cells stably transfected with the hCIN//pIRESNeo2 vector (see Fig. 17 B and E). In GBM6840, the labeling increased significantly after CIN knockdown (two-tailed t-test, $p=0.0176$, $df=6$, $n=4$), from 96.14 ± 6.02 A.U. to 122.0 ± 5.23 A.U. (see Fig. 17 C and E).

CIN expression was examined for every sample *via* routine western blotting (see Fig. 17 F).

These experiments showed that the total F-actin content of U87 and GBM6840 cells is significantly modulated by the cellular CIN level.

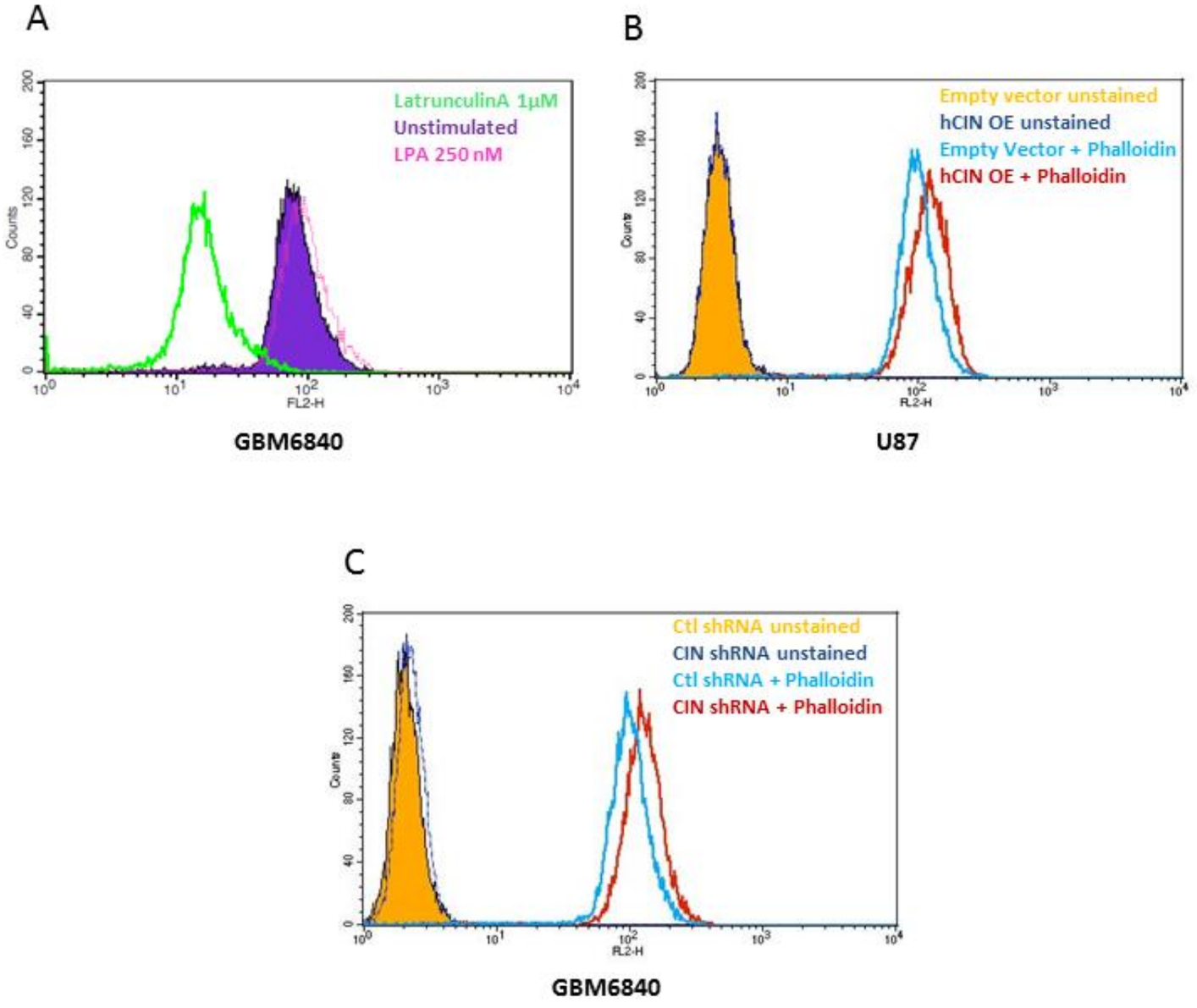
A
LatrunculinA 1µM
Unstimulated
LPA 250 nM
Counts
FL2-H
GBM6840
B
Empty vector unstained
hCIN OE unstained
Empty Vector + Phalloidin
hCIN OE + Phalloidin
Counts
FL2-H
U87
C
Ctl shRNA unstained
CIN shRNA unstained
Ctl shRNA + Phalloidin
CIN shRNA + Phalloidin
Counts
FL2-H
GBM6840

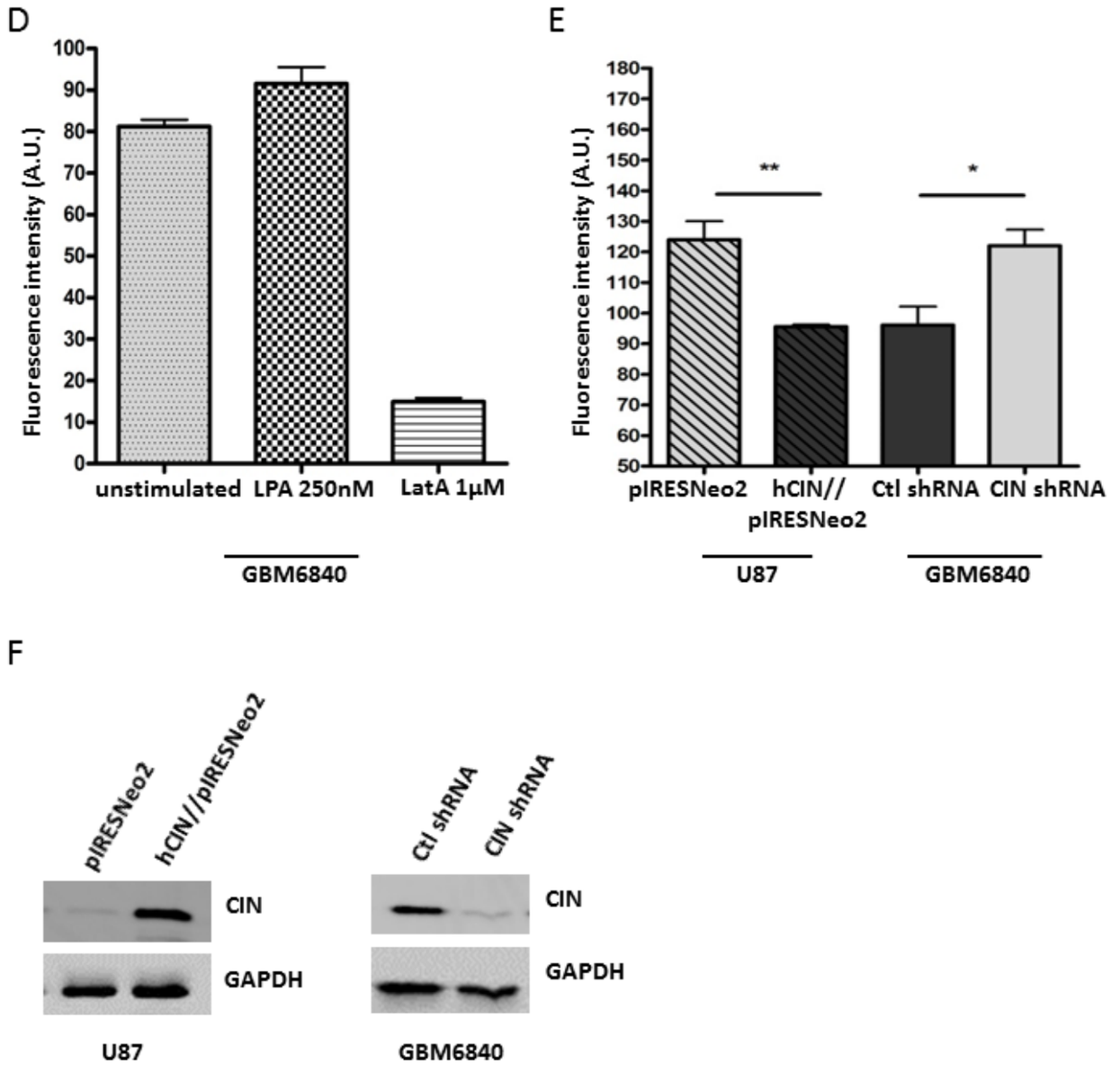

Figure 17: Analysis of F-actin levels *via* FACS based measurement.
(A) Representative histogram of Alexa Fluor 546 phalloidin stained GBM6840 cells after treatment with 1 µM latrunculin A (LatA) or 250 nM LPA for 10´. Latrunculin A treatment drastically reduced the staining intensity, whereas LPA treatment lead to an increase in signal intensity.
(B) Representative histogram of unstained or Alexa Fluor 546 phalloidin stained U87 cells stably transfected with pIRESNeo2 empty vector (referred to as empty vector) or hCIN//pIRESNeo2 (referred to as hCIN OE). hCIN expression led to a reduction in signal intensity.
(C) Representative histogram of GBM6840 cells transduced with Ctl shRNA or CIN shRNA. CIN knockdown led to an increase in signal intensity as compared to Ctl shRNA cells.
(D) Quantification of n=3 as shown in (A).
(E) Quantification of n=3 as shown in (B) and n=4 as shown in (C).
(F) Representative western blot with α-CIN antibody in GBM6840 and U87, GAPDH was used as loading control.

5.5 Analysis of F/G-actin ratios with the spin down assay

The actin spin down assay is based on the separation of cellular G- and F-actin by ultracentrifugation [61]. The G-actin containing supernatant is collected, and the F-actin containing pellet is then resuspended in 8 M urea and the F-actin is depolymerized for 1 h. Afterwards both fractions are run on SDS-PAGE, and the actin content in the fractions and the F/G-actin ratio can be calculated. The advantage compared to the flow cytometry based assay as described in 5.4 is that there is no need for trypsinization. The disadvantage is that the samples have to be centrifuged for 1 h and incubated at 37°C. This long term incubation at a physiological temperature can give rise to changes in the cytoskeletal components.

In U87, hCIN expression led to a reduction in the F/G-actin ratio (two-tailed t-test, p=0.1376, df=4, see Fig. 18 A and C), and CIN knockdown in GBM6840 led to a significant increase in the F/G-actin ratio (two-tailed t-test, p=0.0014, df=4, see Fig. 18 B and D). In line with the results of the flow cytometry based assay, treatment of GBM6840 cells with 1µM LPA for 10´ led to an increase, whereas treatment with 1 µM latrunculin A for 10´ led to a strong reduction in the F/G-actin ratio (see Fig. 18 E and F).

These experiments suggested that the F/G-actin ratio was regulated by the cellular CIN level in GBM6840 and U87, as had been shown for the total F-actin content in 5.4.

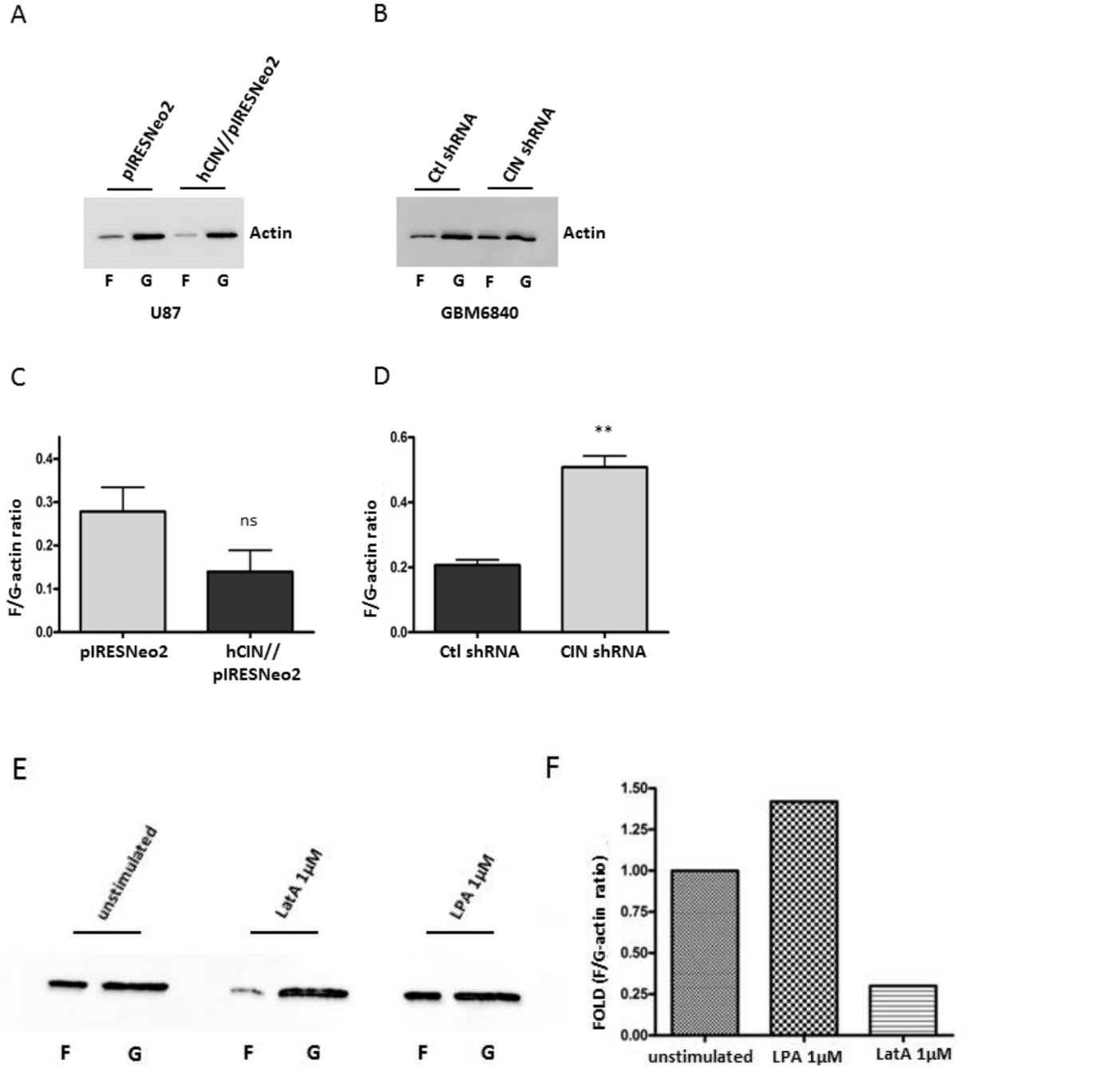

Figure 18: Analysis of F/G-actin ratios in glioma cells *via* actin spin down assay.
(A) Representative western blot with α-ß-actin antibody for F-and G-actin containing fractions of U87 cells stably transfected with pIRESNeo2 or hCIN//pIRESNeo2.
(B) Representative western blot with α-ß-actin antibody for F-and G-actin containing fractions of GBM6840 cells transduced with Ctl shRNA or CIN shRNA encoding plasmids.
(C) Quantification of n=3 as shown in (A).
(D) Quantification of n=3 as shown in (B).
(E) Western blot with α-ß-actin antibody for F-and G-actin containing fractions of GBM6840 cells that were unstimulated or stimulated with LPA or latrunculin A (LatA).
(F) Quantification of the western blot in (E).

5.6 Analysis of SRE reporter activity

The serum response element (SRE) is regulated by the G-actin level in the cell, and SRE activity has been shown to be essential for invasion and experimental metastasis in breast carcinoma and melanoma cells [120]. LIMK activity has been shown to be important for both SRE activity and invasion [121]. Therefore, it was investigated if the knockdown of the functional LIMK antagonist CIN, which led to an altered cellular F/G-actin ratio, was also able to induce changes in SRE activity, possibly contributing to the invasive phenotype of CIN knockdown cells. G-actin binds the serum response factor (SRF) coactivator MAL, and thereby represses SRF activity, although the exact G-actin pool that regulates SRF is not known [122]. The SRE-activity was examined in GBM6840 cells. The assay is based on a firefly luciferase that is expressed from a reporter plasmid under control of a SRE, together with a renilla luciferase that is under control of a constitutively active promoter.

Renilla normalized luminescence intensity in CIN siRNA transfected cells was 0.53 ± 0.09 and substantially lower than in Ctl siRNA transfected cells, which showed a mean intensity of 0.71 ± 0.06 (two-tailed t-test, p=0.2583, df=2, n=2). There was no major difference in Ctl siRNA transfected cells with a mean intensity of 0.07 ± 0.01 and 0.11 ± 0.06 in CIN siRNA transfected in the negative control (see Fig. 19, n=2).

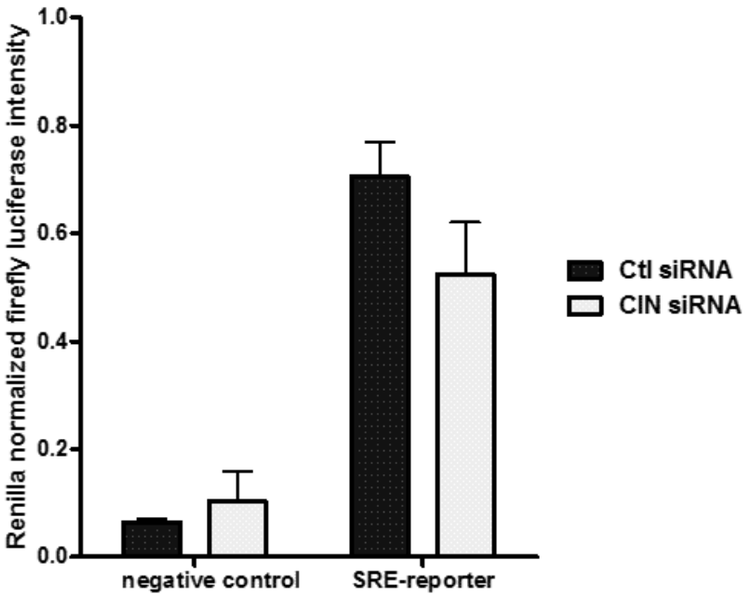

Figure 19: SRE-reporter activity assay in GBM6840.
After transfection with a CIN siRNA reporter activity was reduced as compared to Ctl cells. Shown are means + SEM.

5.7 Changes in the actin cytoskeleton after CIN deregulation

Cofilin is a central regulator of the dynamics of the actin cytoskeleton [36] that is regulated by CIN. In quantitative assays, a significant increase in total F-actin (see 5.4) and an increase in the F/G-actin ratio (see 5.5) were found after CIN knockdown. The opposite phenotype was observed after hCIN expression in U87, as expected.

To investigate where the F-actin accumulates, standard immunocytochemistry with fluorescently labeled phalloidin was performed that selectively labels F-actin, to detect qualitative changes in the actin cytoskeleton.

Interestingly, the hCIN overexpressing U87 cells showed a very dramatic phenotype. The cytoplasmic F-actin and the stress fibers, which were pronounced in control cells, were nearly completely dissolved. After CIN knockdown in GBM6840 cells, an increase in stress fibers could be detected.

Furthermore, a loss of these F-actin structures was seen both after ROCK-inhibitor treatment as has been reported previously [68], and after expression of a RNAi resistant hCIN construct in GBM6840 CIN shRNA cells (see Fig. 20). However, no obvious shape change occurred after CIN deregulation.

Taken together, through the use of immunocytochemistry a loss of stress fibers was correlated with higher CIN expression in GBM6840 and U87. Importantly, the increased stress fiber content after CIN knockdown was reduced after treatment with the ROCK inhibitor Y-27632.

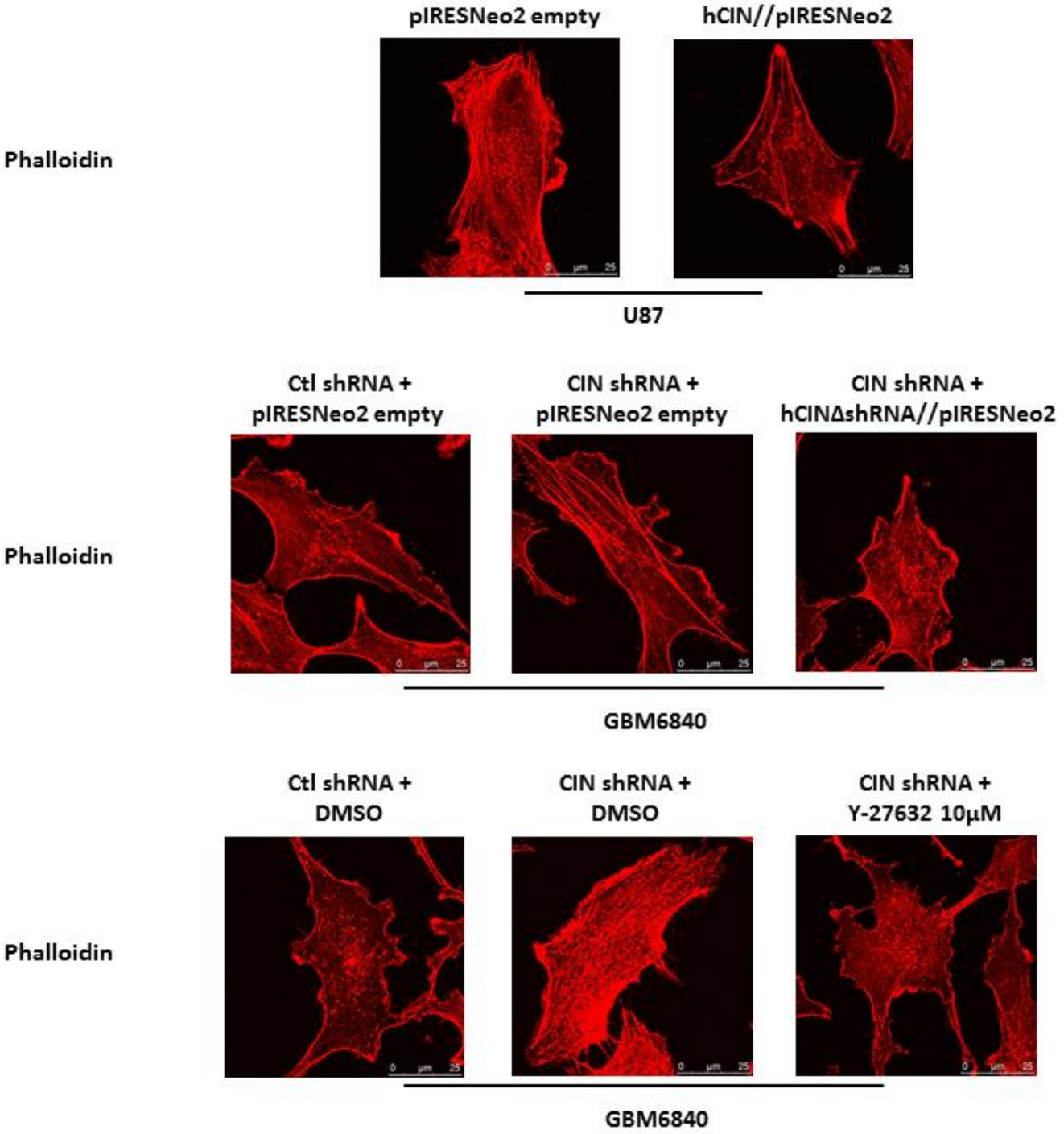

Figure 20: The actin cytoskeleton after CIN deregulation or ROCK-inhibition.

In U87 cells, a dramatic loss of cytoplasmic F-actin and stress fibers was present after expression of hCIN (upper panel). In GBM6840 cells, CIN knockdown led to an increase of these F-actin structures. The phenotype of GBM6840 cells could be reverted by expression of an RNAi resistant hCIN construct (hCINΔshRNA; middle panel) and by ROCK-inhibitor treatment (bottom panel). The pictures shown are maximum projections of at least 30 sections in the z-axis of slice thickness 0.7 µm.

5.8 Analysis of the cofilin phosphorylation pathway in Rembrandt

The cancer genome project provides a wealth of expression data for glioma, as well as information on copy number alterations and mutations [107].

This makes it possible to check the relative expression of the members of the cofilin phosphorylation pathway on mRNA level in normal brain and in GBM tissue. The Rembrandt database was accessed, and the pathway members CFL1, LIMK1, LIMK2, CIN, RhoA, RhoB, RhoC, ROCK1 and ROCK2, as well as the important RhoC effector FMNL3 were analyzed [123]. The downloaded data included 28 normal brain samples and 221 GBM samples.

Upregulated (> 1.5 x) were LIMK2, ROCK1, RhoA and RhoC. Whereas there was no major change of the expression of CFL1, FMNL3, LIMK1 or ROCK2 and SSH genes, CIN was strongly downregulated (see table 6).

Table 6: Gene expression analysis based on Rembrandt.

Normal Brain	Relative Expression in GBM	Symbol	Probe Set
1.00	1.11	CFL1	1555730_a_at
1.00	1.06	CFL1	200021_at
1.00	1,30	FMNL3	227844_at
1.00	1.45	FMNL3	231231_at
1.00	0.84	FMNL3	232249_at
1.00	1.19	FMNL3	238823_at
1.00	0.66	LIMK1	204356_at
1.00	2.27	LIMK2	202193_at
1.00	1.58	RhoA	1555814_a_at
1.00	0.85	RhoA	240337_at
1.00	0.88	RhoB	1553963_at
1.00	1.22	RhoB	212099_at
1.00	0.96	RhoB	226417_at
1.00	4.03	RhoC	200885_at
1.00	4.55	RhoC	235742_at
1.00	1.87	ROCK1	213044_at
1.00	0.80	ROCK1	230239_at
1.00	0.77	ROCK2	202762_at
1.00	1.24	SSH1	1554274_a_at
1.00	1.30	SSH1	1555624_a_at
1.00	0.90	SSH1	221752_at
1.00	0.93	SSH1	221753_at
1.00	1.10	SSH2	1555423_at
1.00	0.89	SSH2	226080_at
1.00	1.08	SSH3	51192_at
1.00	0.36	CIN	223290_at

5.9 Chemotaxis analysis on collagen IV

Actin reorganization regulated by cofilin has been shown to be essential for chemotaxis in mammary carcinoma cells [59]. In metastatic mammary carcinoma cells, reorientation towards the chemoattractant is lost after increasing cofilin phosphorylation by LIMK overexpression [124]. Therefore, the chemotactic behavior of glioma cells after CIN knockdown was analyzed. GBM6840 cells were seeded on collagen IV coated µ-slide chemotaxis chambers. 10 % fetal calf serum (FCS) or 100 ng/ml EGF were then added as chemoattractant (n=1 and n=3, respectively). Both GBM6840 Ctl shRNA and CIN shRNA cells were able to chemotax towards FCS (see Fig. 21 A and B) and there was no obvious difference in their chemotactic behavior. In contrast to FCS, GBM6840 cells showed no major chemotactical response towards EGF (see Fig. 21 C and D). The calculated forward migration index was -0.02 ± 0.04 in CIN shRNA cells and 0.001 ± 0.035 in GBM6840 Ctl shRNA cells, and therefore not significantly different from zero in both cell lines. A forward migration index close to zero indicates that no chemotaxis has taken place.

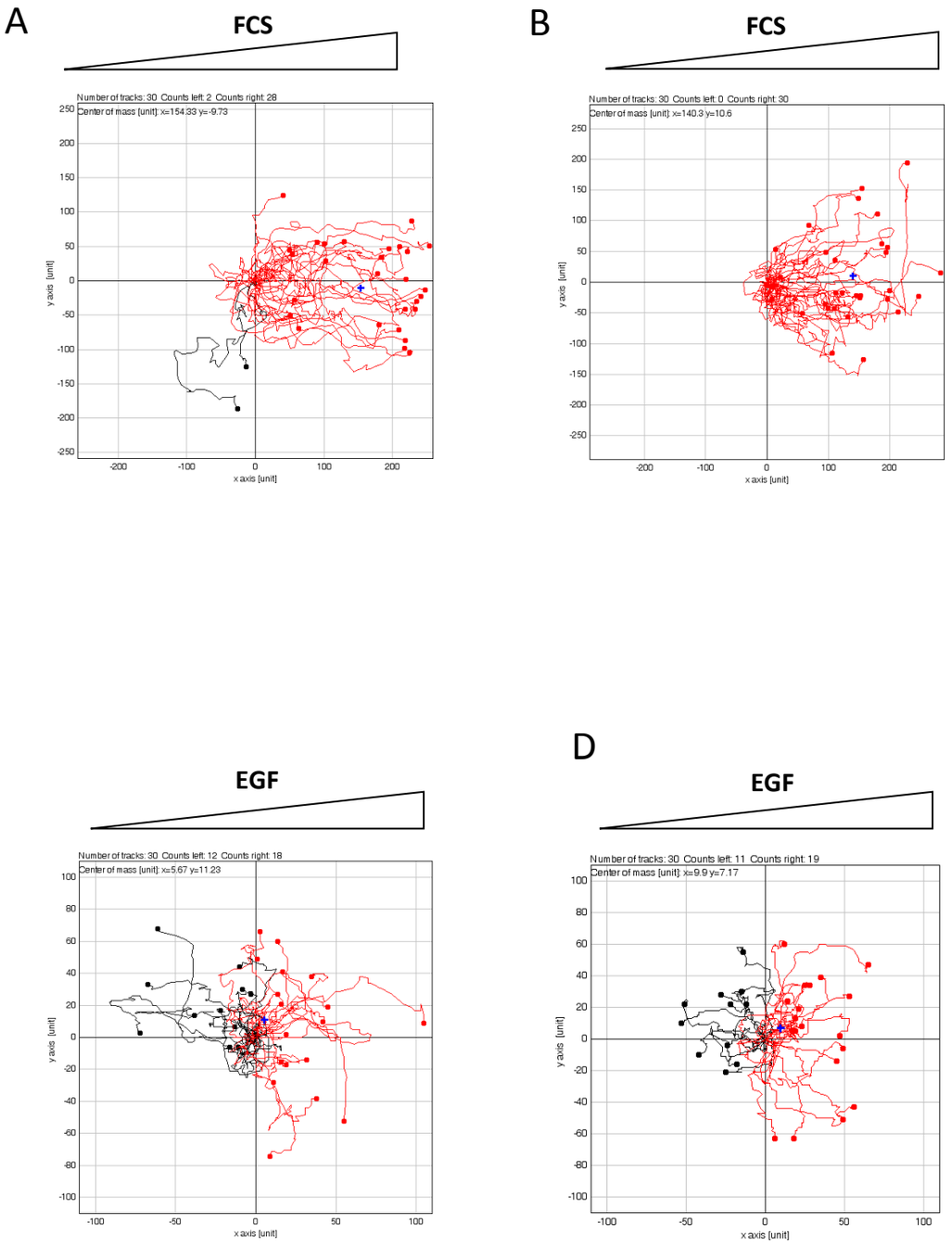

Fig. 21: Analysis of the chemotactical behavior of GBM6840 cells.
(A, B) Rose-plots of the individual tracks of 30 control (Ctl) or chronophin (CIN) shRNA cells in a gradient of FCS.
(C, D) Representative rose-plots of the individual tracks of 30 control (Ctl) or chronophin (CIN) shRNA cells in a gradient of EGF.

5.10 Analysis of cell migration after CIN deregulation in 2D environments

As stated in 5.9, no chemotactic response was seen after application of a gradient of EGF in GBM6840 cells. However, the GBM6840 CIN shRNA cells seemed to migrate in a different, slower but more directional way, as can be seen in Fig. 21 C and D. We therefore quantified speed and directionality of glioma cells in a 2D environment. No chemotactical gradient was applied due to the technical limitations of the 8-well setup, but cellular integrins were stimulated with the collagen IV coating used in all assays. Due to the limited geometry of the chemotaxis chambers, only 30 randomly chosen cells could be analyzed on these chambers. For the quantifications of U87 cells, inhibitor-assays and GFP-expressing cells, at least 50 randomly chosen cells were analyzed for each condition. Immotile (or non-motile) cells and cells that divided during the observation period were excluded from the analysis. Immotile cells were defined as cells that did not migrate more than one cell perimeter during the observation period.

Indeed, quantification of the migratory parameters revealed that there was a significant drop in speed (two-tailed t-test, $p=0.0285$, $n=3$, $df=4$), but an increase in directionality (two-tailed t-test, $p=0.0161$, $n=3$, $df=4$, see Fig. 22 A and B) in GBM6840 cells after CIN knockdown.

In U87 cells, a significant increase in speed could be detected after expression of hCIN (two-tailed t-test, $p=0.0099$, $n=3$, $df=4$), accompanied by a loss of directionality (two-tailed t-test, $p=0.061$, $n=3$, $df=4$, see Fig. 22 C and D).

After treatment of the cell line GBM6840 with the ROCK-inhibitors fasudil and Y-27632 at a concentration of 10 µM, a significant increase in speed could be detected (two-tailed t-test, $p=0.0062$ and 0.0020 respectively, $n=3$, $df=4$), but directionality was decreased as compared to the DMSO treated control samples (two-tailed t-test, $p=0.0232$ and 0.03450 respectively, $n=3$, $df=4$, see Fig. 22 E and F).

The phenotype that was measured in the chemotaxis setup as seen in Fig. 22, could be nicely reproduced with GFP-expressing Ctl shRNA and CIN shRNA GBM6840 cells (see Fig. 22 H and I).

Expression of a constitutively active, non-phosphorylatable CFL1 mutant (CFL1-S3A) [125] fused to GFP, was able to rescue the phenotype. Both an increase in speed and a decrease in directionality were seen after CFL1-S3A expression in GBM6840 CIN shRNA cells (see Fig. 22 H and I). Expression levels of CIN and GFP were examined by routine western blotting for every experiment (see Fig. 22 G and J).

These results pointed towards a specific involvement of CIN in 2D migration, which is mediated by its effect on cofilin phosphorylation.

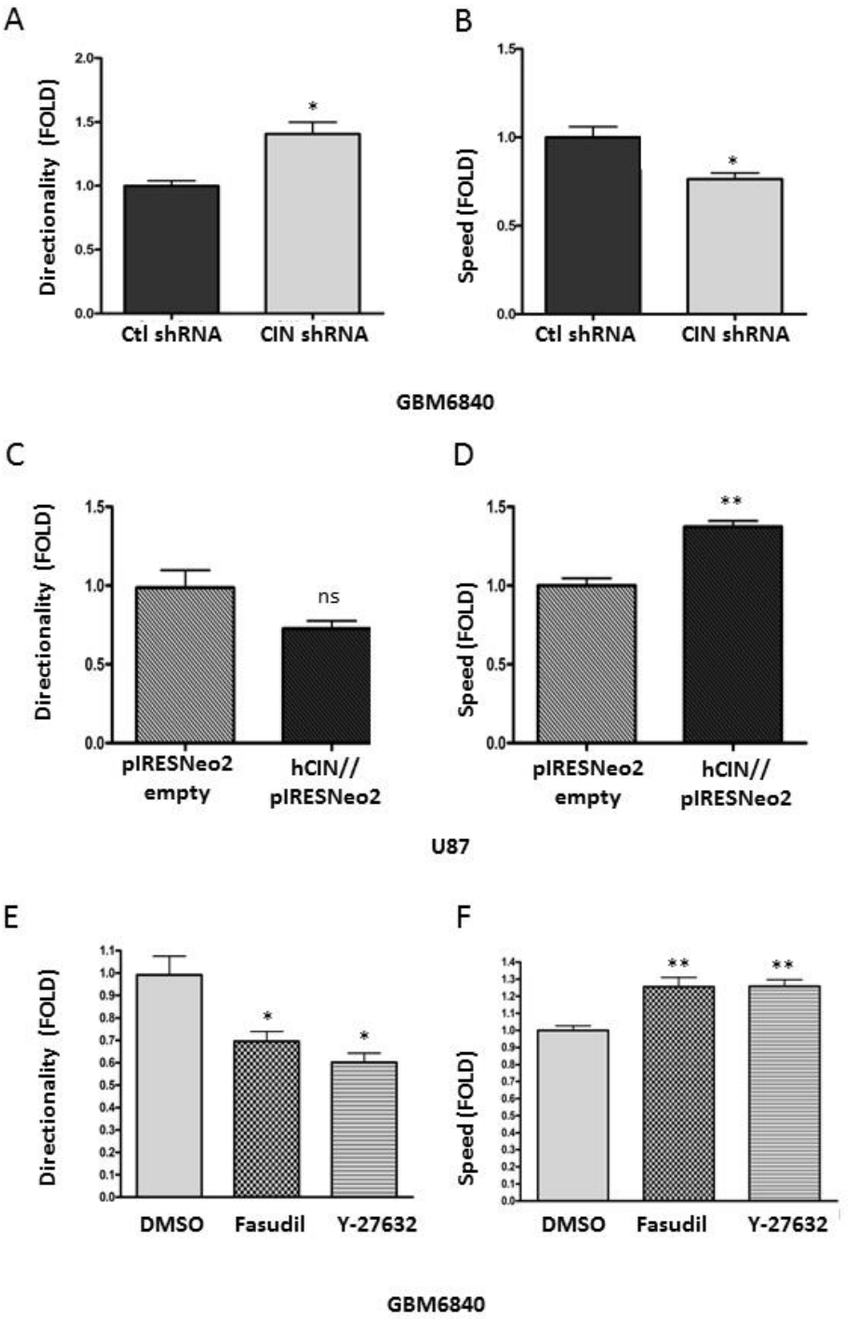

G

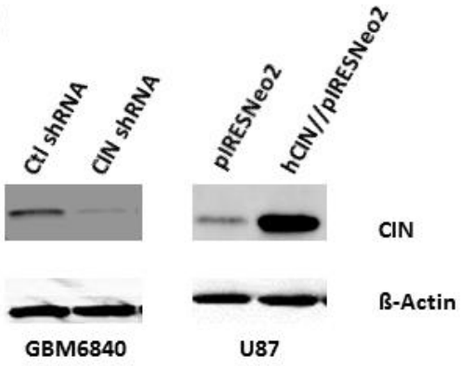
Ctl shRNA
CIN shRNA
pIRESNeo2
hCIN//pIRESNeo2
CIN
ß-Actin
GBM6840
U87

H

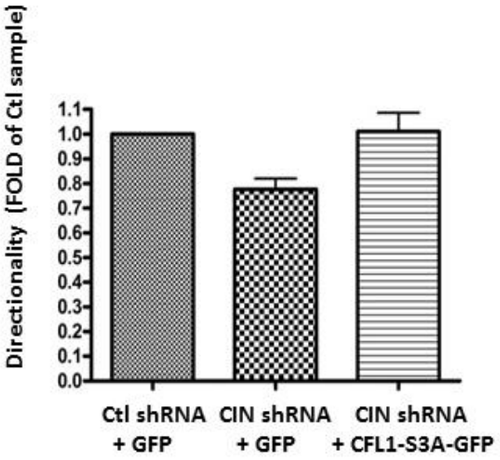
Directionality (FOLD of Ctl sample)
1.1
1.0
0.9
0.8
0.7
0.6
0.5
0.4
0.3
0.2
0.1
0.0
Ctl shRNA + GFP
CIN shRNA + GFP
CIN shRNA + CFL1-S3A-GFP

I

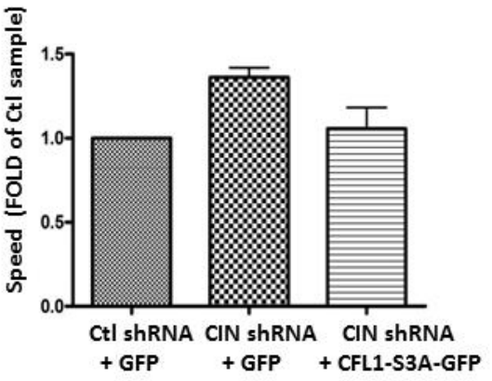
Speed (FOLD of Ctl sample)
1.5
1.0
0.5
0.0
Ctl shRNA + GFP
CIN shRNA + GFP
CIN shRNA + CFL1-S3A-GFP

J

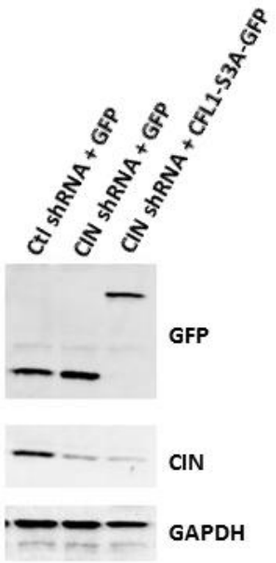
Ctl shRNA + GFP
CIN shRNA + GFP
CIN shRNA + CFL1-S3A-GFP
GFP
CIN
GAPDH

Figure 22: Analysis of glioma cell migration in a 2D environment.
(A) Quantification of the directionality on collagen IV coated µ-slide chemotaxis chambers in GBM6840, n=3, shown are means + SEM.
(B) Quantification of the speed on collagen IV coated µ-slide chemotaxis chambers in GBM6840, n=3, shown are means + SEM.
(C) Quantification of the directionality on collagen IV coated eight-well slides in U87 cells, n=3, shown are means + SEM.
(D) Quantification of the speed on collagen IV coated eight-well slides in U87 cells, n=3, shown are means + SEM.
(E) Quantification of the directionality on collagen IV coated eight-well slides in GBM6840 after DMSO (control) or ROCK-inhibitor treatment.
(F) Quantification of the speed on collagen IV coated eight-well slides in GBM6840 after DMSO (control) or ROCK-inhibitor treatment.
(G) Representative western blot with α-CIN antibody for 2D migration experiments, GAPDH was used as loading control.
(H) Quantification of the directionality on collagen IV coated eight-well slides in Ctl shRNA + GFP, CIN shRNA + GFP and CIN shRNA + CFL1-S3A-GFP expressing GBM6840 cells, n=3.
(I) Quantification of the directionality on collagen IV coated eight-well slides in Ctl shRNA + GFP, CIN shRNA + GFP and CIN shRNA + CFL1-S3A-GFP expressing GBM6840 cells, n=3.
(J) Representative western blot with α-CIN and α-GFP antibody, GAPDH was used as loading control.

5.11 Analysis of cell invasion in the transwell setup

The cell lines GBM6840, U87 and DBTRG-05-MG were tested for their invasive potential in a matrigel invasion assay after CIN deregulation. In this assay the cells migrate across a porous membrane in a gradient of EGF, and have to cross a barrier of ECM-molecules. The cells were incubated for 24 h after seeding onto the upper compartment of the transwell insert, and the concentration of EGF in the lower chamber was 100 ng/ml.

Reduction of CIN levels *via* shRNA mediated knockdown increased the invasive capacity of DBTRG-05-MG cells significantly (Kruskal-Wallis test, p=0.02092, df=1, see Fig. 23 A and E). The invasiveness of GBM6840 cells was significantly higher after CIN knockdown (Kruskal-Wallis test, p-value = 0.04953, df=1), whereas the difference between hCINΔshRNA expressing CIN shRNA cells and Ctl shRNA cells was not significant (Kruskal-Wallis test, p-value = 0.2752, df=1, see Fig. 23 C and D).

In U87 cells, expression of a human full length CIN led to a significant reduction of the number of invasive cells (Kruskal-Wallis test, p-value = 0.04953, df=1, see Fig. 23 B and F).

Furthermore, it was tested if treatment with a ROCK-Inhibitor or expression of a constitutively active CFL1 mutant (CFL1-S3A-GFP) could rescue the pro-invasive phenotype in GBM6840 cells that was observed upon shRNA-mediated chronophin depletion. Treatment with the ROCK-inhibitor Y-27632 at a concentration of 10 µM (see Fig. 23 H) as well as expression of the CFL1-S3A-GFP mutant (see Fig. 23 I) reduced the increased invasion of chronophin-depleted GBM6840 cells back to control levels. CIN and GFP expression were examined for each experiment *via* routine western blotting (see Fig. 23 G and K). Expression of CFL1-GFP, CFL1-S3A-GFP and CFL1-S3E-GFP alone in GBM6840 cells had no influence on the invasiveness (see Fig. 23 M).

Taken together, these results suggested a strong and cell line independent effect of CIN expression on invasion. The increased invasiveness was dependent on active ROCK signaling and increased cofilin phosphorylation after CIN knockdown.

A

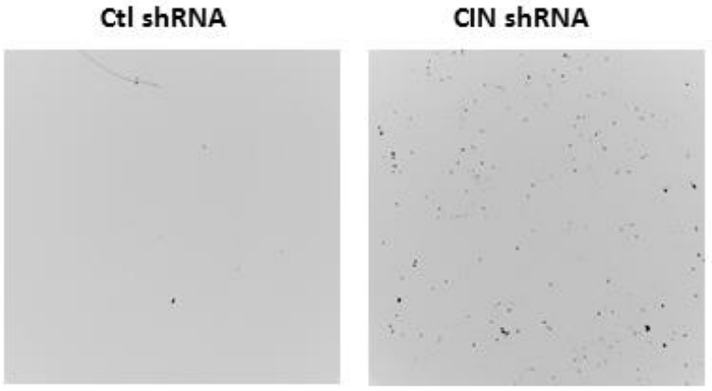

B

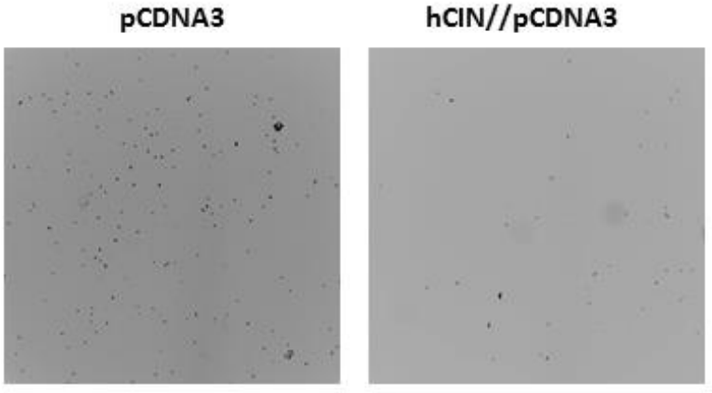

U87

C

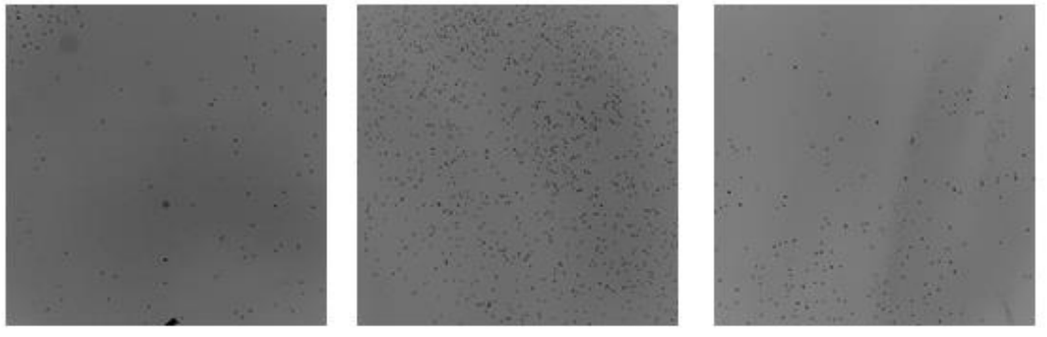

GBM6840

D

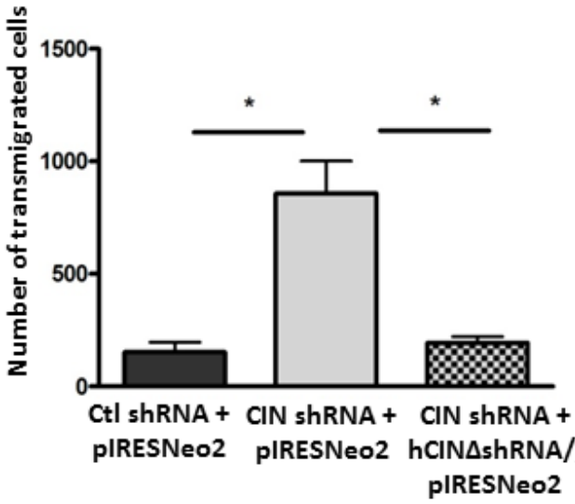
Number of transmigrated cells
1500
1000
500
0
*
*
Ctl shRNA + pIRESNeo2
CIN shRNA + pIRESNeo2
CIN shRNA + hCINΔshRNA// pIRESNeo2

E

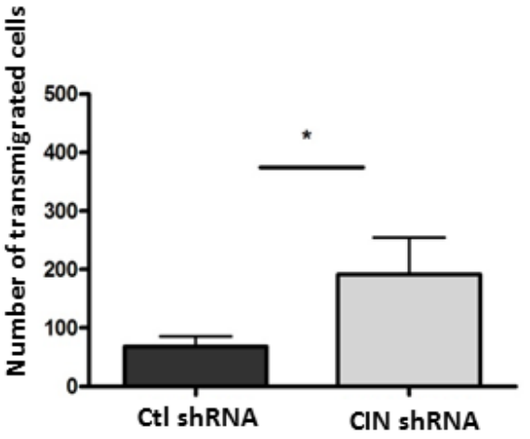
Number of transmigrated cells
500
400
300
200
100
0
*
Ctl shRNA
CIN shRNA

F

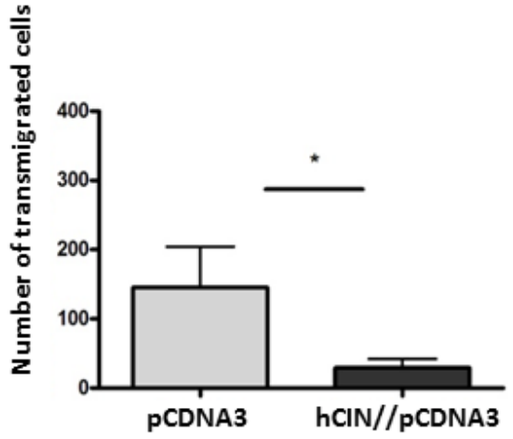
Number of transmigrated cells
400
300
200
100
0
*
pCDNA3
hCIN//pCDNA3

G

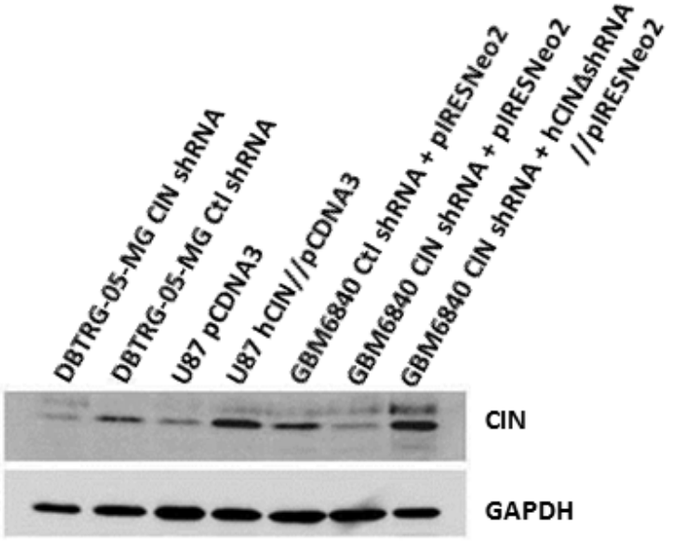
DBTRG-05-MG CIN shRNA
DBTRG-05-MG Ctl shRNA
U87 pCDNA3
U87 hCIN//pCDNA3
GBM6840 Ctl shRNA + pIRESNeo2
GBM6840 CIN shRNA + pIRESNeo2
GBM6840 CIN shRNA + hCINΔshRNA //pIRESNeo2
CIN
GAPDH

H

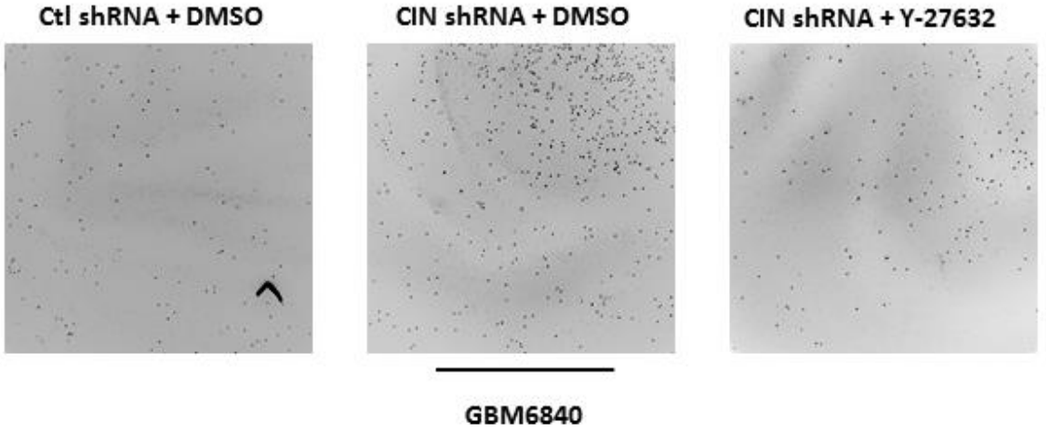
Ctl shRNA + DMSO
CIN shRNA + DMSO
CIN shRNA + Y-27632
GBM6840

I

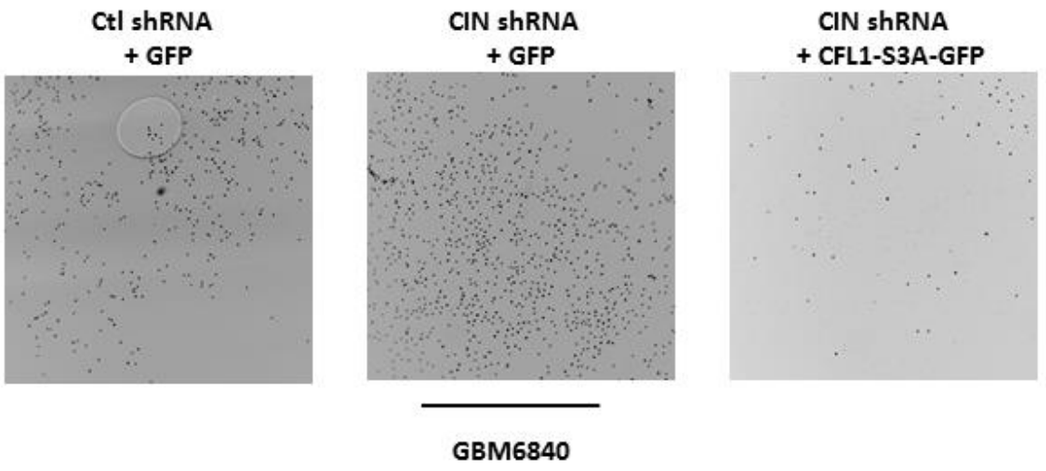
Ctl shRNA
+ GFP
CIN shRNA
+ GFP
CIN shRNA
+ CFL1-S3A-GFP
GBM6840

J

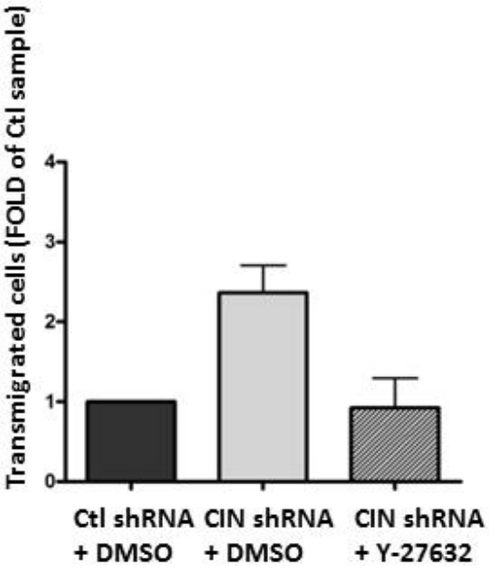
Transmigrated cells (FOLD of Ctl sample)
0
1
2
3
4
Ctl shRNA + DMSO
CIN shRNA + DMSO
CIN shRNA + Y-27632

K

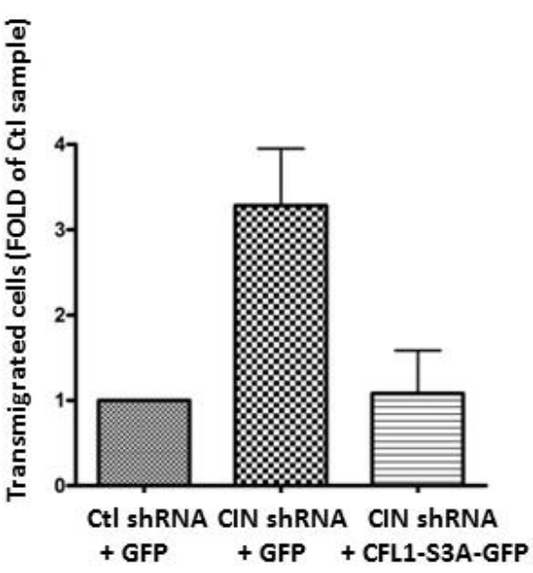
Transmigrated cells (FOLD of Ctl sample)
0
1
2
3
4
Ctl shRNA + GFP
CIN shRNA + GFP
CIN shRNA + CFL1-S3A-GFP

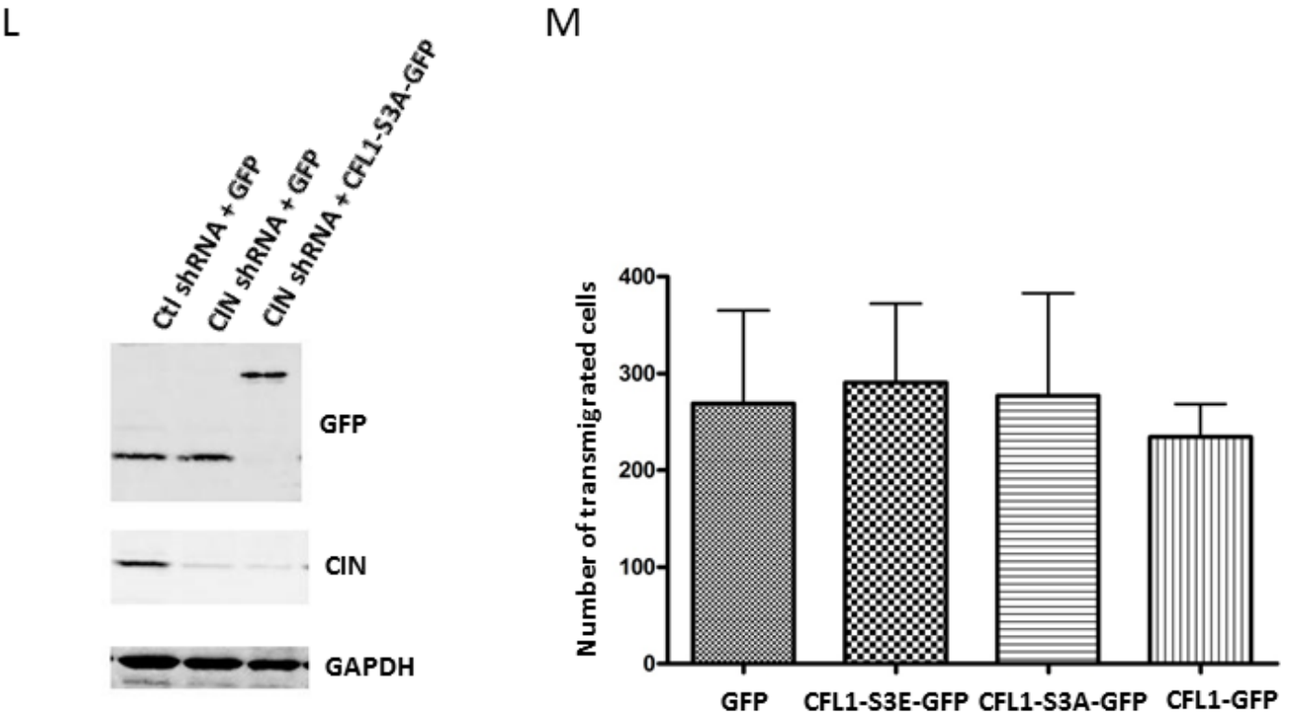

Figure 23: Analysis of glioma cell invasion in the transwell system.
(A) Representative DAPI stained membranes of a matrigel invasion assay in DBTRG-05-MG.
(B) Representative DAPI stained membranes of a matrigel invasion assay in U87.
(C) Representative DAPI stained membranes of a matrigel invasion assay in GBM6840.
(D) Quantification of n=3 as shown in (C).
(E) Quantification of n=4 as shown in (A).
(F) Quantification of n=3 as shown in (B).
(G) Representative western blot with α-CIN antibody, GAPDH was used as loading control.
(H) Representative DAPI stained membranes of a matrigel invasion assay in GBM6840 after Y-27632 or DMSO (control) treatment.
(I) Representative DAPI stained membranes of a matrigel invasion assay in GBM6840 cells expressing Ctl shRNA + GFP, CIN shRNA + GFP and CIN shRNA + CFL1-S3A-GFP.
(J) Quantification of n=3 as shown in (H).
(K) Quantification of n=4 as shown in (I).
(L) Representative western blot with α-CIN and α-GFP antibody, GAPDH was used as loading control.
(M) Quantification of transwell assays with GBM6840 cells expressing GFP, a CFL1 WT-GFP fusion construct, a CFL1-S3A constitutively active mutant and a CFL1-S3E inactive mutant fused to GFP, n=4.

5.12 Regulation of proteases on mRNA and protein level

Different proteases increase glioma cell invasion by dissolving the ECM and releasing growth factors bound to the ECM. Well known to be involved in glioma invasion are MMP2, MMP9, MMP14, CathepsinB, and the uPA-uPAR system [126]. The expression of some of those proteases has already been linked to the phospho regulation of the cofilin protein. MMP2 downregulation has been found after treatment with the ROCK-inhibitor fasudil in glioma cells [67]. An increased expression of uPA and uPAR has been found after overexpression of catalytically active LIMK1 in breast cancer cells [127].

Therefore, GBM6840 cells were analyzed for expression of these proteases after CIN knockdown. However, the expression of MMP2, MMP9, MMP14 and uPA was not altered on the mRNA- and protein-level in Ctl shRNA and CIN shRNA cells (see Fig. 24 A, B, C and D). CatpepsinB could be examined only on mRNA level, but was not significantly altered, too (see Fig. 24 A and B).

A mild but statistically significant uPAR overexpression was detectable on mRNA and protein level in GBM6840. However, this uPAR overexpression was not found in chronophin-depleted DBTRG-05-MG cells, or in U87 cells compared to U87 cells reexpressing CIN (see Fig. 24 E).

A

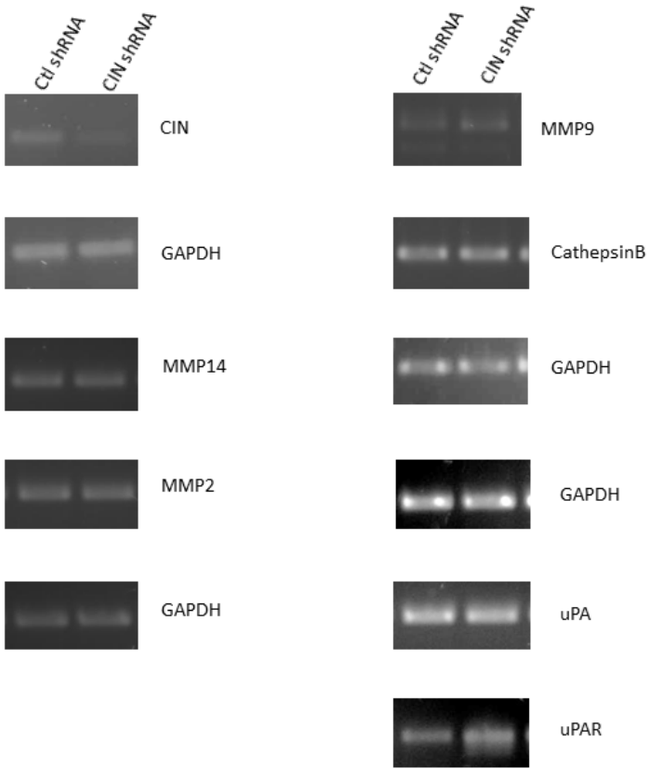
Ctl shRNA
CIN shRNA
CIN
GAPDH
MMP14
MMP2
GAPDH
Ctl shRNA
CIN shRNA
MMP9
CathepsinB
GAPDH
GAPDH
uPA
uPAR

B

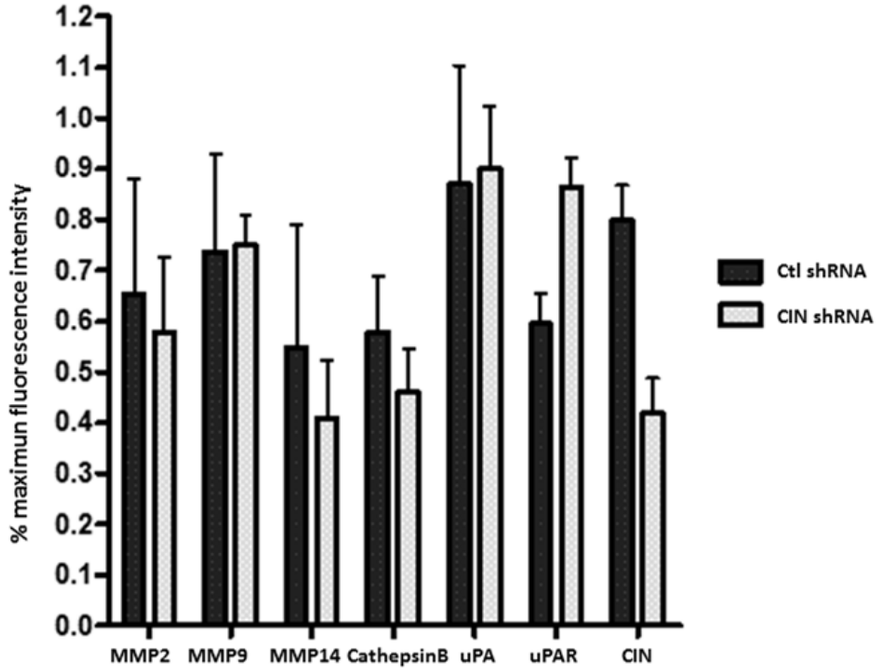
% maximun fluorescence intensity
1.2
1.1
1.0
0.9
0.8
0.7
0.6
0.5
0.4
0.3
0.2
0.1
0.0
MMP2
MMP9
MMP14
CathepsinB
uPA
uPAR
CIN
Ctl shRNA
CIN shRNA

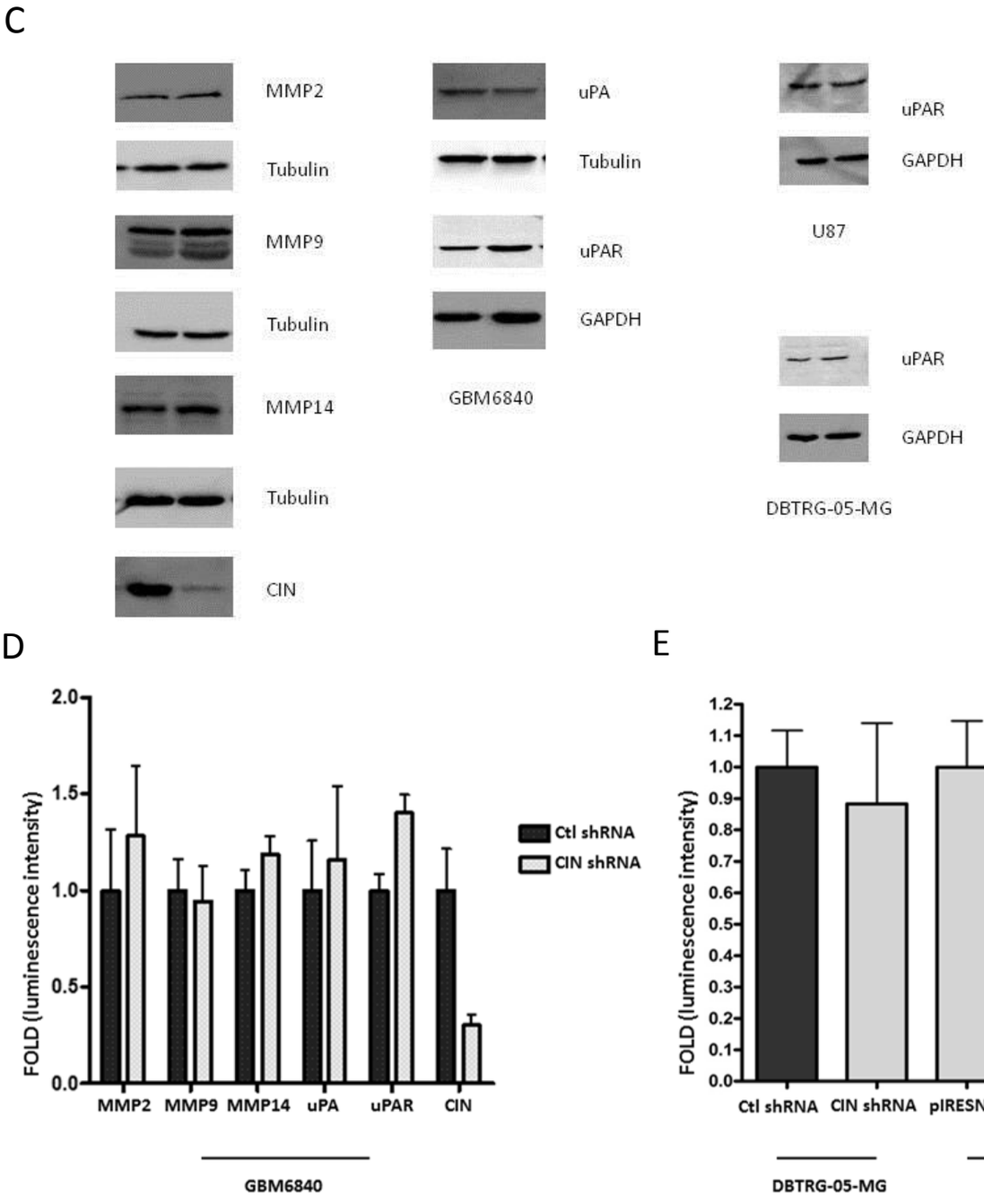

Figure 24: Analysis of protease expression after CIN knockdown.
(A) Representative ethidium bromide stained agarose gels for the PCR analysis of MMP2, MMP14, MMP9, uPA, uPAR, CathepsinB and CIN. GAPDH was used as loading control.
(B) Quantification of n=3 as shown in (A). CIN is efficiently downregulated in CIN shRNA cells as compared to Ctl shRNA cells. There are no significant differences in the expression of MMP2, MMP14, MMP9, uPA und CathepsinB. uPAR is upregulated after CIN knockdown. Shown are means + SEM.
(C) Western blots for MMP2, MMP14, MMP9, uPA and uPAR in GBM6840. In DBTRG-05-MG and U87 only uPAR expression was examined. GAPDH or α-Tubulin were used as loading control.
(D) Quantification of n=3 as shown in (C) for MMP2, MMP14, MMP9, uPA and uPAR in GBM6840. The intensities of the bands were normalized to the GAPDH or α-Tubulin level, and the mean intensity in the three control samples was set to one. Shown are means + SEM.
(E) Quantification of n=3 for uPAR in DBTRG-05-MG and U87 as shown in (C) U87 cells were transfected with pCDNA3 empty vector (EV) or a hCIN encoding plasmid. Shown are means + SEM.

5.13 Live-analysis of proliferation after CIN deregulation using Hoechst 33342

Differences in proliferation can impact the results of the transwell assay as shown in 5.11. LIMK1 overexpression can repress the growth of fibroblasts in cell culture [128].

Therefore, the cell lines GBM6840, DBTRG-05-MG and U87 were tested for their proliferation speed. For that purpose, cells were seeded at low density on 96-well plates, one well from every condition was stained with Hoechst 33342 every day and pictures were taken.

Hoechst is a DNA binding dye that is suitable to stain the DNA of living cells in culture [129], and allows automatic counting of the cell numbers. Within the observation period of five days, all cell lines were proliferating robustly (see Fig. 25 A), although with different doubling time, as has already been reported in the literature [97,98]. However, deregulation of CIN did not affect the proliferation of any cell line (see Fig. 25 C). The knockdown and the expression of CIN were verified by routine western blotting (see Fig. 25 B)

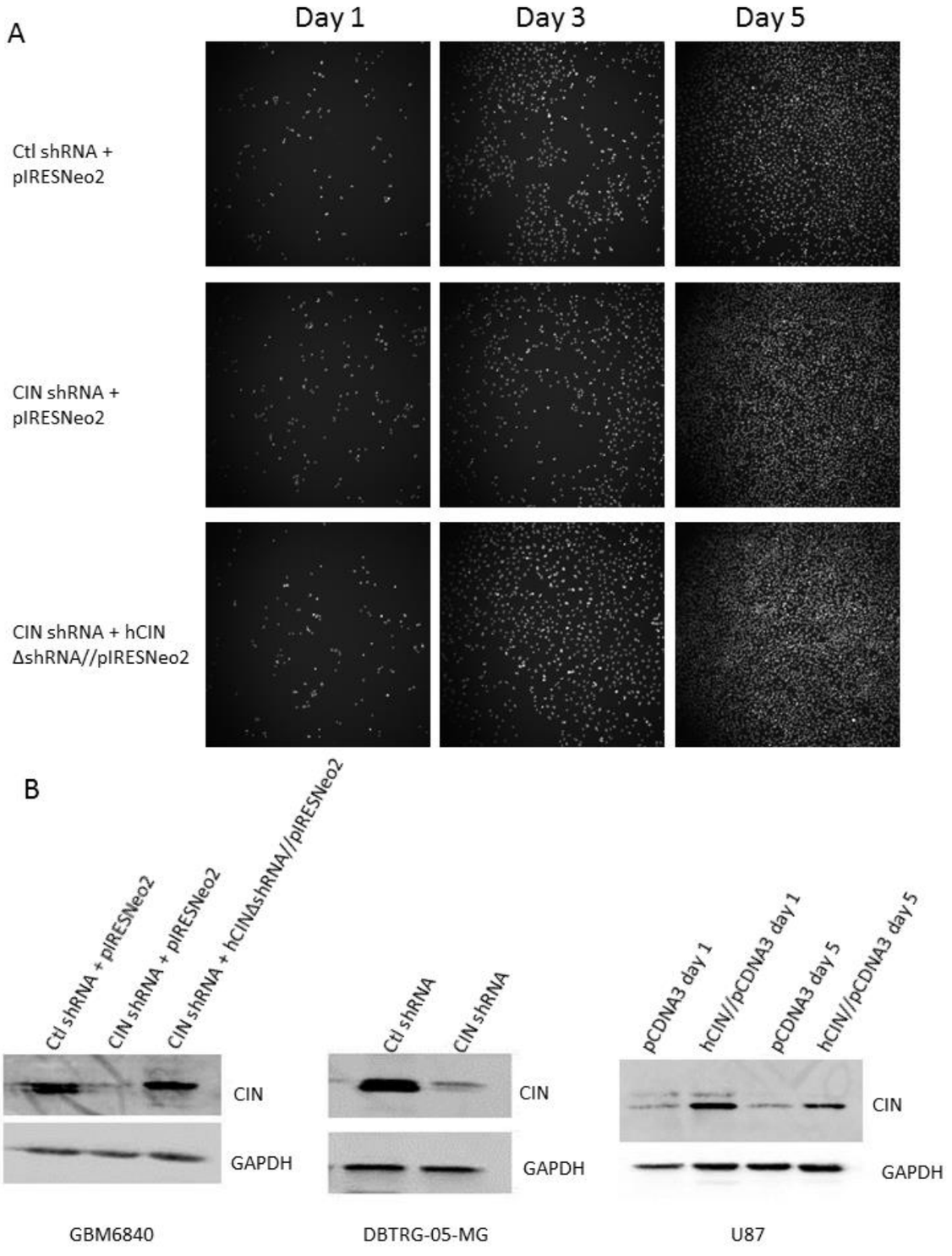
A
Day 1
Day 3
Day 5
Ctl shRNA + pIRESNeo2
CIN shRNA + pIRESNeo2
CIN shRNA + hCIN ΔshRNA//pIRESNeo2
B
Ctl shRNA + pIRESNeo2
CIN shRNA + pIRESNeo2
CIN shRNA + hCINΔshRNA//pIRESNeo2
CIN
GAPDH
GBM6840
Ctl shRNA
CIN shRNA
CIN
GAPDH
DBTRG-05-MG
pCDNA3 day 1
hCIN//pCDNA3 day 1
pCDNA3 day 5
hCIN//pCDNA3 day 5
CIN
GAPDH
U87

C

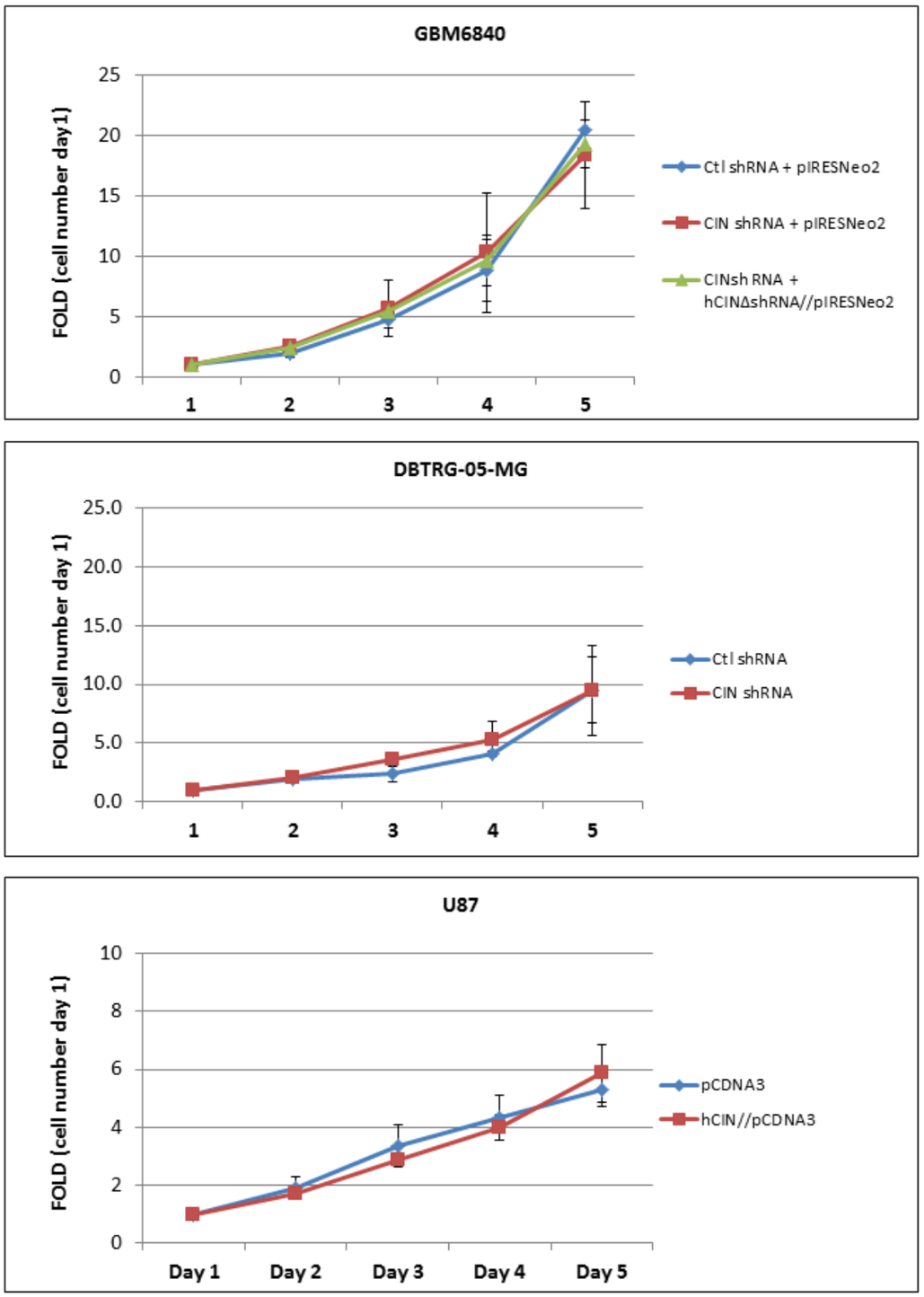

Figure 25: Quantification of glioma cell proliferation after CIN deregulation.
(A) Hoechst 33342 stained GBM6840 cells on day 1, day 3 and day 5 of a proliferation assay.
(B) Representative western blot with α-CIN antibody, GAPDH was used as loading control.
(C) Quantification of n=2 as shown in (A). There is no difference in proliferation in any of the three cell lines after CIN deregulation.

5.14 Analysis of cytokinesis after CIN deregulation

Spatio-temporal control of cofilin phosphorylation is needed for a proper completion of the mitotic process [130], and deregulation of LIMK expression can lead to defects in it [131]. In HeLa cells, cytokinesis is disturbed after acute CIN downregulation [74]. Therefore, it was examined if the stable knockdown or expression of CIN affects the completion of cytokinesis in glioma cells. Cells were seeded in medium containing FCS, then starved to closely mimick the conditions of the transwell setup in 5.11. The number of successfully completed mitoses including a complete cytokinesis (see Fig. 26 A) were counted. There were no differences in the number of completed mitoses after CIN deregulation (see Fig. 26 A and B). At least 100 cells were analyzed in each condition per replicate. These assays were performed in parallel with the transwell assays, and the routine western blotting from the transwell experiments also belongs to this assay.

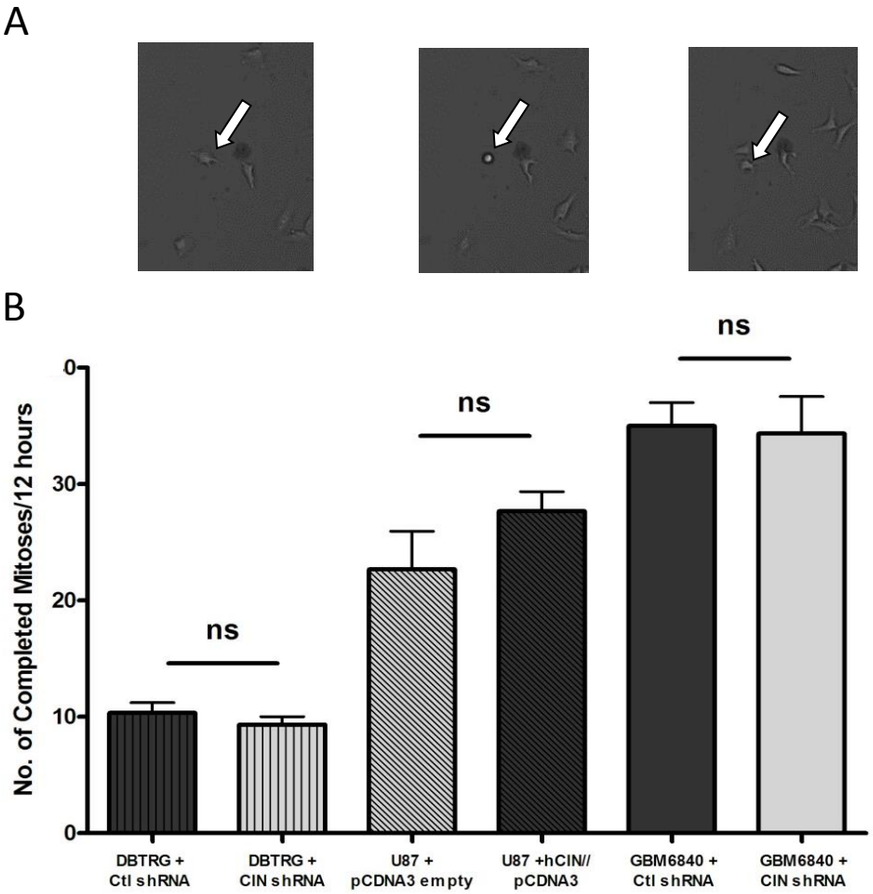

Figure 26: Analysis of completed cytokineses after CIN deregulation.
(A) Time-lapse movie of a GBM6840 cell that is first spread on the culture dish, then rounds up in mitosis and finally divides into two daughter cells (arrows).
(B) Quantification of the number of completed mitoses in DBTRG-05-MG, U87 and GBM6840, n=3 as shown in (A). Shown is the mean + SEM.

5.15 Analysis of cell roundness and area on collagen IV

In GBM6840 CIN shRNA cells that are grown on a glass surface, cell area increases as compared to the Ctl shRNA cells [48]. Therefore, it was tested if the cells show any differences in area or roundness under the conditions of the migration setup as used in 5.10. Cells were stained with fluorescently labeled phalloidin and then photographed with a Nikon T_i eclipse epifluorescence microscope and analyzed *via* automatic image analysis with ImageProPlus 7.0 as shown in Fig. 27 A, followed by manual inspection and correction of every picture. There were no differences in area or roundness after CIN deregulation in GBM6840 and U87 (see Fig. 27). At least 100 cells were analyzed for each condition.

A

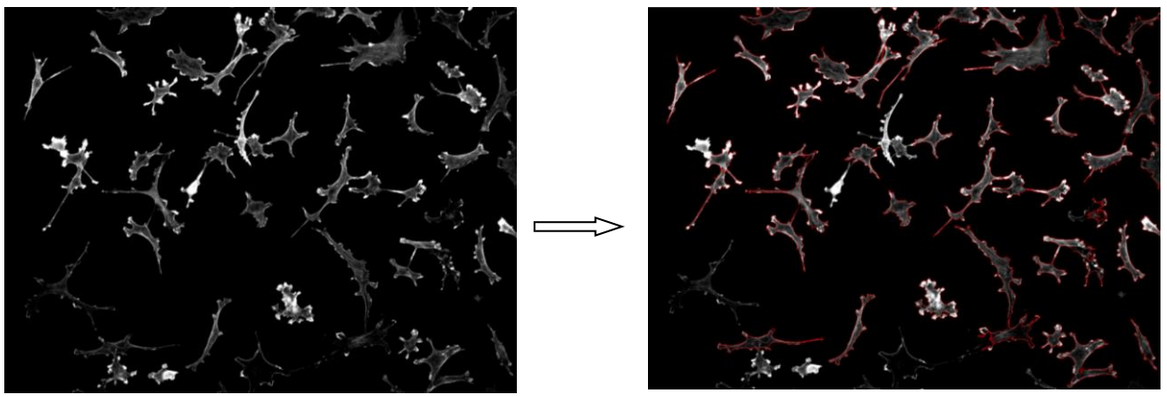

B

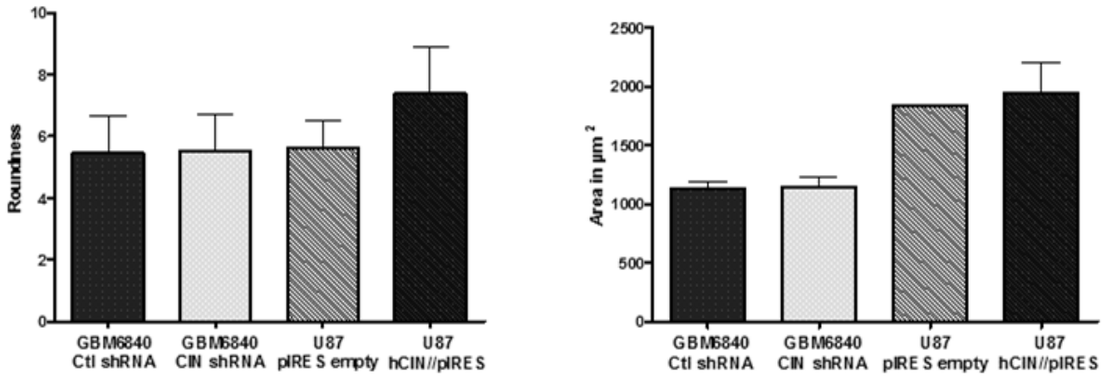

Figure 27: Analysis of glioma cell roundness and area on collagen IV.
(A) GBM6840 cells were stained with phalloidin and then photographed with a Nikon T_i eclipse epifluorescence microscope and analyzed *via* automatic image analysis (cell border detection) with ImageProPlus 7.0 as shown in the right panel. Cell area, width and length were determined from these processed images and the roundness was calculated for each cell.
(B) Quantification of n=2 as shown in (A), CIN deregulation did not influence area or roundness on collagen IV in U87 or GBM6840 cells. Shown are means + SEM.

5.16 Analysis of cell adhesion after CIN knockdown

Changes in adhesion to extracellular matrix (ECM) molecules affect cell migration in 2D and 3D differentially [132], and cofilin phosphorylation is regulated by integrin dependent adhesion [133]. Therefore, it was tested if there were any differences in adhesion to different ECM molecules after CIN knockdown. Cells were stained with calcein AM, allowed to adhere for different time points to an ECM-coated 96-well plate, and then the fluorescence intensities were measured for each condition. The adhesion between CIN shRNA cells and Ctl shRNA cells was not different on fibronectin, collagen IV, vitronectin or collagen I. Only on poly-L-lysine after 40 minutes, the measured signals were higher in CIN shRNA cells as compared to control cells. Under the assay conditions used, the cells adhered faster to the ECM molecules collagen IV and fibronectin than to cell culture plastic or poly-l-lysine alone (see Fig. 28 A). Interestingly, the cells adhered only very weakly to the vitronectin coated surface. CIN knockdown was checked for every experiment *via* routine western blotting (see Fig. 28 B).

A

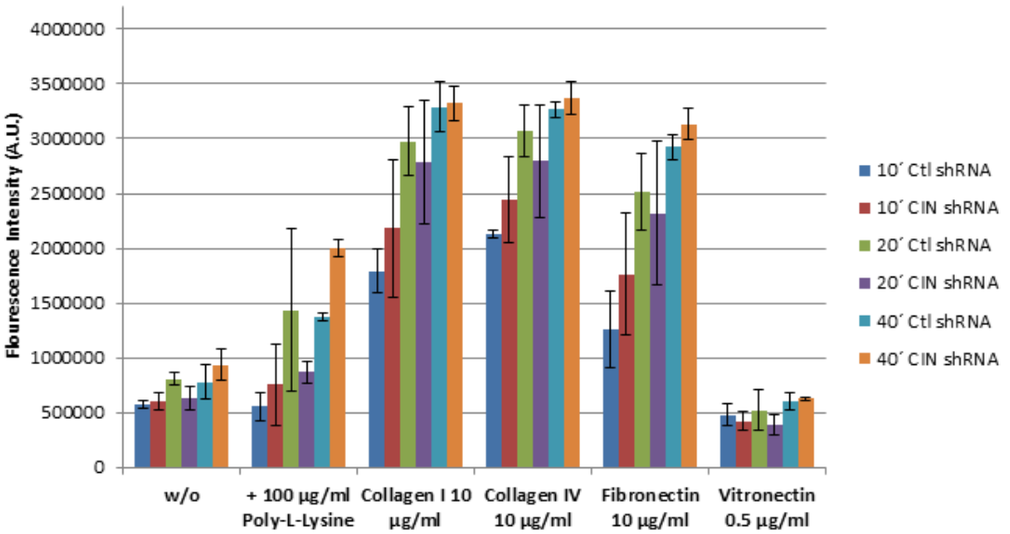

B

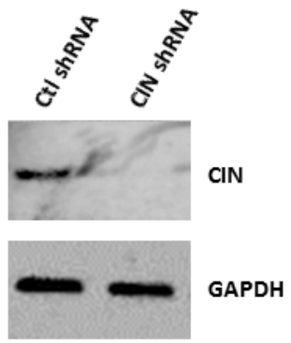

Figure 28: Analysis of cell adhesion after CIN knockdown.
(A) Measurement of fluorescence intensities of calcein AM stained GBM6840 cells. Cell adhesion was increased on fibronectin, collagen I and collagen IV coating as compared to cell culture plastic alone. However, CIN knockdown induced no significant change in cell adhesion on these coatings.
(B) Representative western blot with α-CIN antibody, GAPDH was used as loading control.

5.17 Analysis of tumor growth *in vivo*

The brain ECM is highly hydrated, and difficult to mimic in an *in vitro* setup [134].
Therefore, it is important to monitor cell growth and invasion of the glioma cells *in vivo*. For that purpose, GBM6840 cells were transduced with a construct that encodes a GFP-Luciferase fusion gene. Then clones were selected that possessed a high GFP and adequate CIN Expression (see Fig. 29 A, B and C). The clones Ctl shRNA + pIRESNeo2 16, hereafter named control, CIN shRNA + pIRESNeo2 16, hereafter named knockdown and CIN shRNA + hCINΔshRNA//pIRESNeo2 41, herafter named add-back were used for the following experiments. Luciferase activities in the GBM6840 cell lines were: Control, 6.2×10^3 photons/cell/sec; knockdown, 2.4×10^3 photons/cell/sec; add-back 7.6×10^3 photons/cell/sec.

10,000 cells were injected orthotopically into the brains of immunocompromised NOD-SCID mice by Prof. Dr. A-L. Sirén, and the growth of the cells was monitored by Dr. S. Kraus and Prof. Dr. A-L. Sirén in the center for experimental biomedicine.

Although comparable numbers of cells were injected in each case, as reflected by comparable luminescence intensities on day + 1 after the injection, analysis of the luminescence intensities over time revealed that control cells and chronophin add-back cells grew much faster than knockdown cells (see Fig. 30 A and B). Statistical analysis of the log transformed data with a linear model revealed that there was a highly significant difference between chronophin knockdown and control cells in cell growth (linear model: Luminescence intensity ~ day + shRNA, $p=7.7 \times 10^{-6}$, n=7). Luminescence intensity was modeled against the factors day and shRNA, but interactions between day and shRNA were not included. This means that it was assumed that the effects of the factors day and shRNA are simply additive and no parameters were included in the modeling which would account for interaction between the factors shRNA and day, due to the fact that the number of samples (mice) was not sufficient for estimating this amount of parameters. No significant difference between control and chronophin add-back cells (linear model: Luminescence intensity ~ day + shRNA, p=0.982, n=7) was found.

Histology revealed that most brains injected with control cells contained intraparenchymatic lesions. All control cell injected brains also contained tumor masses that were superficially

positioned on the brain. Both chronophin knockdown and chronophin add-back injected brains did not contain intraparenchymatic lesions at all (see Fig. 31 und Table 7).

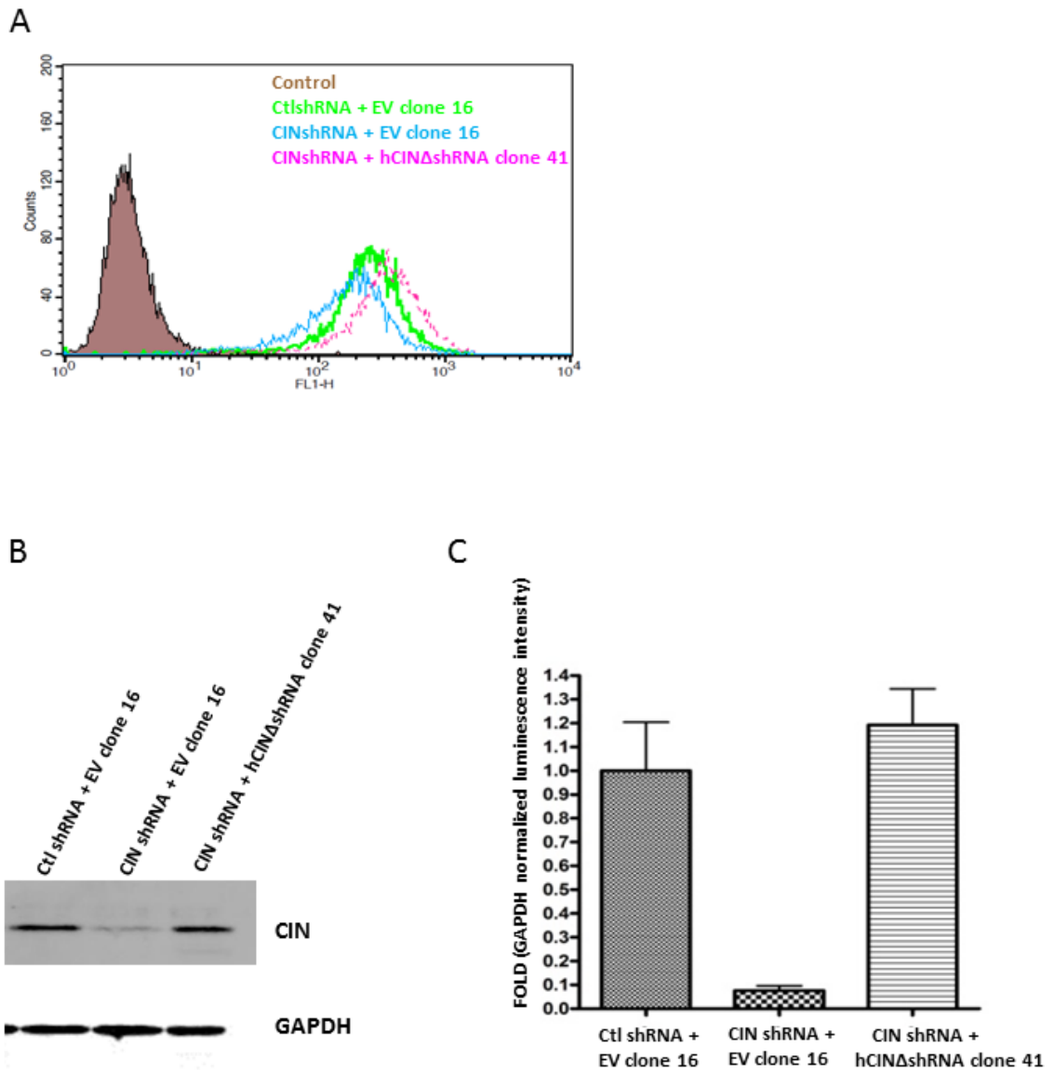

Figure 29: Characterization of GBM6840 clones for *in vivo* assays.
(A) Flow cytometric analysis of GFP expression of the three clones used. There were comparable GFP-expression levels in the three GBM6840 cell lines. Luciferase activities in the GBM6840 cell lines were: Control, 6.2 × 10^3 photons/cell/sec; knockdown, 2.4 × 10^3 photons/cell/sec; chronophin add-back, 7.6 × 10^3 photons/cell/sec.
(B) Western blot with α-CIN antibody, GAPDH was used as loading control.
(C) Quantification of n=2 as shown in (B).

A

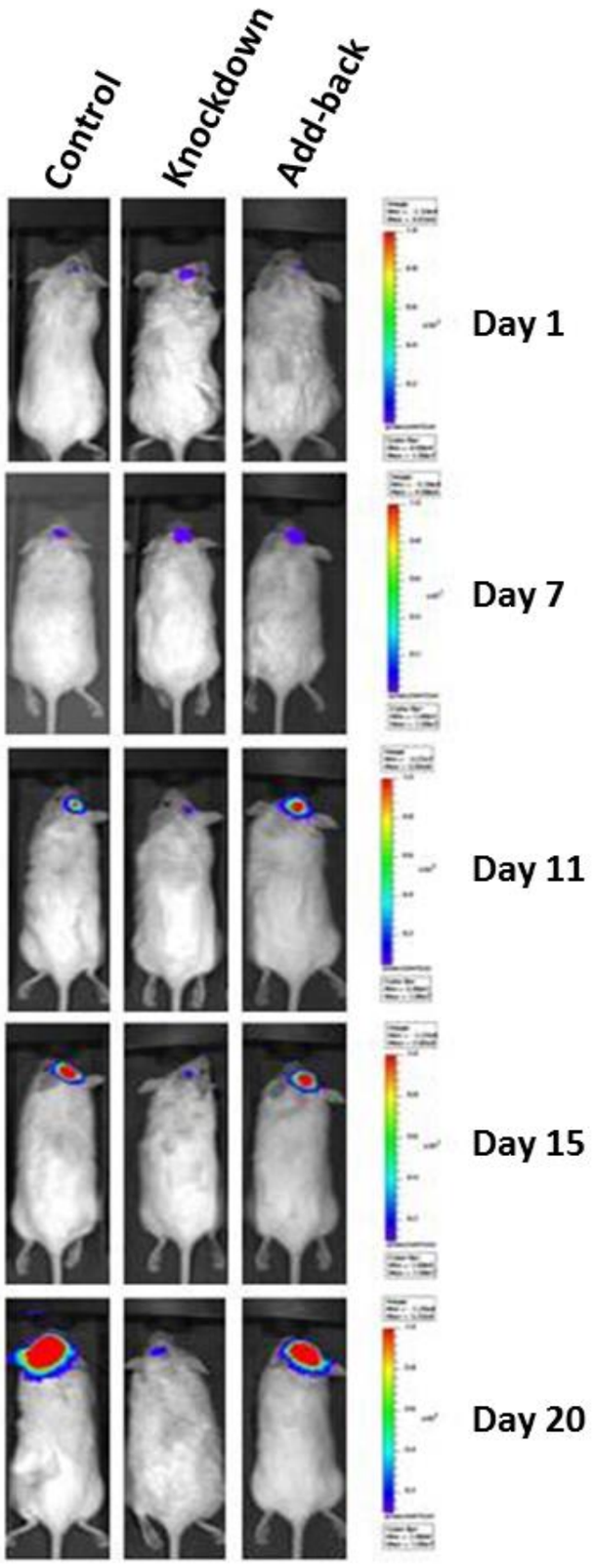

B

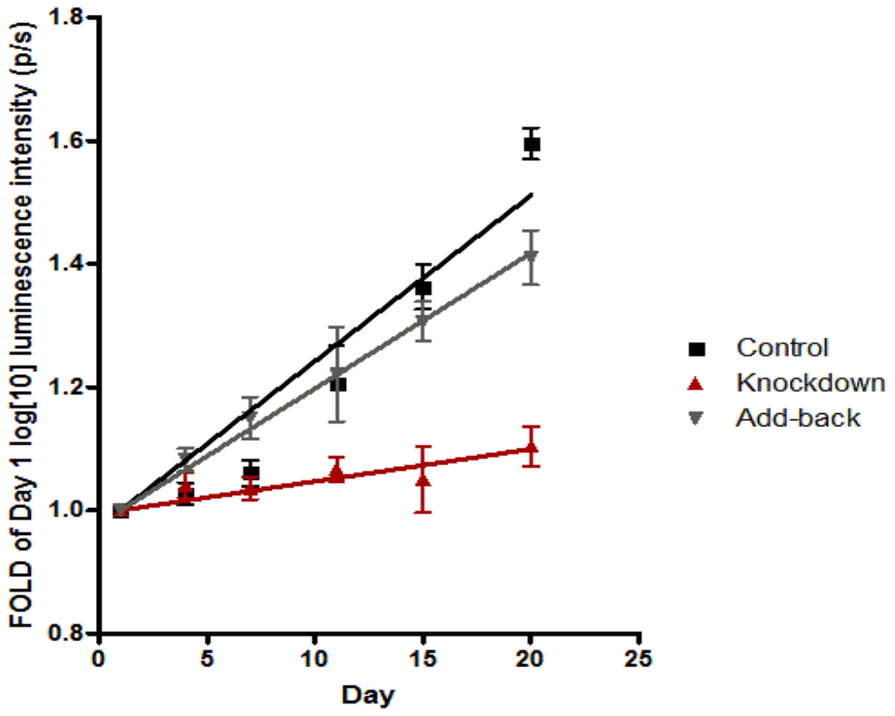

Figure 30: Analysis of GBM6840 cell growth *in vivo* using bioluminescence imaging.
(A) Representative pictures of mice injected with GBM6840 control, knockdown or chronophin add-back cells. Shown is the same mouse, one from each condition, on day 1, 7, 11, 15 and 20 after tumor cell implantation. The luminescence intensity is shown in emitted photons per second.
(B) Quantification of n=7 mice per condition as shown in (A).
Control cells and add-back cells, the chronophin expressing cells, grew much faster than cells with a low chronophin expression, chronophin knockdown cells, during the observation period of 21 days.

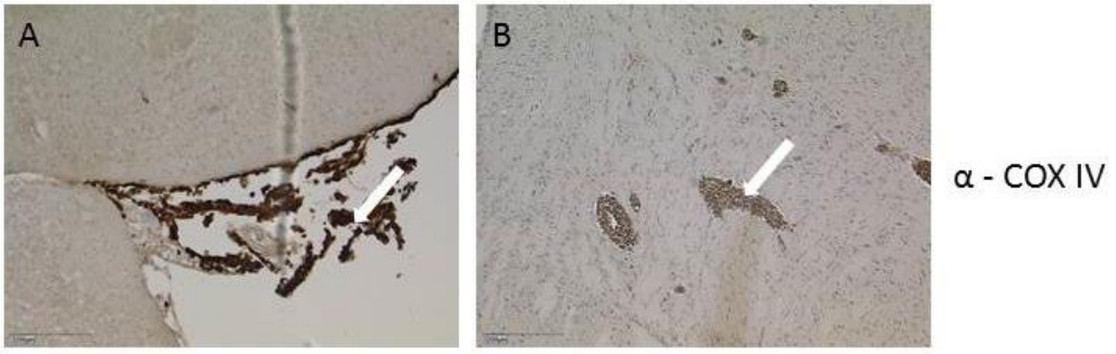

Figure 31: Analysis of GBM6840 cells *in vivo* with immunohistochemistry.
(A) α-COX IV DAB-staining of a mouse brain injected with control cells. Only a superficial lesion is present (arrow). The α-COX IV antibody used recognizes specifically only human cells.
(B) α-COX IV DAB-staining of a mouse brain injected with control cells. Several intraparenchymatic lesions are present (arrow).

Table 7: Histology based scoring of the tumor lesions in the *in vivo* assay.

Every tenth slide from each brain was stained with an antibody specifically staining only human COX IV as indicated in 4.6.5 and 4.6.6. If tumor cells were present on one slide, Yes is indicated in the tumor cells present column.

Animal	Injected cell type	Tumor cells present	Superficial tumor	Intraparenchymatic lesion
51	Control	Yes	Yes	Yes
54	Control	Yes	Yes	Yes
64	Control	Yes	Yes	Yes
65	Control	Yes	Yes	No
66	Control	Yes	Yes	Yes
67	Control	Yes	Yes	Yes
68	Control	Yes	Yes	Yes
69	Knockdown	No	No	No
70	Knockdown	No	No	No
73	Knockdown	No	No	No
74	Knockdown	No	No	No
55	Knockdown	No	No	No
58	Knockdown	No	No	No
72	Knockdown	No	No	No
59	Add-back	Yes	Yes	No
60	Add-back	No	No	No
75	Add-back	No	No	No
76	Add-back	No	No	No
77	Add-back	No	No	No
78	Add-back	Yes	Yes	No
80	Add-back	NA	NA	NA

5.18 Microarray analysis after CIN deregulation in GBM6840

To study the impact of CIN deregulation on transcription in GBM cells, RNA was isolated from GBM6840 Ctl shRNA, CIN shRNA and CIN shRNA + hCIN ΔshRNA expressing cells (hereafter named Rescue). CIN expression was tested *via* western blot. Then, RNA quality was analyzed and a microarray experiment was performed and analyzed by the microarray core facility in Marburg. The chips used were Agilent Human Genome vers. 2.0 Chips.

Then, all deregulated genes (probe sets) in the comparison Ctl shRNA versus CIN shRNA with a logFC ≥ 0.6 were extracted, resulting in 4944 deregulated transcripts. Afterwards, the genes (probe sets) regulated in the opposite direction in the CIN shRNA versus Rescue assay with a logFC ≥ 0.6 were filtered out, leading to 194 probe sets (see Table 8). As expected, CIN was among the top hits in the array, but was not included in the further analyses.

Under the assumption that the most highly deregulated transcripts in the publicly available datasets from patient samples contain potentially important genes, it was tried to identify transcripts regulated specifically by CIN which are involved in progression from a benign to a very malignant tumor entity.

Therefore, the 194 probe sets were filtered against data sets that are available in the GEO database [135].

The first microarray experiment compared GBM to normal brain tissue (GEO Accession GSE 4290, [108]). All genes (Symbols) from this experiment were extracted that showed a logFC ≥ 0.5 at an adjusted p ≤ 0.05 and were also contained in the 194 probe sets identified for control versus chronophin shRNA cells, yielding 40 genes (Symbols) that are marked with (*) in table 8. Only those genes were extracted that were downregulated after chronophin knockdown in GBM6840 as compared to control cells and downregulated in GBM tissue as compared to control tissue or upregulated after chronophin knockdown in GBM6840 as compared to control cells and upregulated in GBM tissue as compared to control tissue. Genes that were downregulated after chronophin knockdown but upregulated in GBM tissue as compared to control tissue or upregulated after chronophin knockdown but downregulated in GBM tissue as compared to control tissue were excluded.

These 40 were then compared to a pilocytic astrocytoma versus GBM dataset that is available in the GEO database (GSE12657, unpublished), and all significantly deregulated genes deregulated in the same direction were extracted leading to two genes (see Fig. 32).

The two genes identified by this approach were EDIL3 and MXI1.

The functional annotation of the 194 probe sets with DAVID [109,110] revealed that the most significantly affected cellular functions were cell proliferation, cell adhesion and cell migration (see Table 9). All those have been examined in GBM6840 cells after CIN deregulation previously in 5.9, 5.13 and 5.16, respectively.

Significantly affected transcription factors were identified through the use of IPA (Ingenuity®Systems, www.ingenuity.com). Identified transcription factors at a p-value ≤ 0.05 that were regulating the highest number of genes were SP1, p53, STAT3 and c-myc (see Fig. 34). As cells with deregulated c-myc activity may contain different levels of total RNA [83], total RNA levels in GBM6840 Ctl shRNA and CIN shRNA were compared. These were not significantly different between Ctl shRNA and CIN shRNA cells (see Fig. 33)

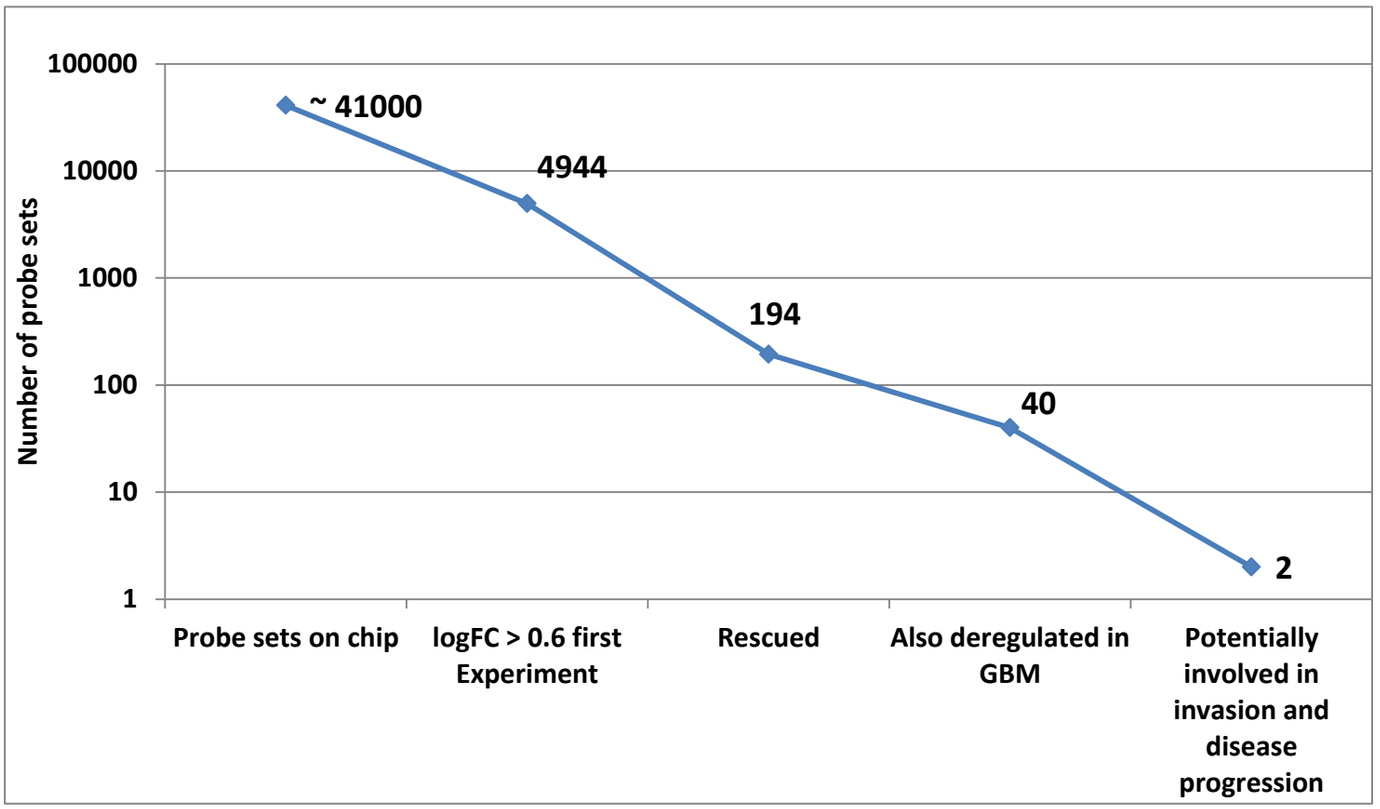

Figure 32: Analysis of the transcriptomic changes after CIN knockdown.
Analysis of the transcriptomic changes induced after CIN knockdown in GBM6840 that are potentially involved in disease progression and invasion. MXI1 and EDIL3 are the most promising candidate genes that are regulated by CIN.

Table 8: List of all 194 genes (probe sets) specifically regulated by CIN.

Shown is the logFC CIN shRNA versus Ctl shRNA, the average expression in the first experiment and the logFC Rescue versus CIN shRNA, n=2.

ID	SYMBOL	logFC CIN shRNA vs Ctl shRNA	AveExpr	logFC Rescue vs CIN shRNA
A_23_P345808	FAM133A (*)	-2.32	6.97	1.93
A_23_P54144	BMP4	-2.14	6.5	0.86
A_33_P3243554	SEPT6	-2.06	5.75	0.90
A_24_P280029	PDXP	-1.71	9.78	2.19
A_33_P3263902	MXI1 (*)	-1.36	6.24	0.87
A_33_P3364240	PAEP	-1.35	10.87	0.67
A_33_P3399453	CAPZA1	-1.34	11.68	1.09
A_33_P3323975	NA	-1.3	4.27	0.65
A_33_P3255647	HNRNPH2	-1.24	9.18	0.81
A_33_P3224858	EIF2AK2	-1.22	7.48	0.65
A_24_P142118	THBS1	-1.21	13.16	0.92
A_23_P404481	S1PR1 (*)	-1.18	4.78	0.69
A_33_P3418833	FLRT3 (*)	-1.17	7.25	1.04
A_24_P179044	SNX9	-1.16	7.97	0.89
A_32_P191895	NA	-1.11	8.24	0.68
A_24_P944991	SREK1IP1	-1.09	7.32	0.77
A_23_P354151	ITK	-1.08	3.32	0.62
A_24_P283928	OBFC2B	-1.07	9.96	0.70
A_24_P76649	GPRIN3	-1.04	3.98	0.65
A_33_P3371493	TOP1	-1.03	8.99	0.87
A_33_P3317988	CMPK1	-1	9.2	0.95
A_23_P55020	CD300LF	-0.99	3.49	0.75
A_23_P160934	ANP32E	-0.99	9.82	0.75
A_33_P3364864	NAMPT	-0.97	8.45	0.63
A_24_P59220	POTEF	-0.97	13.87	0.65
A_33_P3383233	NDRG2 (*)	-0.97	6.38	0.65
A_33_P3415820	THBS1	-0.97	8.42	1.26
A_23_P401606	EDIL3 (*)	-0.96	7.53	0.78
A_33_P3397298	NA	-0.95	10.51	0.69
A_33_P3231277	HIF1A	-0.95	10.14	0.72
A_24_P870620	PTN	-0.95	5.63	0.73
A_33_P3421733	EIF3CL	-0.95	10.54	1.17
A_23_P217015	SET	-0.93	11.65	0.73
A_33_P3362891	HNRNPA2B1	-0.93	12.22	0.84
A_33_P3314031	TMEM154	-0.92	4.46	0.61
A_33_P3314466	NA	-0.92	7.59	1.02
A_24_P942481	GPR180	-0.9	8.85	0.62
A_33_P3259902	NA	-0.89	12.91	0.74
A_33_P3407618	LOC80154	-0.89	7	1.01

ID	SYMBOL	logFC CIN shRNA vs Ctl shRNA	AveExpr	logFC Rescue vs CIN shRNA
A_24_P333326	CTAGE5	-0.89	6.35	1.02
A_24_P6903	ACTBL2	-0.88	13.06	0.62
A_23_P153583	PPP5C	-0.88	9.36	0.70
A_33_P3232294	ITPR2	-0.88	8.18	0.88
A_24_P33444	YWHAE	-0.88	10.45	1.02
A_33_P3338539	NA	-0.87	4.94	0.98
A_33_P3287760	RASGEF1A (*)	-0.86	4.39	0.68
A_24_P201153	TJP2 (*)	-0.86	9.95	0.77
A_32_P810645	FLJ40288	-0.86	4.37	0.86
A_33_P3301394	NA	-0.85	12.85	0.82
A_23_P200772	ZNF644	-0.85	10.18	1.12
A_33_P3283992	ZNF671	-0.84	6.72	0.71
A_33_P3238976	TRMT5	-0.83	12.67	0.66
A_24_P381136	PACSIN3	-0.83	9.39	0.69
A_24_P391260	PTTG1IP	-0.83	10.09	0.72
A_24_P182494	DUSP10	-0.83	6.25	0.77
A_33_P3234859	UTRN	-0.83	6.71	0.79
A_23_P28420	OLA1 (*)	-0.82	12.91	0.75
A_24_P190541	BRWD1 (*)	-0.82	8.04	0.76
A_32_P199252	HSP90AA1	-0.82	14.07	0.84
A_33_P3270776	HTRA3	-0.81	7.06	0.71
A_33_P3276455	KDM5B	-0.8	8.04	0.90
A_33_P3393456	LOC100131129	-0.79	4.82	0.71
A_33_P3323520	KIAA1826	-0.79	7.52	0.72
A_24_P169574	LOC649395	-0.79	10.44	1.05
A_24_P65616	PVR	-0.77	11.96	0.62
A_23_P379550	YARS	-0.77	12.64	0.66
A_33_P3280003	HERC2 (*)	-0.77	6.19	0.87
A_33_P3233105	NA	-0.75	5.58	0.75
A_24_P8454	SPAG9	-0.75	8.26	1.00
A_33_P3258223	MCM7	-0.75	10.63	1.27
A_33_P3325131	CANX	-0.74	9.34	0.64
A_33_P3267948	SLC25A23 (*)	-0.74	8.16	0.72
A_24_P294821	SYNJ2 (*)	-0.74	6.7	0.72
A_23_P60286	EIF4B	-0.74	11.57	0.85
A_33_P3348782	CYP2S1	-0.73	6.28	0.63
A_23_P200310	DEPDC1	-0.73	12.16	0.76
A_23_P373799	CWC22	-0.72	9.71	0.62
A_24_P111134	POMT2	-0.72	9.65	0.65
A_23_P70398	VEGFA	-0.72	9.39	0.65
A_24_P374445	C17orf57	-0.72	4.03	0.78
A_33_P3281816	CAP1	-0.72	10.31	0.81
A_33_P3314468	IMMT	-0.72	8.43	1.02
A_23_P4909	SNRNP70	-0.72	12.38	1.28

ID	SYMBOL	logFC CIN shRNA vs Ctl shRNA	AveExpr	logFC Rescue vs CIN shRNA
A_33_P3260605	CTNNAL1	-0.71	11.68	0.69
A_24_P341187	GBA2 (*)	-0.7	9	1.04
A_33_P3369371	GPX3	-0.69	8.15	1.00
A_24_P392690	ANP32BP1	-0.68	12.79	0.64
A_33_P3311750	CCDC144A	-0.68	6.15	0.81
A_33_P3333507	SENP7	-0.68	6.27	1.00
A_33_P3371381	ANKDD1B	-0.67	4.81	0.61
A_24_P14932	WDR52 (*)	-0.67	5.39	0.64
A_23_P92349	FGFRL1	-0.67	10.38	0.68
A_24_P97825	CCDC69	-0.67	6.46	0.69
A_24_P156267	SOX12	-0.67	5.71	0.80
A_23_P42507	PPIL4	-0.67	9.19	0.82
A_33_P3236267	REXO1L1	-0.67	12.66	0.98
A_23_P426636	AHNAK	-0.67	10.35	1.13
A_24_P128145	ATF2 (*)	-0.67	7.09	1.22
A_33_P3211633	WDR3	-0.67	6.6	1.29
A_23_P20615	ANP32B	-0.66	13.15	0.60
A_24_P415845	LIG4 (*)	-0.66	6.01	0.61
A_24_P81965	RAP2A (*)	-0.66	10.09	0.63
A_33_P3242493	PIBF1	-0.66	6.46	0.67
A_23_P96087	H1FX	-0.66	11.45	0.99
A_33_P3299656	RPGR	-0.65	7.85	0.60
A_32_P144908	ZNF254	-0.65	11.07	0.65
A_33_P3224595	OFD1	-0.65	6.81	0.69
A_23_P411806	SLC44A1 (*)	-0.65	7.73	0.70
A_33_P3332860	STX16	-0.65	8.74	0.75
A_23_P152768	TUBG1	-0.64	11.32	0.61
A_23_P71146	POLD2	-0.64	10.74	0.63
A_23_P371876	ALKBH8	-0.64	8.06	0.65
A_23_P203658	PICALM (*)	-0.64	9.18	0.79
A_24_P106953	PTGES2 (*)	-0.64	11.06	0.86
A_32_P180210	FAM35A	-0.64	7.44	1.07
A_23_P252764	SMARCA2 (*)	-0.64	8.07	1.14
A_24_P345846	ANTXR2	-0.63	8.1	0.61
A_32_P217390	SPATA8	-0.63	5.27	0.65
A_24_P816384	UBE2Q2P1	-0.63	6.59	0.66
A_24_P26177	VPRBP	-0.63	7.92	0.70
A_24_P106363	MARVELD2	-0.63	3.67	0.70
A_23_P125639	ZFX	-0.63	6.24	0.74
A_33_P3288110	PKP4 (*)	-0.63	8.26	0.84
A_32_P83465	NBPF10	-0.63	12.25	1.35
A_33_P3272412	FLJ45482	-0.62	7.72	0.63
A_33_P3212640	NOTCH2NL	-0.62	5.07	0.68
A_24_P384755	NOL10	-0.62	8.72	0.73

ID	SYMBOL	logFC CIN shRNA vs Ctl shRNA	AveExpr	logFC Rescue vs CIN shRNA
A_24_P358381	GTPBP6	-0.62	9.49	0.87
A_33_P3412613	TMPO	-0.62	6.59	1.25
A_33_P3211854	NA	-0.61	3.91	0.60
A_33_P3320277	MFN2 (*)	-0.61	7.82	0.65
A_33_P3289996	USP45	-0.61	7.32	0.65
A_24_P99090	CKAP2	-0.61	8.41	0.70
A_23_P203665	ACER3 (*)	-0.61	6.89	0.76
A_33_P3404701	SEL1L (*)	-0.61	7.98	0.77
A_33_P3380932	ZNF800	-0.61	7.81	0.96
A_33_P3300893	MADD (*)	-0.6	10.12	1.03
A_33_P3411204	GCNT2 (*)	0.6	8.68	-0.60
A_24_P583040	C17orf67	0.62	7.51	-0.64
A_23_P76332	RFX4 (*)	0.63	4.07	-0.79
A_33_P3247331	KCNQ1 (*)	0.64	4.15	-0.76
A_23_P133236	PCDHB14	0.64	8.74	-0.63
A_23_P347525	PATE1	0.65	4.75	-0.66
A_33_P3382276	NA	0.67	4.22	-0.70
A_23_P356717	ANKS1B	0.67	4.31	-0.67
A_23_P42868	IGFBP1 (*)	0.67	9.83	-0.65
A_23_P387585	NCRNA00246	0.68	4.75	-0.67
A_23_P88767	PLA2G10	0.69	4.9	-0.76
A_23_P76234	RPH3A	0.69	3.94	-0.63
A_24_P349117	GPR158	0.7	4.29	-0.88
A_33_P3256391	CRB3	0.71	5.49	-0.60
A_33_P3351536	PTK2B	0.72	6.31	-0.63
A_33_P3216694	HIVEP3 (*)	0.73	5.08	-0.75
A_33_P3299915	NA	0.74	4.52	-0.77
A_23_P7901	TTLL2	0.76	3.94	-0.67
A_23_P42189	SLC17A1	0.76	4.26	-0.60
A_33_P3361102	CAMTA1 (*)	0.77	4.63	-0.71
A_23_P143247	TSHZ2	0.79	4.92	-0.88
A_23_P421401	PDGFRB (*)	0.79	9.18	-0.61
A_33_P3278122	NA	0.82	4.33	-0.68
A_33_P3320648	NA	0.83	4.99	-0.76
A_33_P3342797	LOC401442	0.83	4.23	-0.72
A_33_P3230995	NA	0.83	4.57	-0.61
A_33_P3345678	NA	0.86	4.42	-0.62
A_33_P3330911	BCAS1	0.9	4.16	-0.62
A_24_P929388	TMEM169	0.9	3.71	-0.61
A_24_P187056	LOC375010 (*)	0.91	4.41	-0.63
A_33_P3263307	RANGAP1	0.92	16.39	-0.82
A_24_P254506	PAGE4	0.92	4.6	-0.61
A_33_P3324730	C20orf173	0.95	4.37	-0.73
A_23_P218442	CEACAM6	0.97	3.91	-0.96

ID	SYMBOL	logFC CIN shRNA vs Ctl shRNA	AveExpr	logFC Rescue vs CIN shRNA
A_23_P98580	FADS2 (*)	0.97	12.15	-0.63
A_33_P3229107	LOC642587	1	3.64	-0.66
A_23_P218549	EMR3	1.04	4.88	-0.77
A_23_P205348	TCL6 (*)	1.11	4.41	-0.67
A_33_P3404974	OPN5	1.13	4.02	-0.88
A_32_P206479	ZNF831	1.18	4.31	-0.68
A_23_P23829	CD34 (*)	1.19	4.63	-0.81
A_24_P945096	CACNA1I	1.23	4.31	-0.88
A_33_P3317336	NA	1.23	4.45	-0.67
A_24_P15325	NA	1.28	3.78	-0.63
A_23_P31626	ODF1	1.29	3.91	-0.62
A_33_P3384695	NA	1.32	4.1	-0.75
A_33_P3272957	NA	1.37	3.68	-0.73
A_32_P480330	EYS	1.39	3.62	-0.63
A_33_P3326427	OR4A16	1.48	4.82	-0.84
A_33_P3290477	ZNF648	1.61	3.98	-0.68
A_23_P131676	CXCR7 (*)	1.62	4.01	-0.66
A_24_P935491	COL3A1 (*)	1.66	5.07	-0.98
A_33_P3388192	GTSF1	1.71	4.23	-0.61
A_23_P21120	NA	2.12	3.31	-0.83
A_33_P3324114	NCRNA00295	2.22	4.25	-0.63
A_32_P86578	LOC389023	2.56	3.65	-0.65
A_23_P106405	NDN	2.98	8.44	-0.74

Table 9: Functional Annotation of targets using DAVID.

Term	No. Genes	% of all genes	p-Value
GO:0042127 regulation of cell proliferation	16	9.14	0.0035
GO:0007155 cell adhesion	12	6.86	0.0419
GO:0022610 biological adhesion	12	6.86	0.0423
GO:0008285 negative regulation of cell proliferation	9	5.14	0.0137
GO:0016477 cell migration	8	4.57	0.0105
GO:0051674 localization of cell	8	4.57	0.0180
GO:0048870 cell motility	8	4.57	0.0180
GO:0008284 positive regulation of cell proliferation	8	4.57	0.0702

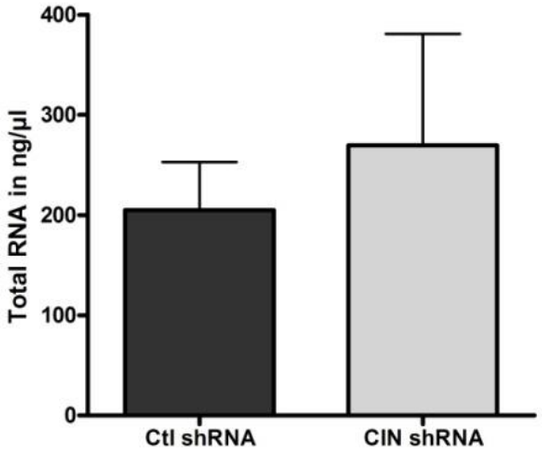

Figure 33: Quantification of total RNA levels in GBM6840.
RNA content did not differ significantly between GBM6840 Ctl shRNA and CIN shRNA cells.

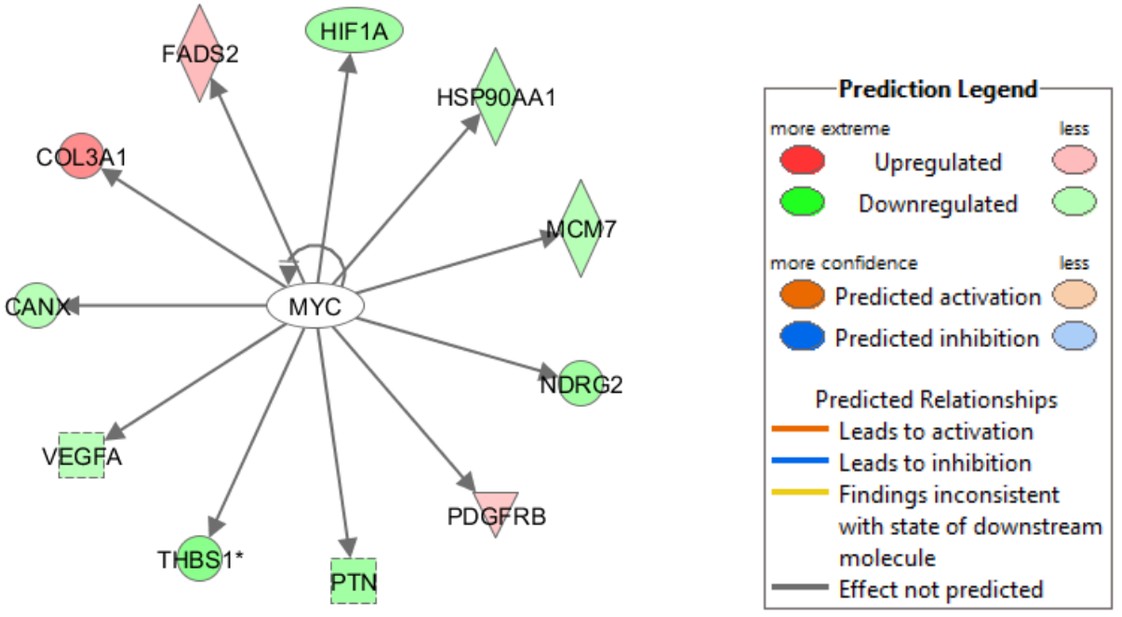

Figure 34: Potentially deregulated myc targets in GBM6840 CIN shRNA cells as compared to Ctl shRNA cells.
Myc targets are shown as predicted by IPA (Ingenuity®Systems, www.ingenuity.com).

5.19 Real-time PCR validation of microarray hits

Several hits from the microarray list in table 8 were reexamined *via* quantitative real-time PCR. The downregulation of THBS1, VEGFA, MXI1 and EDIL3 in CIN shRNA compared to Ctl shRNA cells could be confirmed. For THBS1, VEGFA and EDIL3 a complete rescue of the expression level was achieved in CIN shRNA cells reexpressing CIN. The expression of MXI1 was 1.5 x higher in the rescue cells as compared to the CIN shRNA cells, but remained at about 60 % as compared to Ctl shRNA expressing cells (see Fig. 35, n=3).

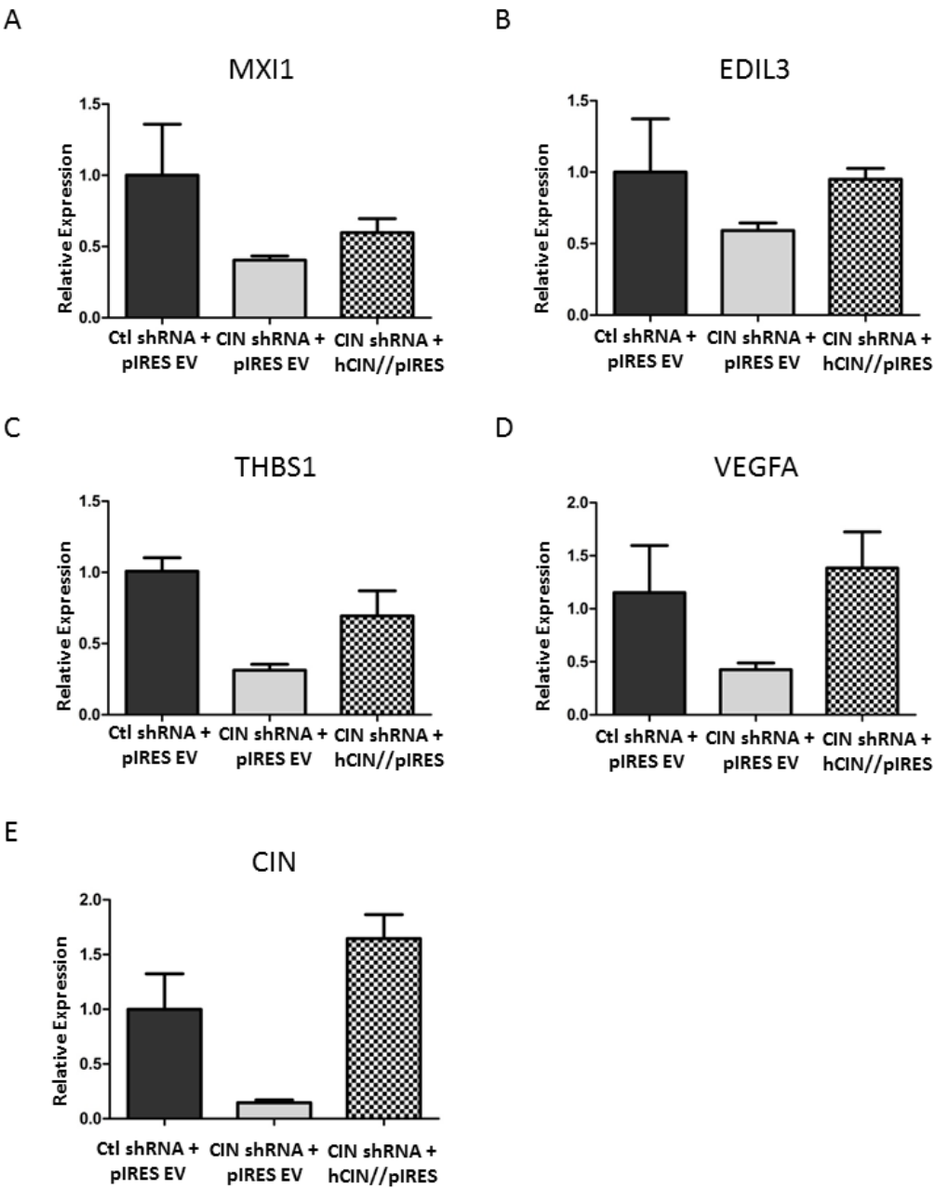

Figure 35: Real-time PCR of selected target genes.
Selected target genes from table 8 were validated by real-time PCR in GBM6840, n=3. The downregulation of THBS1, VEGFA, MXI1 and EDIL3 in CIN shRNA compared to Ctl shRNA could be confirmed.

5.20 Luciferase screening assay

To examine the transcriptional activity of cancer relevant pathways, a Cignal Finder 10-Pathway Reporter Array Cancer was used that monitors the activity of the transcription factors myc/max , E2F/DP1, HIF1A, NFκB, p53, RBP-Jκ , SMAD2/3/4, Elk-1/SRF and TCF/LEF in parallel including a negative and positive control [102]. This assay was performed in GBM6840 cells in a medium containing 0.5 % FCS. The myc/max reporter was the only one that showed reproducible differences in CIN siRNA transfected cells as compared to Ctl siRNA transfected cells (see Fig. 36). The cells were transfected with siRNAs to exclude any artifacts that are potentially introduced by different transfection efficiencies between the different stable cell lines. The myc/max activity was increased after CIN knockdown (two-tailed t-test, p=0.0687, df=4, n=3).

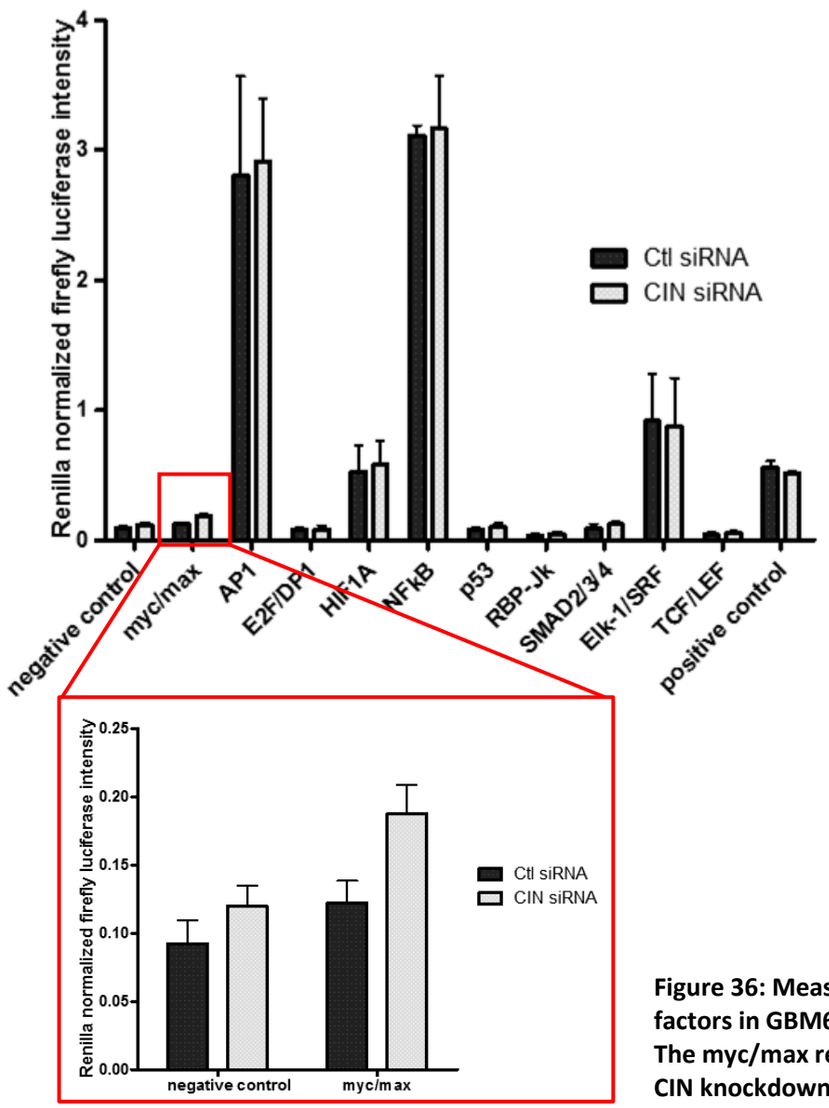

Figure 36: Measurement of the activity of cancer relevant transcription factors in GBM6840.
The myc/max reporter showed a reproducible increase in activity after CIN knockdown (n=3, p=0.0687).

5.21 C-myc luciferase reporter activity in medium containing 5 % FCS

Myc belongs to the immediate early response genes after serum stimulation [136]. Due to the fact that the signals from the myc/max reporter were rather low in the assay described in 5.20, the assay was performed in medium containing 5 % FCS again. Here, the increase of reporter activity after CIN knockdown could be nicely reproduced. The mean of the renilla normalized firefly intensity was 0.067 ± 0.005 in Ctl siRNA transfected GBM6840 cells and increased to 0.11 ± 0.02 in CIN siRNA treated cells (two-tailed t-test, p=0.0643, df=4, n=3). Moreover, expression of hCIN in U87 led to a reduction of the intensity from 0.25 ± 0.03 in pCDNA3 transfected cells to 0.16 ± 0.02 (p=0.0695, df=4, n=3, see Fig. 37). No major difference was observed in the negative control samples (n=3). Interestingly, the endogenous c-myc protein level was significantly reduced after CIN knockdown (see Fig. 37 B and C). Moreover, after transfection of a plasmid encoding full length human c-myc, the c-myc level was much lower in GBM6840 CIN shRNA cells (see Fig. 37 E and F). The CIN knockdown was verified *via* routine western blotting for every sample.

Alltogether, the results from the microarray study and from the c-myc reporter assay pointed towards a deregulation of c-myc activity after deregulation of CIN expression. Higher reporter activity was measured in cells with lower CIN levels in U87 and GBM6840. However, the c-myc protein level was reduced in GBM6840 after CIN knockdown.

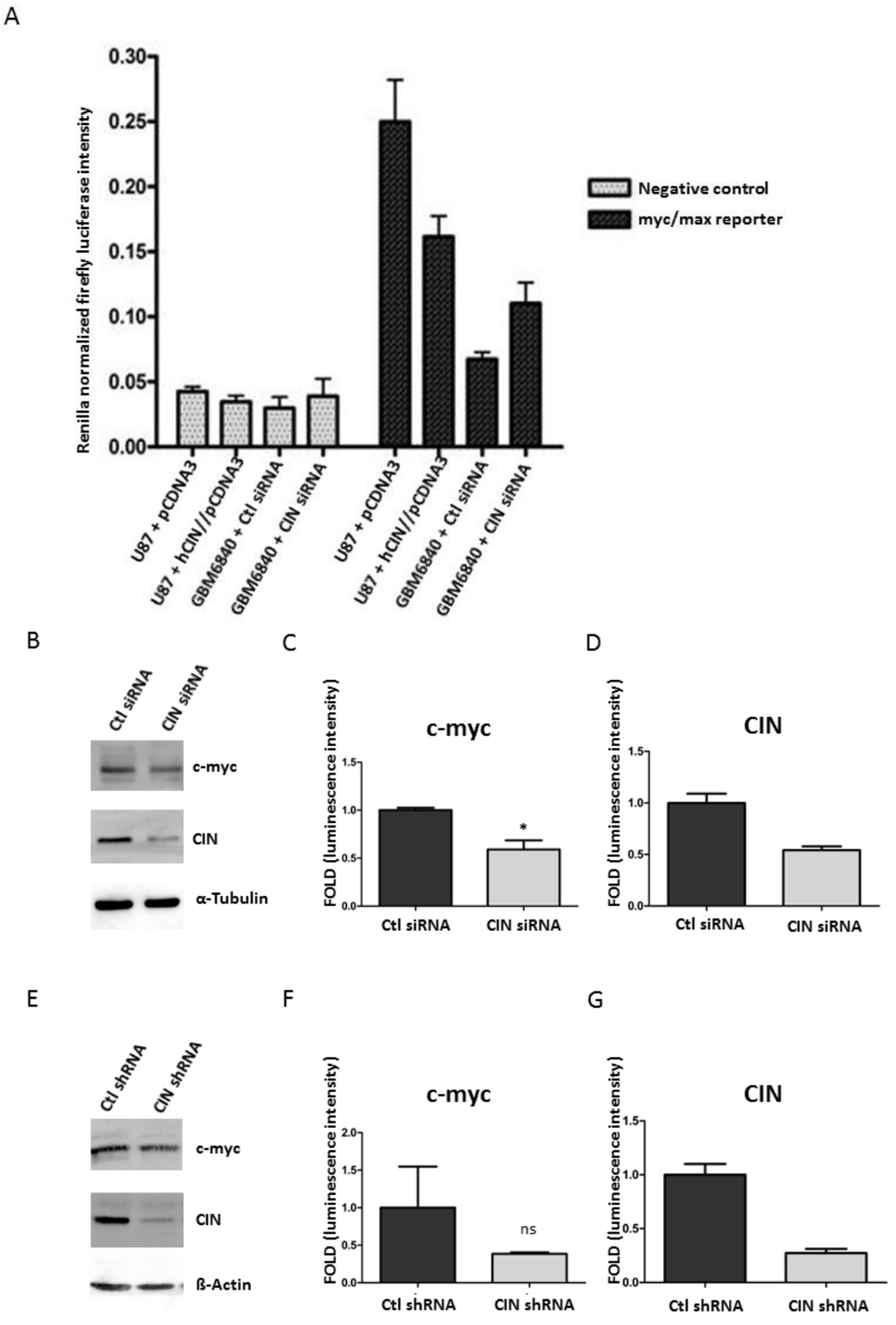

Figure 37: Analysis of myc/max reporter activity in medium containing 5 % FCS.
(A) Myc/max reporter activity was increased after CIN knockdown in GBM6840, but decreased after hCIN reexpression in U87.
(B) Representative western blot with α-CIN and α-c-myc antibody, α-Tubulin was used as loading control.
(C) Quantification of n=3 as shown in (B).
(D) Quantification of n=3 as shown in (B).
(E) Representative western blot with α-CIN and α-c-myc antibody, ß-Actin was used as loading control.
(F) Quantification of n=2 as shown in (E).
(G) Quantification of n=2 as shown in (E).

5.22 Semiquantitative PCR for transcription factors that are deregulated after CIN knockdown according to ingenuity pathway analysis (IPA)

As mentioned in 5.18, the transcription factors p53, SP1, STAT3 and c-myc were identified as potentially altered after CIN deregulation by IPA. Therefore, the expression of these transcription factors and in addition the expression of c-JUN was examined *via* semiquantitative PCR (see Fig. 38 A). Quantification revealed that none of the transcription factors undergoes major changes after CIN knockdown in GBM6840 Ctl shRNA cells compared to CIN shRNA cells on mRNA level (see Fig. 38 B).

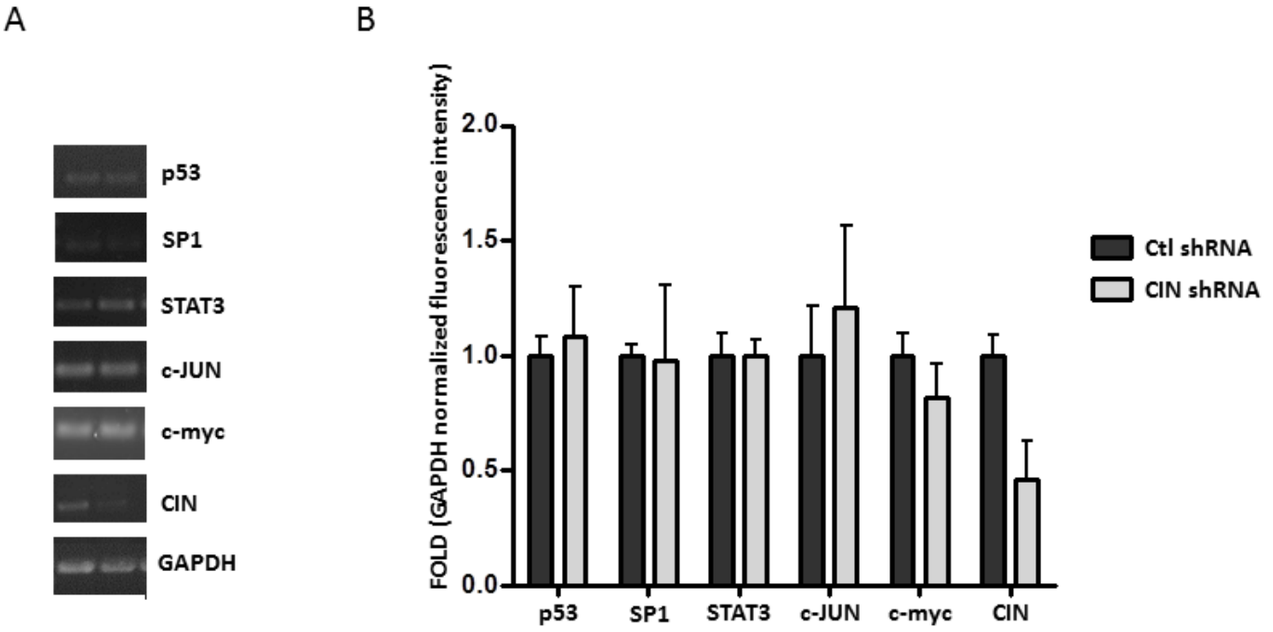

Figure 38: Analysis of transcription factor expression after CIN knockdown.
(A) Representative ethidium bromide stained agarose gels showing PCR product abundance of p53, SP1, STAT3, c-JUN, c-myc and CIN. GAPDH was used as loading control.
(B) Quantification of n=3 as shown in (A). CIN is efficiently downregulated in CIN shRNA cells as compared to Ctl shRNA cells. There are no significant differences in the RNA levels of p53, SP1, STAT3, c-JUN and c-myc.

5.23 Meta-analysis of studies dealing with glioma invasion

In 5.21, it was shown that CIN knockdown increased the reporter activity of a c-myc reporter construct. To examine if deregulated c-myc transcriptional activity can contribute to the invasiveness of glioma cells, an *in silico* analysis of glioma invasion studies was performed. In the last years, a couple of papers have been published that aimed to identify genes involved in glioma invasion by high throughput approaches, including microarrays, 2D PAGE and suppression subtractive hybridization (SSH) [137-140]. However, the identified genes showed little, if any, overlap. This problem has been reported in many other systems and a variety of high throughput studies, e.g. in c-myc dependent transcription profiles [83,84]. Despite the lack of a common target gene, it is possible that (a) common deregulated transcription factor(s) can be identified from the datasets. Therefore, the data sets were reexamined for common, altered transcription factors through the use of IPA (Ingenuity®Systems, www.ingenuity.com).

For that purpose, four datasets were reanalyzed that specifically compare invasive with non invasive cell populations [113-116] (see Table 10). Due to the fact that fold changes were not available in every study, the transcripts were only assigned to two categories (up- or downregulated) in the invasive cell population. A logFC of 2 was arbitrarily assigned to the genes in the category “upregulated”, and a logFC of -2 was assigned to the genes in the category “downregulated” for IPA analysis.

Then, the datasets were analyzed for common transcription factors identified to be altered. The only two hits that were present in every study, and that were accounting for at least ten percent of the identified genes, were c-myc and p53 (see Table 10). However, it should be noted that proteins well known to be involved in glioma invasion, like MMPs and integrins, were not present in the identified gene lists in [113-116].

Table 10: Meta-analysis of studies dealing with glioma invasion.

Reference	Approach	Genes identified	Mapped by IPA	% MYC	% MYC and p53
[113]	Microarray	25	21	33	48
[114]	SSH	18	16	38	56
[115]	2D PAGE	18	17	24	41
[116]	Microarray	118	92	15	33

6. Discussion

6.1 Regulation of cofilin phosphorylation in GBM

Receptor tyrosine kinases (RTKs) are frequently altered in GBM *via* mutation or overexpression [21]. Their signaling boosts cell proliferation and survival of cancer cells. In addition, RTKs influence actin dynamics and are therefore important initiators of cell migration and invasion [34]. In contrast to the RTKs and PI3K, for which a wealth of literature is available dealing with their involvement in glioma invasion, much less is known about their downstream effectors in the signaling to the actin cytoskeleton.

The actin regulatory protein cofilin has been mainly examined in breast cancer cells for its contribution to cell migration, invasion and metastasis [46]. Some studies have found an association of increased cofilin phosphorylation levels with increased invasion in glioma cells [141,142]. In a previous thesis from our laboratory, it was shown that proteins that regulate cofilin phosphorylation are deregulated in gliomas. The kinases LIMK1 and LIMK2 that mediate cofilin phosphorylation are strongly upregulated, whereas the cofilin phosphatase CIN is strongly downregulated in GBM tissue on protein level as shown by western blotting [48].

A concentration dependent motility response to cofilin in glioma cells has been described in a 2D *in vitro* setup. Here, U373 cell clones stably transfected with a cofilin encoding plasmid were examined for their motility and cofilin expression on protein level. Clones with intermediate cofilin expression levels, about 4.5 x above the wild type level, showed the highest motility. In clones expressing cofilin more than 7 x above the wild type level, the motility was only slightly higher than in the control cells [70]. A study that compared the transcriptional profiles of primary rat astrocytes and C6 rat glioma cells by serial analysis of gene expression, to identify markers for glioblastoma growth and motility, has found cofilin to be overexpressed in C6 cells [143].

Recently, it was shown that cofilin activity may be linked to glioma invasion *in vitro* and *in vivo*. In this study, the effects of overexpression of a constitutively active cofilin mutant on migration in 2D and invasion were analyzed [69]. In contrast, cofilin has not been found to be altered on mRNA or protein level in GBM [48]. Furthermore, the data available in the

Rembrandt database also did not show altered cofilin mRNA expression levels in glioma samples compared to normal brain tissue (this study). Fig. 39 summarizes the most important changes in the signaling towards cofilin as mapped by Rembrandt [107]. EGFR and PI3K are frequently mutated in GBMs, whereas for the other shown genes no mutations are known. EGFR and PI3K signaling are activated in a substantial amount of GBM samples [21]. The upregulated LIMK2 and ROCK1 have already been linked to increased invasion [41]. Interestingly, the highly upregulated RhoC has been found to be a driver for invasion and metastasis in breast cancer and melanoma [144-146], although the role of Rho family proteins in glioma invasion is controversially discussed [147]. ROCKs are predicted to bind especially efficiently to RhoC, which is also a potent ROCK activator [148]. The upregulation of cofilin kinases and the loss of CIN expression are commonly found in astrocytic tumors [48].

Therefore, the consequences of a pathophysiological deregulation of cofilin phosphorylation, *via* altered CIN expression, was analyzed here.

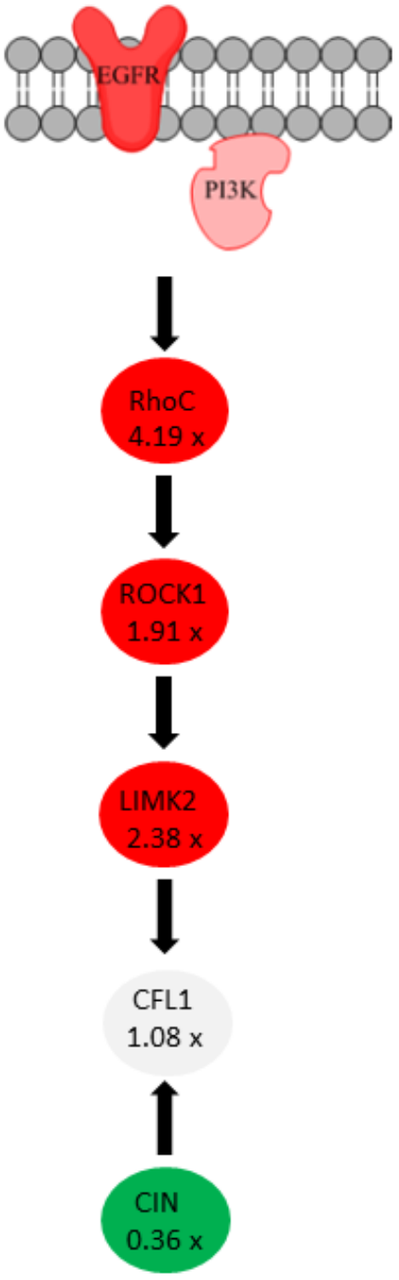

Figure 39: Changes in proteins regulating cofilin phosphorylation as mapped by Rembrandt. EGFR and PI3K are frequently mutated in GBMs, whereas for the other genes shown no mutations are known. RhoC, ROCK1 and LIMK2 are strongly upregulated, whereas CIN is strongly downregulated on mRNA level. Shown are the logFC values for the comparison GBM tissue versus normal brain together with the gene symbols.

6.2 Actin and P-cofilin phenotypes

Upon shRNA-mediated chronophin depletion, the p-cofilin level underwent major changes only in GBM6840 cells, whereas the phenotype in U87 and DBTRG-05-MG cells were rather mild. The cells were grown to high density and starved for these assays, to closely mimick the situation of the transwell setup, in which a strong phenotype was present in all cell lines after CIN deregulation.

Consistent with decreased actin dynamics upon elevated cofilin phosphorylation due to CIN loss, total F-actin levels were increased after CIN knockdown in GBM6840. Conversely, total F-actin levels strongly decreased upon CIN reexpression in U87 cells, as determined by flow cytometry of phalloidin stained cells. In addition, the F/G-actin ratios increased after CIN knockdown in GBM6840, but decreased after CIN expression in U87 as determined in the spin down assay. As both assays showed a strong phenotype in GBM6840 and U87 (see Fig. 17 and 18), it is likely that altered dynamics of the phosphocycling of cofilin are more important than absolute phosphocofilin levels for the regulation of the actin cytoskeleton. Among the growth factors tested, only activation of RhoA *via* LPA stimulation was able to increase phosphocofilin levels substantially (see Fig. 15 H and I). Or in other words, only stress fiber build up, but not induction of lamelliopdia or filopodia was associated with increased levels of phosphocofilin. That fits well to the observation that CIN knockdown induces F-actin accumulation in the cytoplasm and/or at the ventral membrane.

Interestingly, the increased cofilin phosphorylation in GBM6840 was accompanied by an increase in RhoA activity in GBM6840 cells (see Fig. 14 and 15). There are two possibilities that can explain this phenomenon. First, in addition to its function as a cofilin phosphatase downstream of Rho-ROCK signaling, CIN may have a role in the upstream regulation of RhoA. Rho activity is tightly regulated by numerous GEFs and GAPs, which are in turn often regulated by phosphorylation [149]. Therefore, CIN dependent dephosphorylation of a GAP or GEF could be the reason for the difference in basal RhoA activity.

It is also possible that there is a positive feedback loop between increased cofilin phosphorylation and/or changes in protrusive activity and RhoA activity. In PC-3 cells, inhibition of ROCK1 activity by siRNA mediated knockdown or chemical inhibition with fasudil leads to an increase in Rac-GTP levels but to a decrease in RhoA-GTP levels. The

fasudil induced decrease in RhoA activity is dependent on the presence of both Rac1 and Tiam1, a Rac GEF [150]. A positive feedback loop between RhoA and ROCK signaling might be present in glioma cells on the cellular level, although the molecular mechanism has to be different due to the fact that there was no change in Rac protein level and activity after CIN knockdown in GBM6840 cells.

A feedback regulation between Rac and Rho proteins is also known from fibroblasts, where activation of Rac downregulates RhoA activity [151]. Until now it was not examined if changes in cofilin phosphorylation could also be part of the feedback between RhoA, Rac and ROCK, because cofilin is also a Rac signaling effector.

Although primarily focusing on adhesion, it was reported that altered cytoskeletal tension can regulate RhoA activity [152]. CIN knockdown increased cofilin phosphorylation levels in GBM6840 (see Fig. 14). Cofilin competes with myosin for F-actin binding [153]. Therefore, increased cofilin phosphorylation potentially increases myosin association with actin and cytoskeletal tension, which could lead to elevated RhoA activity.

In a study that examined ruffle formation and migratory behavior of human keratinocytes on different surfaces, it was found that differences in protrusive activity go hand in hand with changes in small GTPase activity. It was found that RhoA activity was highest under conditions that supported optimal cell substrate adhesion and lamellipodial persistence [154]. Although no obvious change in lamellipodia size or number occurred in CIN shRNA cells, it was not examined if protrusive persistence is altered. Protrusion persistence is the best indicator of 3D migratory behavior [155]. However, in epithelial cells the increase in RhoA activity is accompanied by changes in ruffle formation and Rac activity [154], and there were no global cellular changes in Rac activity measurable in GBM6840 cells after CIN knockdown (see Fig. 15 A). This suggests that the molecular mechanism for RhoA activation in GBM6840 cells is different from the one reported for keratinocytes.

U87 cells overexpressing hCIN showed no reduction in RhoA-GTP levels (see Fig. 15 C). Therefore, the cellular background and the presence of other regulatory proteins might be important for CIN regulation of RhoA activity in U87 compared to GBM6840 cells. U87 cells were established from a grade IV astrocytoma that occurred in a male individual, whereas GBM6840 cells were established from a GBM that occurred in a young female individual. It is

not known to which molecular GBM subtype the original tumors belonged. Therefore, the molecular characteristics of the two cell lines can be quite different.

That CIN downregulation leads to an accumulation of F-actin has been described previously [48]. This study has added a quantification of the observed phenotype *via* flow cytometry and actin spin down assays to the previous results (see Fig. 17 and 18). Moreover, through the use of the ROCK-inhibitor Y-27632 and hCIN overexpressing cells, important evidence for the CIN and phosphocofilin specificity of the observed phenotypes was collected.

The observed phenotype on the actin level, the loss of stress fibers (see Fig. 20) , fits well to already published data after ROCK-inhibition in glioma cells [68].

An increased invasiveness after CIN knockdown has been described in GBM6840 [48]. This study extends the finding to two other cell lines, U87 and DBTRG-05-MG. Through examination of U87 cells reexpressing CIN, and through expression of a RNAi-resistant CIN construct in GBM6840, further evidence in support of the specificity of the observed phenotype was generated (see Fig. 23 D, E and F).

As both ROCK-inhibitor treatment and expression of a constitutively active cofilin mutant were able to normalize invasion back to control levels, at least in GBM6840, the migration and invasion phenotype depended on increased phosphorylation of cofilin (see Fig. 23 J and K).

Changes in cofilin phosphorylation have a significant impact on actin dynamics, and can therefore change serum response factor activity [122]. The SRF is a widely expressed transcription factor that controls mitogen-activated genes, among them many cytoskeletal genes, and muscle specific target genes. Its activity is regulated, among other mechanisms, by cellular G-actin binding to its coactivator MAL [122]. SRF has already been published to be important for invasive behavior of glioma cells, in a study that showed that SRF knockdown in A172 cells reduces their invasive potential, and that SRF positively regulates the transcription of RTVP-1, which is a proinvasive gene [156].

LIMK activity is needed both for SRF activity and for cellular invasion [121]. Therefore the hypothesis was tested if CIN induced cell invasion is also accompanied by an increase in SRF activity.

However, SRF activity was reduced after CIN knockdown (see Fig. 19). Lower levels of G-actin, which were indeed observed after CIN depletion, are actually expected to increase SRF activity [122], as does LIMK expression [157] . However, the reporters used in the studies on LIMK are different from the reporter used in this study. The commercially available reporter used here contains a TRE of serum response elements, and is validated only for the serum and growth factor dependent MAPK/ELK-1 mediated stimulation of transcription that is an alternative activation mechanism in contrast to MAL activation of SRF. The reporter used in the LIMK study contains the 3D.ACAT promoter as described in [158], and has been extensively used in the study of actin dependent regulation of SRF activity [157]. It is possible that an increase in MAL dependent activation leads to a decrease in activity in the MAPK dependent transcriptional element, what might explain the observed results.

Furthermore, the exact nature of the actin pool mediating the SRF regulation is not known. It would be interesting to examine the nuclear actin concentrations in CIN shRNA cells compared to Ctl shRNA cells.

Therefore, due to the technical differences in the methods used, the involvement of SRF activity in the invasive process needs further investigation.

6.3 Migration and invasion

Cofilin [46,117] as well as the LIMKs [127,159,160] have been shown to be important regulators of migration and invasion in 3D culture systems and *in vivo* models.

In 2D culture conditions, some cells show no migratiory phenotype after altered cofilin phosphorylation as has been reported for immune cells [161] as well as fibroblasts [51]. In contrast, in these studies strong phenotypes in 3D culture conditions, like the matrigel system, were observed.

It was also reported that actin itself plays only a minor role in the 2D motility of glioma cells [118]. Although the treatments applied in this study were rather drastic, it is important to note that 2D motility in glioma cells might be less dependent on F-actin than in other systems, which would nicely explain the rather mild phenotypes found in this study.

Other studies have found a significant impact of cofilin expression levels on the 2D migratory behavior of cancer cells. More specifically, a cofilin knockdown increases speed and directionality in metastatic breast cancer cells, the Mtln3 cells. [117] In the same cells, expression of the kinase domain of LIMK1 abolishes protrusion and reactivity towards EGF [124].

For CIN, this is the first study that describes a migratory phenotype after CIN deregulation under 2D culture conditions. This phenotype nicely fits to the results of the transwell system. In contrast to other studies dealing with glioma cell invasion [162,163] a decrease in the speed under 2D migration conditions was correlated with an increase in matrigel invasion in transwell assays (see Fig. 22 and 23). One explanation for this observation is that the different conditions examined in these reports [162,163], malignancy grade and response to growth factor stimulation, are different from the actin regulatory pathway affected in CIN depleted glioma cells. Importantly, a recent report has also found a decrease in 2D motility and an increase in invasiveness after manipulation of actin regulatory proteins. It was found that knockdown of the SCAR/WAVE complex in A431 squamous carcinoma cells strongly decreases their migration in a wound healing assay, but promotes their invasion into matrigel *via* N-WASP activation. This leads to the conclusion that the actin machinery is utilized differently in 2D and 3D migration [164].

Increased invasion in 3D but a decreased speed in 2D can also be explained by increased force build up through cancer cells by a more stable actin cytoskeleton.

Increased actomyosin contractility is present after ROCK overexpression in melanoma cells [65], and ROCK also plays a role in cancer initiation and progression [165]. A decrease in actomyosin contractility after the treatment of GBM6840 cells with Y-27632 could be responsible for the decrease in invasion observed.

In line with an elevated ROCK activity, increased cofilin phosphorylation can lead to an increase in actomyosin assembly, and force build up [153]. This mechanism could be of crucial importance in the brain, as the brain ECM is highly hydrated, and may be more susceptible to deformation by cancer cells than other tissue barriers [134].

Importantly, inhibitors for both ROCKs and LIMKs are available [166,167], and LIMK inhibitors have been shown to inhibit glioma cell invasion *in vitro* recently [168].

6.4 *In vivo* studies

In the orthotopic implantation model that was used here, a significant growth delay could be detected after CIN downregulation in GBM6840 *in vivo* (see Fig. 30).

Slower growth is associated with increased invasion in glioma [169,170]. It is possible that in addition to that a reduction of angiogenesis through transcriptional silencing of VEGFA and the loss of c-myc protein expression (see Fig. 35 D and 37 F) contributed to the growth reduction *in vivo*.

However, no intraparenchymatic lesions could be detected in CIN knockdown or rescue cell injected animals (see Fig. 31 and Table 7), and neither angiogenesis nor stem cell properties could be examined in the xenografts in CIN knockdown and rescue cells. It is possible that the numbers of the injected cells were too low to allow observation of invasiveness during the observation period, as cell numbers can greatly influence the outcome in an implantation experiment [171].

It is also possible that the cells have lost their potential to form invasive lesions *in vivo* by an off target or integration effect of the shRNA construct used. It would be very interesting to create other CIN shRNA knockdown cell lines with different shRNAs and to analyze them *in vivo* and to inject higher cell numbers. It would be also very interesting to see if other CIN knockdown lines show a specific growth retardation *in vivo*, as *in vitro* assays under 2D culture conditions did not yield any evidence for differences in proliferation after CIN deregulation. However, the cells might proliferate differentially under 3D culture conditions and not under 2D conditions *in vitro*, as has been reported in other systems [172,173].

6.5 Transcription

The analysis of the glioma cell transcriptome has identified two CIN specific regulated transcripts, EDIL3 and MXI1, which are potentially involved in disease progression and invasion (see Table 8 and Fig. 32). The hits from the microarray analysis could be nicely verified in an independently harvested set of RNAs *via* real-time quantitative PCR (see Fig. 35). Interestingly, a negative regulator of c-myc dependent transcription, MXI1, is downregulated upon CIN depletion in GBM6840. MXI1 is known to be a regulator of

differentiation and tumorigenesis [174]. On the other hand, c-myc protein levels were reduced after CIN depletion (see Fig. 37), suggesting a complex relationship between CIN expression and c-myc activity. Overall, the measured activity of the c-myc reporter construct was higher after CIN depletion, which might indicate that the effect of the loss of MXI1 expression overrides the effect of c-myc protein reduction *in vitro* (see Fig. 37).

The phenotypes in the c-myc reporter assays in GBM6840 and U87 were rather mild, but seemed to be CIN specific. Moreover, c-myc was identified by IPA as one of the significantly altered regulators of transcription (see Fig. 34). MXI1 has been reported to act as a tumor suppressor in glioma cells [92], and influences the growth of glioma cells *in vitro* and *in vivo* [175,176]. Therefore, despite the rather small differences in reporter activity, these phenotypes might be highly relevant for glioma initiation and progression induced by CIN. It has to be taken into consideration that promoters containing E-Boxes, like the ß-Thymosin promoter, can also have overlapping binding sites for other transcription factors like AP2 and it is possible that the E-Box reporter used is not completely c-myc specific [177].

As myc/max activity could be reduced by expression of CIN in U87 cells (see Fig. 37), it would be very interesting to check if MXI1 is upregulated by CIN expression in this cell line. Additionally, detailed studies of mRNA- and protein-levels of MXI1 and c-myc are needed in GBM6840 and U87, to clarify the role of chronophin in myc regulation in glioma. As phosphorylation on Threonin 58 and Serine 62 influences myc stability and regulates myc dependent transcription, it would be interesting to quantifiy the levels of these phosphoproteins in the two cell lines.

A possible functional role for MXI1 in glioma initiation is its impact on mitochondrial biogenesis, which is mediated *via* HIF-1 signaling [178]. It would be promising to reinvestigate the observed phenotypes under hypoxia, due to the fact that CIN has also been reported to be regulated by cellular ATP levels [80], and to measure mitochondrial biogenesis after CIN deregulation.

It would also be possible to measure myc-reporter activity after treatment of cells with ROCK- and LIMK-inhibitors, to determine if the observed phenotypes are cofilin specific.

A meta-analysis of different studies on glioma invasion identified c-myc and p53 as significantly altered transcription factors in all studies analyzed (see Table 6). There were

some contradictionary results regarding the question if c-myc activity is enhanced or inhibited. A reason for this discrepancy could be the small number of genes identified in some studies.

Recently, the upregulation of p53 and downregulation of c-myc activity have been reported to be correlated with motility in glioma cells. In addition, it was shown that c-myc downregulation by siRNA knockdown increases migration and slows down growth of GBM cells *in vitro* [179].

Until now there is only limited information on the impact of c-myc on glioma invasion. Myc has been reported to be overexpressed in glioma [89], and has a significant impact on tumor initiation [91,180] and stem cell renewal in this tumor [90].

However, there are numerous studies on the pro-and anti-invasive roles of c-myc in other cancers [181,182].

In medulloblastoma, silencing of THBS1 is important for the c-myc mediated invasion [183]. THBS1 was downregulated in CIN knockdown cells in the microarray experiment, too.

CIN has previously been linked to c-myc regulation [75]. It was identified together with PP1 and PP2A in a screen for phosphatases that regulate nuclear receptor coactivator / steroid receptor coactivator 3 (NCOA3/SRC-3) activity. HEK293T cells expressing NCOA3 and estrogen receptor were transfected with a phosphatase library and screened for differences in NCOA3 phosphorylation. CIN was identified as important negative regulator of NCOA3 activity, and found to influence the hormone dependent expression of NCOA3 target genes [75]. However, the mechanism of CIN dependent myc regulation in this published report and in the present study has to be different. In the previous study c-myc is upregulated after CIN knockdown and estrogen stimulation. C-myc is a known target gene of estrogen receptor signaling and NCOA3. In the system examined, CIN, and other phosphatases, function as negative regulators of NCOA3 coactivation by dephosphorylation. Therefore, the induction of c-myc mRNA after estrogen stimulation is increased after CIN knockdown. In GBM6840, there was no alteration in c-myc expression on mRNA level after CIN knockdown, but a decrease on protein level.

P-cofilin might be the mediator of c-myc regulation, as RhoA induced cytoskeletal rearrangements have been shown to be connected to c-myc activity in NIH3T3 fibroblasts. Here, overexpression of c-myc was able to reduce the F-actin content in NIH3T3 fibroblasts that were transformed with the oncogenic $RhoA^{Q63L}$ mutant [93].

It has been reported that increases in LIMK expression, and therefore cofilin phosphorylation, can alter STAT3 activity and c-myc expression. LIMK1 overexpression in keratinocytes leads to a reduction in c-myc protein levels. Moreover, expression of a cofilin-S3A construct together with LIMK1 is able to rescue the c-myc protein level, and chemical inhibition of ROCK by Y-27632 treatment results in an increase in c-myc protein. Both Y-27632 and expression of S3A cofilin are able to increase STAT3 phosphorylation on tyrosine 705 [94]. The reduction of c-myc protein following increased cofilin phosphorylation is in line with the finding that c-myc levels were reduced on protein level in GBM6840 after CIN depletion.

Another possible mechanism by which cofilin phosphorylation could influence c-myc activity is *via* MYCBP. MYCBP has been found in a yeast two hybrid screen as interaction partner of cofilin, as reported in the STRING database. It is possible that altered cofilin phosphorylation *via* CIN impacts cofilins interaction with MYCBP and influences transcription.

A kinase that can induce both c-myc degradation and cofilin phosphorylation is GSK3ß.
In neutrophils, GSK3ß increases cofilin phosphorylation *via* inhibition of SSH2 [184] and GSK3ß is well known to phosphorylate c-myc on Threonin 58, targeting it for degradation [185].
Interestingly, the transcription of GSK3ß is upregulated in mice fed with a vitamin B deficient diet, linking CIN that is a phosphatase for active vitamin B6, to the transcriptional regulation of GSK3ß [186]. Therefore, study of GSK3ß mRNA and protein levels might provide a mechanistic insight into the regulation of both molecules. However, it has to be mentioned that CIN depletion should lead to an increase in active vitamin B6, and therefore to a reduction of GSK3ß activity, if the regulation is according to [186].

Due to the fact that MMP2 and uPA/uPAR expression have already been linked to altered cofilin phosphorylation, it was examined if these proteins are deregulated after CIN knockdown. In GBM6840, only a mild upregulation of uPAR was detected. This upregulation

was not present in DBTRG-05-MG and U87 cells. It is possible that the upregulation of uPAR contributed to the invasive phenotype of GBM6840 CIN shRNA cells. However, because DBTRG-05-MG and U87 cells had a strong phenotype in the transwell assay, uPAR upregulation was not the only factor that contributed to increased invasiveness after CIN knockdown.

7. Summary

Glioblastomas, primary brain tumors, represent a tumor entity with a dismal prognosis and a median survival of only about one year. Invasion into the healthy brain parenchyma contributes substantially to the malignancy of this type of brain tumor. Therefore, a better understanding of the mechanisms promoting the invasive behavior of these brain tumors is needed to identify new therapeutic targets.

Cofilin, an actin regulatory protein, has been shown to be an important regulator of the invasive behavior of tumor cells in other types of cancer and the actin cytoskeleton is involved in the formation of a variety of cellular structures important for cell migration and invasion. Cofilin is regulated by phosphorylation on a single residue, serine 3. The aim of this thesis was to examine the role of the cofilin regulatory phosphatase chronophin for glioma cell migration and invasion.

First, it was established that chronophin depletion in the cell line GBM6840 leads to an increase in the ratio of phosphorylated cofilin to total cofilin. Higher chronophin levels were correlated with a decrease in F-actin in the cell lines GBM6840 and U87 as measured in an actin spin down assay and in a flow cytometry based assay.

Furthermore, it was shown that knockdown of chronophin in two different cell lines, GBM6840 and DBTRG-05-MG, strongly increased their invasiveness *in vitro*. Expression of human chronophin in the cell line U87 decreased its invasiveness substantially. There was no difference in cell proliferation between GBM6840 and DBTRG-05-MG cells expressing a chronophin targeting shRNA or a control shRNA and U87 cells transfected with an empty vector or a human chronophin encoding plasmid. The increase in invasiveness after chronophin depletion could be correlated with an increase in directionality in cell migration under 2D culture conditions in the cell lines U87 and GBM6840. Moreover, treatment with the ROCK inhibitor Y-27632 decreased directionality in GBM6840 cells under 2D culture conditions and reduced the invasiveness of GBM6840 chronophin shRNA cells back to control levels.

Expression of a non-phosphorylatable cofilin mutant, the S3A mutant, was able to reduce invasiveness and to reduce directionality under 2D culture conditions back to control levels in GBM6840 chronophin shRNA cells.

This provides important evidence for the involvement of cofilin phosphoregulation in the phenotypes described above.

In vivo, when injected into NOD-SCID mice, chronophin depleted cells showed a dramatic growth reduction as compared to control and rescue cells.

Transciptomic characterization of GBM6840 cells by microarray analysis and subsequent comparison of the data with microarray profiles of normal brain tissues and different glioma entities identified two specifically chronophin regulated transcripts potentially involved in tumor progression and invasion, MXI1 and EDIL3. Moreover, c-myc was identified as a significantly altered transcription factor after chronophin deregulation based on the number of c-myc target molecules in the microarray dataset.

MXI1 is a potential negative regulator of c-myc dependent transcription, and was strongly downregulated after chronophin knockdown in GBM6840. In line with this, the activity of a c-myc reporter plasmid was increased after chronophin depletion in GBM6840 and reduced after chronophin expression in U87 cells.

However, the protein level of the c-myc protein was reduced after chronophin depletion in GBM6840.

Finally, anaylsis of the expression of proteases known to be important for glioblastoma pathogenesis revealed no major changes in protease expression between chronophin depleted and control cells.

Therefore, a comprehensive analysis of chronophin in the context of glioma pathogenesis has been performed in this thesis. It has been shown that chronophin depletion strongly enhanced invasiveness of glioma cells and that it induced transcriptomic changes potentially involved in tumor progression. The proteins regulating cofilin phosphorylation are therefore valuable therapeutic targets for anti-invasive therapy in glioblastomas. Inhibitors for kinases upstream of cofilin, e.g. LIMKs and ROCKs, are available, and might be promising agents for anti-invasive therapy.

8. Zusammenfassung

Glioblastome sind primäre Gehirntumore, die eine besonders schlechte Prognose besitzen und bei denen die mediane Überlebenszeit nur ca. ein Jahr beträgt. Zur Malignität dieses Tumortyps trägt entscheidend das Eindringen der Tumorzellen in das gesunde Hirnparenchym bei. Daher ist es notwendig die molekularen Mechanismen zu verstehen, die diesem Phänomen zu Grunde liegen, um neue therapeutische Zielmoleküle zu identifizieren.
Cofilin, ein Protein das das Aktinzytoskellet reguliert, ist in anderen Krebsarten als wichtiger Regulator des invasiven Verhaltens von Zellen bekannt und das Aktinzytoskellet ist an der Bildung einer Vielzahl von zellulären Strukturen beteiligt, die wichtig für die Zellmigration und –invasion sind. Cofilin wird über die Phosphorylierung einer einzigen Aminosäure, des Serin 3, reguliert. Das Ziel dieser Arbeit war es, die Rolle der Cofilin regulatorischen Phosphatase Chronophin für Zellmigration und -invasion zu untersuchen.
Zuerst konnte gezeigt werden, dass eine Chronophin Depletion in der Zelllinie GBM6840 zu einer Zunahme des Anteils von P-Cofilin am Gesamtcofilin führt. Ebenso war ein hohes Chronophin Level in den Zelllinien GBM6840 und U87 mit einer Abnahme des F-Actin Levels korreliert, was in einem Aktin spin down Assay als auch mittels Durchflusszytrometrie gemessen werden konnte.
Es konnte weiter gezeigt werden, dass eine shRNA vermittelte Depletion des Chronphin zu einer starken Zunahme der Invasivität in den Zelllinien GBM6840 und DBTRG-05-MG *in vitro* führt. Chronophin Expression in der Zelllinie U87 führte zu einer starken Abnahme der Invasivität. Es gab hingegen keinen Chronophin abhängigen Unterschied in der Proliferation von GBM6840 und DBTRG-05-MG Zellen, die entweder eine Kontroll- oder eine Chronophin gerichtete shRNA exprimierten, sowie keinen zwischen U87 Zellen, die mit einem Leervektor oder einem Chronophin codierenden Konstrukt transfiziert worden waren. Die Zunahme der Invasion nach Chronophin Depletion konnte mit einer Zunahme der Direktionalität der Zellen bei der Migration in einer 2D Umgebung korreliert werden. Desweiteren konnte durch Behandlung mit dem ROCK-Inhibitor Y-27632 in GBM6840 Zellen eine Erniedrigung der Direktionalität bei der Migration in 2D Kultur ebenso erreicht werden, wie eine Reduktion der Invasivität von Chronophin shRNA exprimierenden GBM6840 Zellen auf Kontrollniveau.

Die Expression einer nicht-phosphorylierbaren Cofilin Mutante, der S3A Mutante, erniedrigte sowohl die Direktionalität in der 2D Migration als auch die Invasivität von GBM6840 Chronophin shRNA exprimierenden Zellen zurück auf Kontrollniveau.
Diese Experimente lieferten wichtige Hinweise darauf, dass die Phosphoregulation von Cofilin ursächlich an der Entstehung der Phänotypen beteiligt war, die nach Chronophin Knockdown beobachtet wurden.
In vivo konnte nach Injektion in NOD-SCID Mäuse eine dramatische Wachstumsreduktion der Chronophin depletierten Zellen gemessen werden.
Durch Charakterisierung des Transkriptoms der Zelllinie GBM6840 mittels Microarrays und nachfolgender Vergleich der Ergebnisse mit Microarray-Profilen von Normalhirngewebe und verschiedenen Gliomentitäten konnten zwei spezifisch Chronophin abhängig regulierte Transkripte identifiziert werden, MXI1 und EDIL3, die potentiell mit der Progression und Invasivität von Gliomen verknüpft sind.
MXI1, ein potentieller negativer Regulator der c-myc abhängigen Transkription, war nach Chronophin Herunterregulation in GBM6840 stark herunterreguliert. In Übereinstimmung mit diesem Befund war die Aktiviät eines c-myc Reporterplasmids nach Chronophin Herunterregulation in GBM6840 erhöht, nach Chronophin Expression in U87 jedoch erniedrigt. Das c-myc Protein selbst wies eine deutliche Reduktion nach Chronophin Depletion in GBM6840 auf.

Abschließend wurde die Expression von Proteasen untersucht, für die eine Rolle in der Gliominvasion bekannt ist. Hier wurden jedoch keine größeren Chronophin abhängigen Expressionsunterschiede gefunden.

Zusammenfassend gesagt konnte eine umfassende Charakterisierung der Rolle des Chronophin in der Gliompathogenese erreicht werden. Zum einen konnte gezeigt werden, dass Chronophin ein äußerst wichtiger Regulator der Invasion ist, zum anderen dass es zu Chronophin abhängigen transkriptomischen Veränderungen kommt, die potentiell zur Malignisierung des Tumors beitragen.
Daher sind die Proteine die die Cofilinphosphorylierung regulieren potentielle therapeutische Zielmoleküle für eine anti-invasive Therapie im Glioblastom. Inhibitoren für die Kinasen, die Regulatoren des Cofilin sind, die ROCK- und LIM-Kinasen, sind verfügbar und stellen möglicherweise vielversprechende Substanzen für die anti-invasive Therapie dar.

9. References

1. Pellegrin S, Mellor H (2007) Actin stress fibres. J Cell Sci 120: 3491-3499.
2. Doolittle ND (2004) State of the science in brain tumor classification. Semin Oncol Nurs 20: 224-230.
3. Gladson CL, Prayson RA, Liu WM (2010) The pathobiology of glioma tumors. Annu Rev Pathol 5: 33-50.
4. Alcantara Llaguno S, Chen J, Kwon CH, Jackson EL, Li Y, et al. (2009) Malignant astrocytomas originate from neural stem/progenitor cells in a somatic tumor suppressor mouse model. Cancer Cell 15: 45-56.
5. Friedmann-Morvinski D, Bushong EA, Ke E, Soda Y, Marumoto T, et al. (2012) Dedifferentiation of neurons and astrocytes by oncogenes can induce gliomas in mice. Science 338: 1080-1084.
6. Riede UN MW, HE. Schaefer (2004) Allgemeine und spezielle Pathologie. Stuttgart: Georg Thieme Verlag. 1236 p.
7. Huse JT, Holland EC (2010) Targeting brain cancer: advances in the molecular pathology of malignant glioma and medulloblastoma. Nat Rev Cancer 10: 319-331.
8. Bondy ML, Scheurer ME, Malmer B, Barnholtz-Sloan JS, Davis FG, et al. (2008) Brain tumor epidemiology: consensus from the Brain Tumor Epidemiology Consortium. Cancer 113: 1953-1968.
9. Wrensch M, Jenkins RB, Chang JS, Yeh RF, Xiao Y, et al. (2009) Variants in the CDKN2B and RTEL1 regions are associated with high-grade glioma susceptibility. Nat Genet 41: 905-908.
10. Purow B, Schiff D (2009) Advances in the genetics of glioblastoma: are we reaching critical mass? Nat Rev Neurol 5: 419-426.
11. Masuhr K. NM (2007) Neurologie. Stuttgart: Georg Thieme Verlag. 595 p.
12. Stupp R, Hegi ME, Gilbert MR, Chakravarti A (2007) Chemoradiotherapy in malignant glioma: standard of care and future directions. J Clin Oncol 25: 4127-4136.
13. Friedman HS, Kerby T, Calvert H (2000) Temozolomide and treatment of malignant glioma. Clin Cancer Res 6: 2585-2597.
14. Yamanaka R (2008) Cell- and peptide-based immunotherapeutic approaches for glioma. Trends Mol Med 14: 228-235.
15. Castro MG, Candolfi M, Kroeger K, King GD, Curtin JF, et al. (2011) Gene therapy and targeted toxins for glioma. Curr Gene Ther 11: 155-180.
16. Stommel JM, Kimmelman AC, Ying H, Nabioullin R, Ponugoti AH, et al. (2007) Coactivation of receptor tyrosine kinases affects the response of tumor cells to targeted therapies. Science 318: 287-290.
17. Norden AD, Drappatz J, Wen PY (2009) Antiangiogenic therapies for high-grade glioma. Nat Rev Neurol 5: 610-620.
18. Verhoeff JJ, van Tellingen O, Claes A, Stalpers LJ, van Linde ME, et al. (2009) Concerns about anti-angiogenic treatment in patients with glioblastoma multiforme. BMC Cancer 9: 444.
19. Huveldt D, Lewis-Tuffin LJ, Carlson BL, Schroeder MA, Rodriguez F, et al. (2013) Targeting Src family kinases inhibits bevacizumab-induced glioma cell invasion. PLoS One 8: e56505.
20. Munson JM, Fried L, Rowson SA, Bonner MY, Karumbaiah L, et al. (2012) Anti-invasive adjuvant therapy with imipramine blue enhances chemotherapeutic efficacy against glioma. Sci Transl Med 4: 127ra136.
21. (2008) Comprehensive genomic characterization defines human glioblastoma genes and core pathways. Nature 455: 1061-1068.
22. Parsons DW, Jones S, Zhang X, Lin JC, Leary RJ, et al. (2008) An integrated genomic analysis of human glioblastoma multiforme. Science 321: 1807-1812.
23. Chen J, McKay RM, Parada LF (2012) Malignant glioma: lessons from genomics, mouse models, and stem cells. Cell 149: 36-47.

24. Huse JT, Holland E, DeAngelis LM (2013) Glioblastoma: molecular analysis and clinical implications. Annu Rev Med 64: 59-70.
25. Wikstrand CJ, McLendon RE, Friedman AH, Bigner DD (1997) Cell surface localization and density of the tumor-associated variant of the epidermal growth factor receptor, EGFRvIII. Cancer Res 57: 4130-4140.
26. Fan QW, Cheng CK, Gustafson WC, Charron E, Zipper P, et al. (2013) EGFR phosphorylates tumor-derived EGFRvIII driving STAT3/5 and progression in glioblastoma. Cancer Cell 24: 438-449.
27. Verhaak RG, Hoadley KA, Purdom E, Wang V, Qi Y, et al. (2010) Integrated genomic analysis identifies clinically relevant subtypes of glioblastoma characterized by abnormalities in PDGFRA, IDH1, EGFR, and NF1. Cancer Cell 17: 98-110.
28. Sturm D, Witt H, Hovestadt V, Khuong-Quang DA, Jones DT, et al. (2012) Hotspot mutations in H3F3A and IDH1 define distinct epigenetic and biological subgroups of glioblastoma. Cancer Cell 22: 425-437.
29. Noushmehr H, Weisenberger DJ, Diefes K, Phillips HS, Pujara K, et al. (2010) Identification of a CpG island methylator phenotype that defines a distinct subgroup of glioma. Cancer Cell 17: 510-522.
30. Brennan CW, Verhaak RG, McKenna A, Campos B, Noushmehr H, et al. (2013) The somatic genomic landscape of glioblastoma. Cell 155: 462-477.
31. Carro MS, Lim WK, Alvarez MJ, Bollo RJ, Zhao X, et al. (2010) The transcriptional network for mesenchymal transformation of brain tumours. Nature 463: 318-325.
32. Shen R, Mo Q, Schultz N, Seshan VE, Olshen AB, et al. (2012) Integrative subtype discovery in glioblastoma using iCluster. PLoS One 7: e35236.
33. Brennan C, Momota H, Hambardzumyan D, Ozawa T, Tandon A, et al. (2009) Glioblastoma subclasses can be defined by activity among signal transduction pathways and associated genomic alterations. PLoS One 4: e7752.
34. Chicoine MR, Silbergeld DL (1997) Mitogens as motogens. J Neurooncol 35: 249-257.
35. Bugyi B, Carlier MF (2010) Control of actin filament treadmilling in cell motility. Annu Rev Biophys 39: 449-470.
36. Bravo-Cordero JJ, Magalhaes MA, Eddy RJ, Hodgson L, Condeelis J (2013) Functions of cofilin in cell locomotion and invasion. Nat Rev Mol Cell Biol.
37. Vartiainen MK, Mustonen T, Mattila PK, Ojala PJ, Thesleff I, et al. (2002) The three mouse actin-depolymerizing factor/cofilins evolved to fulfill cell-type-specific requirements for actin dynamics. Mol Biol Cell 13: 183-194.
38. Chhabra ES, Higgs HN (2007) The many faces of actin: matching assembly factors with cellular structures. Nat Cell Biol 9: 1110-1121.
39. Nurnberg A, Kitzing T, Grosse R (2011) Nucleating actin for invasion. Nat Rev Cancer 11: 177-187.
40. Pollard TD, Borisy GG (2003) Cellular motility driven by assembly and disassembly of actin filaments. Cell 112: 453-465.
41. Mizuno K (2013) Signaling mechanisms and functional roles of cofilin phosphorylation and dephosphorylation. Cell Signal 25: 457-469.
42. Albinsson S, Nordstrom I, Hellstrand P (2004) Stretch of the vascular wall induces smooth muscle differentiation by promoting actin polymerization. J Biol Chem 279: 34849-34855.
43. Rochelle T, Daubon T, Van Troys M, Harnois T, Waterschoot D, et al. (2013) p210bcr-abl induces amoeboid motility by recruiting ADF/destrin through RhoA/ROCK1. FASEB J 27: 123-134.
44. Ohashi K, Nagata K, Maekawa M, Ishizaki T, Narumiya S, et al. (2000) Rho-associated kinase ROCK activates LIM-kinase 1 by phosphorylation at threonine 508 within the activation loop. J Biol Chem 275: 3577-3582.
45. Sumi T, Matsumoto K, Nakamura T (2001) Specific activation of LIM kinase 2 via phosphorylation of threonine 505 by ROCK, a Rho-dependent protein kinase. J Biol Chem 276: 670-676.
46. Wang W, Mouneimne G, Sidani M, Wyckoff J, Chen X, et al. (2006) The activity status of cofilin is directly related to invasion, intravasation, and metastasis of mammary tumors. J Cell Biol 173: 395-404.

47. van Rheenen J, Condeelis J, Glogauer M (2009) A common cofilin activity cycle in invasive tumor cells and inflammatory cells. J Cell Sci 122: 305-311.
48. Fedorchenko O (2009) Rolle von Chronophin für die Cofilin-vermittelte

Aktin-Dynamik in astrozytären Tumorzellen [Inaugural Dissertation]. Düsseldorf: Heinrich-Heine Universität Düsseldorf. 107 p.
49. Samuel MS, Lopez JI, McGhee EJ, Croft DR, Strachan D, et al. (2011) Actomyosin-mediated cellular tension drives increased tissue stiffness and beta-catenin activation to induce epidermal hyperplasia and tumor growth. Cancer Cell 19: 776-791.
50. Davila M, Frost AR, Grizzle WE, Chakrabarti R (2003) LIM kinase 1 is essential for the invasive growth of prostate epithelial cells: implications in prostate cancer. J Biol Chem 278: 36868-36875.
51. Scott RW, Hooper S, Crighton D, Li A, Konig I, et al. (2010) LIM kinases are required for invasive path generation by tumor and tumor-associated stromal cells. J Cell Biol 191: 169-185.
52. Manetti F (2012) LIM kinases are attractive targets with many macromolecular partners and only a few small molecule regulators. Med Res Rev 32: 968-998.
53. Wang W, Eddy R, Condeelis J (2007) The cofilin pathway in breast cancer invasion and metastasis. Nat Rev Cancer 7: 429-440.
54. Amano M, Nakayama M, Kaibuchi K (2010) Rho-kinase/ROCK: A key regulator of the cytoskeleton and cell polarity. Cytoskeleton (Hoboken) 67: 545-554.
55. Bernstein BW, Bamburg JR (2010) ADF/cofilin: a functional node in cell biology. Trends Cell Biol 20: 187-195.
56. van Rheenen J, Song X, van Roosmalen W, Cammer M, Chen X, et al. (2007) EGF-induced PIP2 hydrolysis releases and activates cofilin locally in carcinoma cells. J Cell Biol 179: 1247-1259.
57. Desmarais V, Yamaguchi H, Oser M, Soon L, Mouneimne G, et al. (2009) N-WASP and cortactin are involved in invadopodium-dependent chemotaxis to EGF in breast tumor cells. Cell Motil Cytoskeleton 66: 303-316.
58. Linder S (2007) The matrix corroded: podosomes and invadopodia in extracellular matrix degradation. Trends Cell Biol 17: 107-117.
59. Ghosh M, Song X, Mouneimne G, Sidani M, Lawrence DS, et al. (2004) Cofilin promotes actin polymerization and defines the direction of cell motility. Science 304: 743-746.
60. Sun CX, Magalhaes MA, Glogauer M (2007) Rac1 and Rac2 differentially regulate actin free barbed end formation downstream of the fMLP receptor. J Cell Biol 179: 239-245.
61. Kiuchi T, Ohashi K, Kurita S, Mizuno K (2007) Cofilin promotes stimulus-induced lamellipodium formation by generating an abundant supply of actin monomers. J Cell Biol 177: 465-476.
62. Unwin RD, Craven RA, Harnden P, Hanrahan S, Totty N, et al. (2003) Proteomic changes in renal cancer and co-ordinate demonstration of both the glycolytic and mitochondrial aspects of the Warburg effect. Proteomics 3: 1620-1632.
63. Turhani D, Krapfenbauer K, Thurnher D, Langen H, Fountoulakis M (2006) Identification of differentially expressed, tumor-associated proteins in oral squamous cell carcinoma by proteomic analysis. Electrophoresis 27: 1417-1423.
64. Keshamouni VG, Michailidis G, Grasso CS, Anthwal S, Strahler JR, et al. (2006) Differential protein expression profiling by iTRAQ-2DLC-MS/MS of lung cancer cells undergoing epithelial-mesenchymal transition reveals a migratory/invasive phenotype. J Proteome Res 5: 1143-1154.
65. Sanz-Moreno V, Gaggioli C, Yeo M, Albrengues J, Wallberg F, et al. (2011) ROCK and JAK1 signaling cooperate to control actomyosin contractility in tumor cells and stroma. Cancer Cell 20: 229-245.
66. An L, Liu Y, Wu A, Guan Y (2013) microRNA-124 Inhibits Migration and Invasion by Down-Regulating ROCK1 in Glioma. PLoS One 8: e69478.
67. Deng L, Li G, Li R, Liu Q, He Q, et al. (2010) Rho-kinase inhibitor, fasudil, suppresses glioblastoma cell line progression in vitro and in vivo. Cancer Biol Ther 9: 875-884.

68. Salhia B, Rutten F, Nakada M, Beaudry C, Berens M, et al. (2005) Inhibition of Rho-kinase affects astrocytoma morphology, motility, and invasion through activation of Rac1. Cancer Res 65: 8792-8800.
69. Nagai S, Moreno O, Smith CA, Ivanchuk S, Romagnuolo R, et al. (2011) Role of the cofilin activity cycle in astrocytoma migration and invasion. Genes Cancer 2: 859-869.
70. Yap CT, Simpson TI, Pratt T, Price DJ, Maciver SK (2005) The motility of glioblastoma tumour cells is modulated by intracellular cofilin expression in a concentration-dependent manner. Cell Motil Cytoskeleton 60: 153-165.
71. Seifried A, Schultz J, Gohla A (2013) Human HAD phosphatases: structure, mechanism, and roles in health and disease. FEBS J 280: 549-571.
72. Gao GJ, Fonda ML (1994) Kinetic analysis and chemical modification of vitamin B6 phosphatase from human erythrocytes. J Biol Chem 269: 7163-7168.
73. Gao G, Fonda ML (1994) Identification of an essential cysteine residue in pyridoxal phosphatase from human erythrocytes. J Biol Chem 269: 8234-8239.
74. Gohla A, Birkenfeld J, Bokoch GM (2005) Chronophin, a novel HAD-type serine protein phosphatase, regulates cofilin-dependent actin dynamics. Nat Cell Biol 7: 21-29.
75. Li C, Liang YY, Feng XH, Tsai SY, Tsai MJ, et al. (2008) Essential phosphatases and a phospho-degron are critical for regulation of SRC-3/AIB1 coactivator function and turnover. Mol Cell 31: 835-849.
76. Zoudilova M, Min J, Richards HL, Carter D, Huang T, et al. (2010) beta-Arrestins scaffold cofilin with chronophin to direct localized actin filament severing and membrane protrusions downstream of protease-activated receptor-2. J Biol Chem 285: 14318-14329.
77. Jang YM, Kim DW, Kang TC, Won MH, Baek NI, et al. (2003) Human pyridoxal phosphatase. Molecular cloning, functional expression, and tissue distribution. J Biol Chem 278: 50040-50046.
78. Boe AS, Bredholt G, Knappskog PM, Storstein A, Vedeler CA, et al. (2004) Pyridoxal phosphatase is a novel cancer autoantigen in the central nervous system. Br J Cancer 91: 1508-1514.
79. Kim JE, Ryu HJ, Kim MJ, Kim DW, Kwon OS, et al. (2010) Pyridoxal-5'-phosphate phosphatase/chronophin induces astroglial apoptosis via actin-depolymerizing factor/cofilin system in the rat brain following status epilepticus. Glia 58: 1937-1948.
80. Huang TY, Minamide LS, Bamburg JR, Bokoch GM (2008) Chronophin mediates an ATP-sensing mechanism for cofilin dephosphorylation and neuronal cofilin-actin rod formation. Dev Cell 15: 691-703.
81. Nakamura M, Ishida E, Shimada K, Kishi M, Nakase H, et al. (2005) Frequent LOH on 22q12.3 and TIMP-3 inactivation occur in the progression to secondary glioblastomas. Lab Invest 85: 165-175.
82. Ji H, Wu G, Zhan X, Nolan A, Koh C, et al. (2011) Cell-type independent MYC target genes reveal a primordial signature involved in biomass accumulation. PLoS One 6: e26057.
83. Lin CY, Loven J, Rahl PB, Paranal RM, Burge CB, et al. (2012) Transcriptional amplification in tumor cells with elevated c-Myc. Cell 151: 56-67.
84. Nie Z, Hu G, Wei G, Cui K, Yamane A, et al. (2012) c-Myc is a universal amplifier of expressed genes in lymphocytes and embryonic stem cells. Cell 151: 68-79.
85. (2013) Unlocking the mysterious mechanisms of Myc. Nat Med 19: 26-27.
86. Walz S, Lorenzin F, Morton J, Wiese KE, von Eyss B, et al. (2014) Activation and repression by oncogenic MYC shape tumour-specific gene expression profiles. Nature 511: 483-487.
87. Hurlin PJ, Huang J (2006) The MAX-interacting transcription factor network. Semin Cancer Biol 16: 265-274.
88. Herms JW, von Loewenich FD, Behnke J, Markakis E, Kretzschmar HA (1999) c-myc oncogene family expression in glioblastoma and survival. Surg Neurol 51: 536-542.
89. Vita M, Henriksson M (2006) The Myc oncoprotein as a therapeutic target for human cancer. Semin Cancer Biol 16: 318-330.

90. Zheng H, Ying H, Yan H, Kimmelman AC, Hiller DJ, et al. (2008) p53 and Pten control neural and glioma stem/progenitor cell renewal and differentiation. Nature 455: 1129-1133.
91. Radke J, Bortolussi G, Pagenstecher A (2013) Akt and c-Myc induce stem-cell markers in mature primary p53(-)/(-) astrocytes and render these cells gliomagenic in the brain of immunocompetent mice. PLoS One 8: e56691.
92. Manni I, Tunici P, Cirenei N, Albarosa R, Colombo BM, et al. (2002) Mxi1 inhibits the proliferation of U87 glioma cells through down-regulation of cyclin B1 gene expression. Br J Cancer 86: 477-484.
93. Sauzeau V, Berenjeno IM, Citterio C, Bustelo XR (2010) A transcriptional cross-talk between RhoA and c-Myc inhibits the RhoA/Rock-dependent cytoskeleton. Oncogene 29: 3781-3792.
94. Honma M, Benitah SA, Watt FM (2006) Role of LIM kinases in normal and psoriatic human epidermis. Mol Biol Cell 17: 1888-1896.
95. Livak KJ, Schmittgen TD (2001) Analysis of relative gene expression data using real-time quantitative PCR and the 2(-Delta Delta C(T)) Method. Methods 25: 402-408.
96. Kinoshita E, Kinoshita-Kikuta E, Koike T (2009) Separation and detection of large phosphoproteins using Phos-tag SDS-PAGE. Nat Protoc 4: 1513-1521.
97. Kruse CA, Mitchell DH, Kleinschmidt-DeMasters BK, Franklin WA, Morse HG, et al. (1992) Characterization of a continuous human glioma cell line DBTRG-05MG: growth kinetics, karyotype, receptor expression, and tumor suppressor gene analyses. In Vitro Cell Dev Biol 28A: 609-614.
98. Di Tomaso E, Pang JC, Lam HK, Tian XX, Suen KW, et al. (2000) Establishment and characterization of a human cell line from paediatric cerebellar glioblastoma multiforme. Neuropathol Appl Neurobiol 26: 22-30.
99. Ponten J, Macintyre EH (1968) Long term culture of normal and neoplastic human glia. Acta Pathol Microbiol Scand 74: 465-486.
100. Wilson RC, Doudna JA (2013) Molecular mechanisms of RNA interference. Annu Rev Biophys 42: 217-239.
101. Carthew RW, Sontheimer EJ (2009) Origins and Mechanisms of miRNAs and siRNAs. Cell 136: 642-655.
102. Devgan V HA, Jiang Q, Pattison S (2012) Cignal Reporter Assay Kit: A high-performance tool for assessing the functions of genes, biologics, and small molecule compounds.
103. Chopra M, Kraus S, Schwinn S, Ritz M, Mattenheimer K, et al. (2013) Non-invasive bioluminescence imaging to monitor the immunological control of a plasmablastic lymphoma-like B cell neoplasia after hematopoietic cell transplantation. PLoS One 8: e81320.
104. Gargett CE, Schwab KE, Zillwood RM, Nguyen HP, Wu D (2009) Isolation and culture of epithelial progenitors and mesenchymal stem cells from human endometrium. Biol Reprod 80: 1136-1145.
105. Prochazka M, Gaskins HR, Shultz LD, Leiter EH (1992) The nonobese diabetic scid mouse: model for spontaneous thymomagenesis associated with immunodeficiency. Proc Natl Acad Sci U S A 89: 3290-3294.
106. Siolas D, Hannon GJ (2013) Patient-derived tumor xenografts: transforming clinical samples into mouse models. Cancer Res 73: 5315-5319.
107. Madhavan S, Zenklusen JC, Kotliarov Y, Sahni H, Fine HA, et al. (2009) Rembrandt: helping personalized medicine become a reality through integrative translational research. Mol Cancer Res 7: 157-167.
108. Sun L, Hui AM, Su Q, Vortmeyer A, Kotliarov Y, et al. (2006) Neuronal and glioma-derived stem cell factor induces angiogenesis within the brain. Cancer Cell 9: 287-300.
109. Huang da W, Sherman BT, Lempicki RA (2009) Systematic and integrative analysis of large gene lists using DAVID bioinformatics resources. Nat Protoc 4: 44-57.
110. Huang da W, Sherman BT, Lempicki RA (2009) Bioinformatics enrichment tools: paths toward the comprehensive functional analysis of large gene lists. Nucleic Acids Res 37: 1-13.
111. Crawley M (2005) Statistics: An introduction using R: John Wiley & Sons. 342 p.

112. Zaga-Clavellina V, Garcia-Lopez G, Flores-Herrera H, Espejel-Nunez A, Flores-Pliego A, et al. (2007) In vitro secretion profiles of interleukin (IL)-1beta, IL-6, IL-8, IL-10, and TNF alpha after selective infection with Escherichia coli in human fetal membranes. Reprod Biol Endocrinol 5: 46.
113. Kinoshita E, Kinoshita-Kikuta E, Koike T (2012) Phos-tag SDS-PAGE systems for phosphorylation profiling of proteins with a wide range of molecular masses under neutral pH conditions. Proteomics 12: 192-202.
114. Kinoshita E, Kinoshita-Kikuta E, Ujihara H, Koike T (2009) Mobility shift detection of phosphorylation on large proteins using a Phos-tag SDS-PAGE gel strengthened with agarose. Proteomics 9: 4098-4101.
115. Hall A, Nobes CD (2000) Rho GTPases: molecular switches that control the organization and dynamics of the actin cytoskeleton. Philos Trans R Soc Lond B Biol Sci 355: 965-970.
116. Hall A (1998) Rho GTPases and the actin cytoskeleton. Science 279: 509-514.
117. Sidani M, Wessels D, Mouneimne G, Ghosh M, Goswami S, et al. (2007) Cofilin determines the migration behavior and turning frequency of metastatic cancer cells. J Cell Biol 179: 777-791.
118. Panopoulos A, Howell M, Fotedar R, Margolis RL (2011) Glioblastoma motility occurs in the absence of actin polymer. Mol Biol Cell 22: 2212-2220.
119. Machesky LM, Hall A (1997) Role of actin polymerization and adhesion to extracellular matrix in Rac- and Rho-induced cytoskeletal reorganization. J Cell Biol 138: 913-926.
120. Medjkane S, Perez-Sanchez C, Gaggioli C, Sahai E, Treisman R (2009) Myocardin-related transcription factors and SRF are required for cytoskeletal dynamics and experimental metastasis. Nat Cell Biol 11: 257-268.
121. Morin P, Wickman G, Munro J, Inman GJ, Olson MF (2011) Differing contributions of LIMK and ROCK to TGFbeta-induced transcription, motility and invasion. Eur J Cell Biol 90: 13-25.
122. Posern G, Treisman R (2006) Actin' together: serum response factor, its cofactors and the link to signal transduction. Trends Cell Biol 16: 588-596.
123. Institute NC (2005) REMBRANDT home page.
124. Zebda N, Bernard O, Bailly M, Welti S, Lawrence DS, et al. (2000) Phosphorylation of ADF/cofilin abolishes EGF-induced actin nucleation at the leading edge and subsequent lamellipod extension. J Cell Biol 151: 1119-1128.
125. Mouneimne G, DesMarais V, Sidani M, Scemes E, Wang W, et al. (2006) Spatial and temporal control of cofilin activity is required for directional sensing during chemotaxis. Curr Biol 16: 2193-2205.
126. Rao JS (2003) Molecular mechanisms of glioma invasiveness: the role of proteases. Nat Rev Cancer 3: 489-501.
127. Bagheri-Yarmand R, Mazumdar A, Sahin AA, Kumar R (2006) LIM kinase 1 increases tumor metastasis of human breast cancer cells via regulation of the urokinase-type plasminogen activator system. Int J Cancer 118: 2703-2710.
128. Higuchi O, Baeg GH, Akiyama T, Mizuno K (1996) Suppression of fibroblast cell growth by overexpression of LIM-kinase 1. FEBS Lett 396: 81-86.
129. Darzynkiewicz Z (2011) Critical aspects in analysis of cellular DNA content. Curr Protoc Cytom Chapter 7: Unit 7 2.
130. Amano T, Kaji N, Ohashi K, Mizuno K (2002) Mitosis-specific activation of LIM motif-containing protein kinase and roles of cofilin phosphorylation and dephosphorylation in mitosis. J Biol Chem 277: 22093-22102.
131. Hsu FF, Lin TY, Chen JY, Shieh SY (2010) p53-Mediated transactivation of LIMK2b links actin dynamics to cell cycle checkpoint control. Oncogene 29: 2864-2876.
132. Fraley SI, Feng Y, Krishnamurthy R, Kim DH, Celedon A, et al. (2010) A distinctive role for focal adhesion proteins in three-dimensional cell motility. Nat Cell Biol 12: 598-604.
133. Marcoux N, Vuori K (2005) EGF receptor activity is essential for adhesion-induced stress fiber formation and cofilin phosphorylation. Cell Signal 17: 1449-1455.

134. Bellail AC, Hunter SB, Brat DJ, Tan C, Van Meir EG (2004) Microregional extracellular matrix heterogeneity in brain modulates glioma cell invasion. Int J Biochem Cell Biol 36: 1046-1069.
135. Edgar R, Domrachev M, Lash AE (2002) Gene Expression Omnibus: NCBI gene expression and hybridization array data repository. Nucleic Acids Res 30: 207-210.
136. Chandriani S, Frengen E, Cowling VH, Pendergrass SA, Perou CM, et al. (2009) A core MYC gene expression signature is prominent in basal-like breast cancer but only partially overlaps the core serum response. PLoS One 4: e6693.
137. Holtkamp N, Afanasieva A, Elstner A, van Landeghem FK, Konneker M, et al. (2005) Brain slice invasion model reveals genes differentially regulated in glioma invasion. Biochem Biophys Res Commun 336: 1227-1233.
138. Maruo T, Ichikawa T, Kanzaki H, Inoue S, Kurozumi K, et al. (2013) Proteomics-based analysis of invasion-related proteins in malignant gliomas. Neuropathology 33: 264-275.
139. Tatenhorst L, Puttmann S, Senner V, Paulus W (2005) Genes associated with fast glioma cell migration in vitro and in vivo. Brain Pathol 15: 46-54.
140. Hoelzinger DB, Mariani L, Weis J, Woyke T, Berens TJ, et al. (2005) Gene expression profile of glioblastoma multiforme invasive phenotype points to new therapeutic targets. Neoplasia 7: 7-16.
141. Guo H, Gu F, Li W, Zhang B, Niu R, et al. (2009) Reduction of protein kinase C zeta inhibits migration and invasion of human glioblastoma cells. J Neurochem 109: 203-213.
142. Ma Y, Wang B, Li W, Liu X, Wang J, et al. (2011) Intersectin1-s is involved in migration and invasion of human glioma cells. J Neurosci Res 89: 1079-1090.
143. Gunnersen JM, Spirkoska V, Smith PE, Danks RA, Tan SS (2000) Growth and migration markers of rat C6 glioma cells identified by serial analysis of gene expression. Glia 32: 146-154.
144. Clark EA, Golub TR, Lander ES, Hynes RO (2000) Genomic analysis of metastasis reveals an essential role for RhoC. Nature 406: 532-535.
145. Simpson KJ, Dugan AS, Mercurio AM (2004) Functional analysis of the contribution of RhoA and RhoC GTPases to invasive breast carcinoma. Cancer Res 64: 8694-8701.
146. Vega FM, Fruhwirth G, Ng T, Ridley AJ (2011) RhoA and RhoC have distinct roles in migration and invasion by acting through different targets. J Cell Biol 193: 655-665.
147. Khalil BD, El-Sibai M (2012) Rho GTPases in primary brain tumor malignancy and invasion. J Neurooncol 108: 333-339.
148. Wheeler AP, Ridley AJ (2004) Why three Rho proteins? RhoA, RhoB, RhoC, and cell motility. Exp Cell Res 301: 43-49.
149. Cherfils J, Zeghouf M (2013) Regulation of small GTPases by GEFs, GAPs, and GDIs. Physiol Rev 93: 269-309.
150. Tang AT, Campbell WB, Nithipatikom K (2012) ROCK1 feedback regulation of the upstream small GTPase RhoA. Cell Signal 24: 1375-1380.
151. Sander EE, ten Klooster JP, van Delft S, van der Kammen RA, Collard JG (1999) Rac downregulates Rho activity: reciprocal balance between both GTPases determines cellular morphology and migratory behavior. J Cell Biol 147: 1009-1022.
152. Bhadriraju K, Yang M, Alom Ruiz S, Pirone D, Tan J, et al. (2007) Activation of ROCK by RhoA is regulated by cell adhesion, shape, and cytoskeletal tension. Exp Cell Res 313: 3616-3623.
153. Wiggan O, Shaw AE, DeLuca JG, Bamburg JR (2012) ADF/cofilin regulates actomyosin assembly through competitive inhibition of myosin II binding to F-actin. Dev Cell 22: 530-543.
154. Borm B, Requardt RP, Herzog V, Kirfel G (2005) Membrane ruffles in cell migration: indicators of inefficient lamellipodia adhesion and compartments of actin filament reorganization. Exp Cell Res 302: 83-95.
155. Meyer AS, Hughes-Alford SK, Kay JE, Castillo A, Wells A, et al. (2012) 2D protrusion but not motility predicts growth factor-induced cancer cell migration in 3D collagen. J Cell Biol 197: 721-729.

156. Ziv-Av A, Taller D, Attia M, Xiang C, Lee HK, et al. (2011) RTVP-1 expression is regulated by SRF downstream of protein kinase C and contributes to the effect of SRF on glioma cell migration. Cell Signal 23: 1936-1943.
157. Geneste O, Copeland JW, Treisman R (2002) LIM kinase and Diaphanous cooperate to regulate serum response factor and actin dynamics. J Cell Biol 157: 831-838.
158. Mohun T, Garrett N, Treisman R (1987) Xenopus cytoskeletal actin and human c-fos gene promoters share a conserved protein-binding site. EMBO J 6: 667-673.
159. Ahmed T, Shea K, Masters JR, Jones GE, Wells CM (2008) A PAK4-LIMK1 pathway drives prostate cancer cell migration downstream of HGF. Cell Signal 20: 1320-1328.
160. Vlecken DH, Bagowski CP (2009) LIMK1 and LIMK2 are important for metastatic behavior and tumor cell-induced angiogenesis of pancreatic cancer cells. Zebrafish 6: 433-439.
161. Klemke M, Kramer E, Konstandin MH, Wabnitz GH, Samstag Y (2010) An MEK-cofilin signalling module controls migration of human T cells in 3D but not 2D environments. EMBO J 29: 2915-2929.
162. Chicoine MR, Silbergeld DL (1995) The in vitro motility of human gliomas increases with increasing grade of malignancy. Cancer 75: 2904-2909.
163. Pedersen PH, Ness GO, Engebraaten O, Bjerkvig R, Lillehaug JR, et al. (1994) Heterogeneous response to the growth factors [EGF, PDGF (bb), TGF-alpha, bFGF, IL-2] on glioma spheroid growth, migration and invasion. Int J Cancer 56: 255-261.
164. Tang H, Li A, Bi J, Veltman DM, Zech T, et al. (2013) Loss of Scar/WAVE complex promotes N-WASP- and FAK-dependent invasion. Curr Biol 23: 107-117.
165. Samuel MS, Olson MF (2011) Actomyosin contractililty: force power drives tumor growth. Cell Cycle 10: 3409-3410.
166. Olson MF (2008) Applications for ROCK kinase inhibition. Curr Opin Cell Biol 20: 242-248.
167. Ross-Macdonald P, de Silva H, Guo Q, Xiao H, Hung CY, et al. (2008) Identification of a nonkinase target mediating cytotoxicity of novel kinase inhibitors. Mol Cancer Ther 7: 3490-3498.
168. Park JB, Agnihotri S, Golbourn B, Bertrand KC, Luck A, et al. (2014) Transcriptional profiling of GBM invasion genes identifies effective inhibitors of the LIM kinase-Cofilin pathway. Oncotarget.
169. Lu KV, Chang JP, Parachoniak CA, Pandika MM, Aghi MK, et al. (2012) VEGF inhibits tumor cell invasion and mesenchymal transition through a MET/VEGFR2 complex. Cancer Cell 22: 21-35.
170. Horing E, Harter PN, Seznec J, Schittenhelm J, Buhring HJ, et al. (2012) The "go or grow" potential of gliomas is linked to the neuropeptide processing enzyme carboxypeptidase E and mediated by metabolic stress. Acta Neuropathol 124: 83-97.
171. Binda E, Visioli A, Giani F, Lamorte G, Copetti M, et al. (2012) The EphA2 receptor drives self-renewal and tumorigenicity in stem-like tumor-propagating cells from human glioblastomas. Cancer Cell 22: 765-780.
172. Ki CS, Shih H, Lin CC (2013) Effect of 3D Matrix Compositions on the Efficacy of EGFR Inhibition in Pancreatic Ductal Adenocarcinoma Cells. Biomacromolecules.
173. Stegemann JP, Nerem RM (2003) Altered response of vascular smooth muscle cells to exogenous biochemical stimulation in two- and three-dimensional culture. Exp Cell Res 283: 146-155.
174. Foley KP, Eisenman RN (1999) Two MAD tails: what the recent knockouts of Mad1 and Mxi1 tell us about the MYC/MAX/MAD network. Biochim Biophys Acta 1423: M37-47.
175. Chen J, Willingham T, Margraf LR, Schreiber-Agus N, DePinho RA, et al. (1995) Effects of the MYC oncogene antagonist, MAD, on proliferation, cell cycling and the malignant phenotype of human brain tumour cells. Nat Med 1: 638-643.
176. Roy B, Reisman D (1995) Inducible expression of Mad accelerates growth arrest of serum deprived human glioblastoma cells. Cell Biol Int 19: 307-313.
177. Gaubatz S, Imhof A, Dosch R, Werner O, Mitchell P, et al. (1995) Transcriptional activation by Myc is under negative control by the transcription factor AP-2. EMBO J 14: 1508-1519.

178. Zhang H, Gao P, Fukuda R, Kumar G, Krishnamachary B, et al. (2007) HIF-1 inhibits mitochondrial biogenesis and cellular respiration in VHL-deficient renal cell carcinoma by repression of C-MYC activity. Cancer Cell 11: 407-420.
179. Dhruv HD, McDonough Winslow WS, Armstrong B, Tuncali S, Eschbacher J, et al. (2013) Reciprocal activation of transcription factors underlies the dichotomy between proliferation and invasion of glioma cells. PLoS One 8: e72134.
180. Kim HS, Woolard K, Lai C, Bauer PO, Maric D, et al. (2012) Gliomagenesis arising from Pten- and Ink4a/Arf-deficient neural progenitor cells is mediated by the p53-Fbxw7/Cdc4 pathway, which controls c-Myc. Cancer Res 72: 6065-6075.
181. Liu H, Radisky DC, Yang D, Xu R, Radisky ES, et al. (2012) MYC suppresses cancer metastasis by direct transcriptional silencing of alphav and beta3 integrin subunits. Nat Cell Biol 14: 567-574.
182. Chan CH, Lee SW, Li CF, Wang J, Yang WL, et al. (2010) Deciphering the transcriptional complex critical for RhoA gene expression and cancer metastasis. Nat Cell Biol 12: 457-467.
183. Zhou L, Picard D, Ra YS, Li M, Northcott PA, et al. (2010) Silencing of thrombospondin-1 is critical for myc-induced metastatic phenotypes in medulloblastoma. Cancer Res 70: 8199-8210.
184. Tang W, Zhang Y, Xu W, Harden TK, Sondek J, et al. (2011) A PLCbeta/PI3Kgamma-GSK3 signaling pathway regulates cofilin phosphatase slingshot2 and neutrophil polarization and chemotaxis. Dev Cell 21: 1038-1050.
185. Vervoorts J, Luscher-Firzlaff J, Luscher B (2006) The ins and outs of MYC regulation by posttranslational mechanisms. J Biol Chem 281: 34725-34729.
186. Nicolia V, Fuso A, Cavallaro RA, Di Luzio A, Scarpa S (2010) B vitamin deficiency promotes tau phosphorylation through regulation of GSK3beta and PP2A. J Alzheimers Dis 19: 895-907.

Publications

Czakai, K., K. Muller, P. Mosesso, G. Pepe, M. Schulze, A. Gohla, D. Patnaik, W. Dekant, J. M. Higgins, and A. Mally. "Perturbation of Mitosis through Inhibition of Histone Acetyltransferases: The Key to Ochratoxin a Toxicity and Carcinogenicity?" *Toxicol Sci* 122, no. 2 (2011): 317-29.

Hagemann, C., B. Weigelin, S. Schommer, M. Schulze, N. Al-Jomah, J. Anacker, S. Gerngras, S. Kuhnel, A. F. Kessler, B. Polat, R. I. Ernestus, R. Patel, and G. H. Vince. "The Cohesin-Interacting Protein, Precocious Dissociation of Sisters 5a/Sister Chromatid Cohesion Protein 112, Is up-Regulated in Human Astrocytic Tumors." *Int J Mol Med* 27, no. 1 (2011): 39-51.

Schulze, M., and A. Gohla. "Kinases and Phosphatases: Key Enzymes in Targeted Cancer Therapy." *Dtsch Med Wochenschr* 138, no. 9 (2013): 437-40.

Affidavit

I hereby confirm that my thesis entitled “Role of Chronophin for glioma invasion and migration” is the result of my own work. I did not receive any help or support from commercial consultants. All sources and / or materials applied are listed and specified in the thesis.
Furthermore, I confirm that this thesis has not yet been submitted as part of another examination process neither in identical nor in similar form.

Place, Date Signature

Eidesstattliche Erklärung

Hiermit erkläre ich an Eides statt, die Dissertation „Die Rolle von Chronophin für die Migration und Invasion von Gliomzellen“ eigenständig, d.h. insbesondere selbständig und ohne Hilfe eines professionellen Promotionsberaters, angefertigt und keine anderen als die von mir angegebenen Quellen und Hilfsmittel verwendet zu haben.
Ich erkläre außerdem, dass die Dissertation weder in gleicher noch in ähnlicher Form bereits in einem anderen Prüfungsverfahren vorgelegen hat.

Ort, Datum Unterschrift

Acknowledgements

First of all, thanks to Prof. Dr. Antje Gohla for the opportunity to work on this fascinating and challenging project. Thanks for the time invested in supervision, the helpful discussions about the theoretical and technical aspects, and for the support of my research. And of course altogether for the excellent supervision of the project, the support for this phd work and the scientific experience gained during that time.

Thanks to:

Dr. Elisabeth Jeanclos for introduction into the laboratory, microscopy and assays. Thanks for many helpful discussions and the support during the daily life in the lab

Prof. Dr. Martin Eilers for helpful discussions about the project and his excellent supervision of my phd thesis

Prof. Dr. Anna-Leena Sirén for the *in vivo* implantation experiments, the time spent for imaging and histology and thanks of course for the excellent supervision of of my phd thesis

Dr. Andreas Beilhack for the great support of the *in vivo* experiments

Dr. Sabrina Kraus for the great help with the *in vivo* luciferase imaging and the *in vivo* experiments

To all people involved in the *in vivo* setup: It was a great opportunity to test our hypothesis *in vivo*, thanks a lot!

Dr. Stefan Kissler for providing the viral packaging plasmids

Dr. Michael Krause and Lykas Rycak for the microarray studies and their analysis

Christian Linden for the cell sorting

Beate Vogt for the time consuming sectioning of the IHC slides

Alexandra Bohl for providing primary mouse astrocytes

Prof. Dr. Martin Lohse for the excellent working atmosphere at the institute of Pharmacology

My colleagues Gunnar, Anni, Angela, Volker, Gabriela, Juliane, Thomas S., Thomas F., Ambrish, Prashant, Angelika, Kerstin, Beate and Karina, for the nice working atmosphere and activities in the group

Thanks to my family and friends, who supported me the whole time and without whom this work would not have been possible